Aalto University
School of Chemical
Engineering

Özgul Agbaba Sener

CARBON DIOXIDE METHANATION OVER HYDROTALCITE-BASED NICKEL CATALYSTS

Master´s Programme in Chemical, Biochemical and Materials Engineering
Major in Chemical Engineering

Master's thesis for the degree of Master of Science in Technology
submitted for inspection, Espoo, 09 April, 2017.

Supervisor Professor Ville Alopaeus

Instructor M.Sc. Johanna Kihlman
D.Sc. Reetta Karinen

Aalto University
School of Chemical
Engineering

Aalto University, P.O. BOX 11000, 00076 AALTO
www.aalto.fi

Abstract of master's thesis

Author	Özgul Agbaba Sener
Title of thesis	Carbon Dioxide Methanation over Hydrotalcite-based Nickel Catalysts
Department	Department of Biotechnology and Chemical Technology
Major	Chemical Engineering
Thesis supervisor	Professor Ville Alopaeus
Thesis advisor(s) / Thesis examiner(s)	M.Sc. Johanna Kihlman, D.Sc. Reetta Karinen
Date 09.04.2017	**Number of pages** 88+9 **Language** English

Abstract

Global warming and energy shortage have driven modern society to search for alternative and sustainable energy sources to replace with the fossil fuels. Innovative solutions are required for mitigating CO_2 emissions to the atmosphere and storing H_2 due to the intermittency of the renewable energy sources. With this thesis it is possible to cover both of these concerns at the same time while utilizing CO_2 to produce CH_4 as a synthetic fuel that could also be transported into already existing infrastructures or as a chemical compound that could store H_2.

Hydrotalcite-based nickel catalysts were synthesized via various techniques such as wet impregnation, co-precipitation and sol-gel with different nickel contents utilising a one-pot synthesis approach. The main approach of utilizing catalysts was with the washcoating of the newly synthesized catalysts inside the reactor tubes with a diameter of 4 mm and a length of 17.5 cm. Catalytic performance of the catalysts was investigated for the hydrogenation of carbon dioxide under atmospheric pressure in a temperature range of 250-500^{o}C. These synthesized catalysts were compared with a Ni/Al_2O_3 catalyst, which was prepared as benchmark, in terms of CO_2 conversion-to-CH_4. Additionally, throughout this thesis, the effect of many parameters to the performance of the catalysts had been studied, including but not limited to, nickel content, GHSV, catalyst amount, reduction temperature and addition of Ce as well as Zr. Furthermore, the stability of the catalysts was investigated through long-term tests.

The CO_2 methanation was already initiated below 220^{o}C (X_{CO2}=10.2 %, S_{CO2}=98.4 %) which was ~100^{o}C lower than that over Ni/Al_2O_3 and reached 80% conversion of CO_2 at 300^{o}C with 99.9 % selectivity of CH_4 on 15 w% Ni/Mg/Al HT by co-precipitation method. When further increment in the temperature, at 350^{o}C a complete conversion (99.5 %) of CO_2 was achieved with ~100 % of CH_4 selectivity. The catalysts was also utilised as packed-beds, among those 5 w% Ni/Mg/Al HT by sol-gel showed the highest activity at 300^{o}C, 95.0% conversion of CO_2 with 99.8% CH_4 selectivity. The performance of the catalysts reduced with an increase in GHSV, while enhanced catalytic activity results obtained in the presence of excess amount of H_2 in the feeding gas mixture. Furthermore, additional catalyst amount which was assured by repeating washcoating cycles significantly improved the activity results. Finally, long-term tests proved good stability of the catalysts.

This superior performance of hydrotalcite-based nickel catalysts could decrease the reaction temperature of CO_2 methanation to lower temperatures and replace the usage of expensive Ru based catalysts and conventional Ni catalysts supported on various oxides.

Keywords carbon dioxide methanation, hydrogenation, CO2 utilization, CO2 conversion, nickel, hydrotalcite, layered double hydroxides, heterogeneous catalysis, washcoat, basic catalyst, Ni/Al2O3, co-precipitation, sol-gel synthesis

FOREWORD

This master's thesis has been conducted from September 2016 to April 2017 in the team of Catalyst Technologies at VTT, Technical Research Centre of Finland, for the Tekes-funded Neo-Carbon Energy project.

First and foremost, I would like to thank Prof. Juha Lehtonen for suggesting me as a master's thesis worker and to Pekka Simell for giving me the opportunity to perform my thesis in his group.

I would like to express my gratitude to my supervisor Prof. Ville Alopaeus and my advisors Johanna Kihlman and Reetta Karinen for their valuable comments, remarks and engagement through the learning process of this thesis. Furthermore I would like to thank Mari-Leena Koskinen-Soivi for introducing me to the laboratory as well for the support on the way. I would also like to thank all members of the Catalyst Technologies group for being very friendly and helpful.

I wish to thank my husband for encouraging me to turn back to academia and supporting me on the way of life, to my family in Turkey her zaman benimlesiniz!

Espoo, April 9, 2017

Özgul Agbaba Sener

TABLE OF CONTENTS

LIST OF FIGURES

LIST OF TABLES

LIST OF APPENDICES

NOMENCLATURE

Abbreviations

CSS	Carbon sequestration and storage
GHG	Greenhouse gases
HTs	Hydrotalcites
LDH	Layered double hydroxides
GHSV	Gas hourly space velocity
NASA	National Aeronautics and Space Administration
DRIFTS	Diffuse reflectance infrared Fourier transform spectroscopy
TEM	Transmission electron microscopy
XRD	X-ray diffraction
TOF	Turnover frequency
BET	Brunauer-Emmett-Teller
TPR	Temperature programmed reduction
TPD	Temperature programmed desorption
SEM	Scanning electron microscopy
XRF	X-ray fluorescence

Symbols

ΔH	Enthalpy [kJ/mol]
ΔG	Gibbs free energy [kJ/mol]
F_i	Molar flow rate of the component i
X_i	Conversion of the component i
Y_i	Yield of the component i
S_i	Selectivity of the component i
L	Particle size

k	Scherrer constant related to the shape and index of the crystals
w%	Weight percentage

Greek Letters

λ	Wavelength of the X-ray
β	Full width at half-height of the peaks
θ	Diffraction angle of the peak

Subscripts

i	Component index
in	Inlet
out	Outlet
ads	Adsorbed species on the surface of the catalysts

CHAPTER 1 INTRODUCTION

The demand for energy has rapidly increased in the chemical, power and transportation industries due to the rise in population and economic growth [1-4]. Energy production relies heavily on fossil fuels that are non-renewable energy sources. The growing use of fossil fuels inevitably leads to an increasing amount of carbon dioxide released into the atmosphere [2- 5]. Moreover, the rising CO_2 concentration in the atmosphere has resulted in the greenhouse effect and climate change. Therefore, growing efforts have been devoted to reducing atmospheric CO_2. Various approaches have been developed to capture carbon dioxide directly from either the air or the flue gas of fossil-fuelled power plants, biomass and industrial processes [2, 4, 6, 7]. Carbon sequestration and storage (CSS) has been implemented to capture and store CO_2 underground or in deep oceans [5, 6]. However, CSS can be challenging due to many reasons, including the cost, the distance from safe sequestration sites, small or medium sized sources, a diluted concentration of CO_2 in the emitting gas and having no information about the long-term impact on environment [2, 8].

One potential alternative to this problem would be utilization of CO_2 whose cycle is shown in Figure 1 [9]. As can be seen in the figure, captured CO_2 from industrial sources or atmosphere can be converted into a variety of valuable products with the addition of any secondary reagents to the process and the required energy being supplied from renewable sources. Currently, the utilization of CO_2 as chemical feedstock is limited to very few processes including synthesis of urea (mainly), salicylic acid as a pharmaceutical ingredient and polycarbonates. CO_2 conversion into fuels, such as methane or methanol, has gained recent interest due to having many advantages. [8, 10-12]

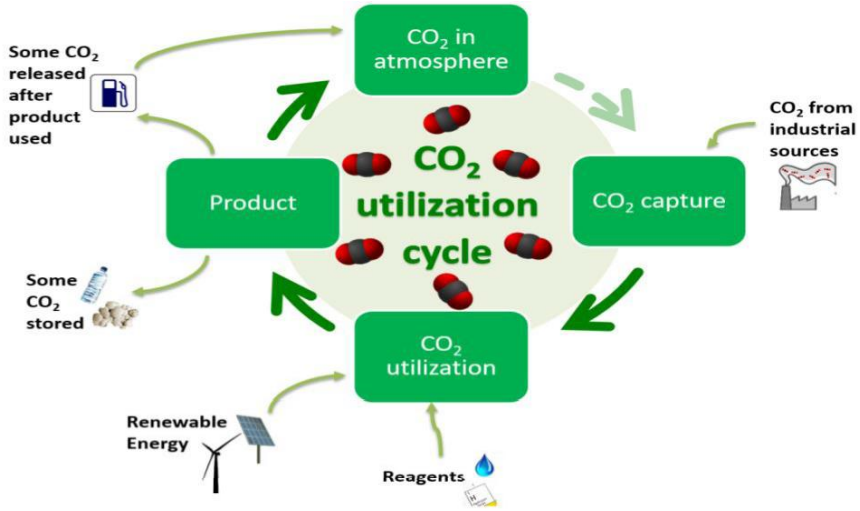

Figure 1: CO_2 utilization cycle [9].

In recent years, the methanation reaction, known also as Sabatier reaction, has gained great interest due to being a valuable solution for conversion of CO_2 which is the most abundant GHGs, a chemical storage of excess amount of hydrogen as well as a source of production of synthetic natural gas [1, 10, 13-18]. The Sabatier reaction catalytically hydrogenates carbon dioxide to methane. The reaction is operated at temperatures of 250-500 ^{o}C with pressures of 1-80bar, while utilizing catalysts. However the reaction is exothermic and thus being limited by the equilibrium at high temperatures and favouring methane formation at lower temperatures [10, 16]. On the basis of the equilibrium limitations of the methanation reaction, the greatest challenge is to find a proper catalyst for indicating high activity and selectivity towards methane at moderate temperatures and pressures [19, 20]. Various compounds have been chosen as catalysts for methanation reaction, including Ru and Ni with the best activities [10, 14, 16, 21-25]. Due to the high cost of Ru, Ni remains the best and most studied catalyst for CO_2 methanation [15, 24, 26]. Numerous studies have been devoted to improving the performance of Ni and to avoid sintering of the Ni particles by controlling the particle size distribution of active metal on Al_2O_3 support, addition of promoters or choosing a different support materials [27-32]. A support material which can activate CO_2 could be beneficial for higher CH_4 yields. Although high CO_2 conversion and methane yields have been achieved utilising Ni as active material at high temperatures, these catalysts have lower

activities at moderate temperatures [33-39]. Hydrotalcites (HTs) as one of the groups among layered double hydroxides (LDHs) have recently been utilised for the CO_2 hydrogenation reaction. However, few studies have utilised hydrotalcites as catalysts or catalyst supports for the CO_2 methanation reaction.

Therefore, the aim of this master's thesis is to produce hydrotalcite-based Ni catalysts using three preparation methods: impregnation, co-precipitation and sol-gel, with different Ni loadings. These synthesized catalysts are compared through CO_2 methanation reaction with Ni/Al_2O_3 catalysts, prepared as benchmarks, based on the performance of the catalysts. Furthermore, another aim is to determine the effect of several parameters (i.e., gas hourly space velocity (GHSV), the feeding compositions of reactants, reduction temperature and catalyst amount) on the activity and selectivity of the catalysts for this reaction. Ni-loaded Ce- and Zr-doped HTs which are commercially available will also be tested.

In line with these objectives, the rest of this thesis is organized as follows. Chapter 2 reviews the literature covering the details of the heterogeneous catalytic CO_2 methanation reaction, various employed reactor concepts and the importance of some parameters that may affect the performance of catalyst materials. Furthermore, HTs are introduced including their properties, preparation techniques and applications. Previous studies are reviewed in terms of HTs utilization as catalysts for the CO_2 methanation reaction. Chapter 3 describes the catalyst synthesis methods as well as the characterization analysis. This chapter also explains the experimental setup and activity test procedures. Chapter 4 reports and discusses the results of the activity tests at a temperature range 250-500^{o}C, including but not limited to the effect of feed composition as well as feeding flow rate. Chapter 6 concludes the thesis by discussing the limitations and future directions for research on this topic.

CHAPTER 2 LITERATURE REVIEW

2.1. CO_2 Methanation

CO_2 is an attractive C_1 building block due to being highly functional, abundant and renewable carbon source. Since the storage of CO_2 is costly, utilization of carbon dioxide has gained more interest [11]. One of the utilization approaches is methanation of carbon dioxide which can also be stated as hydrogenation of CO_2. The reaction has a range of applications including the purification of synthesis gas for the production of ammonia and the production of natural gas [10]. Furthermore the final product of hydrogenation of CO_2 which is CH_4 can further be employed to transform into hydrogen by steam reforming. Another interesting application of methanation of CO_2 has been studied by the National Aeronautics and Space Administration (NASA) regarding to converting the atmosphere of Mars of which main component is CO_2 to methane and water for fuel and astronaut life-support systems [40].

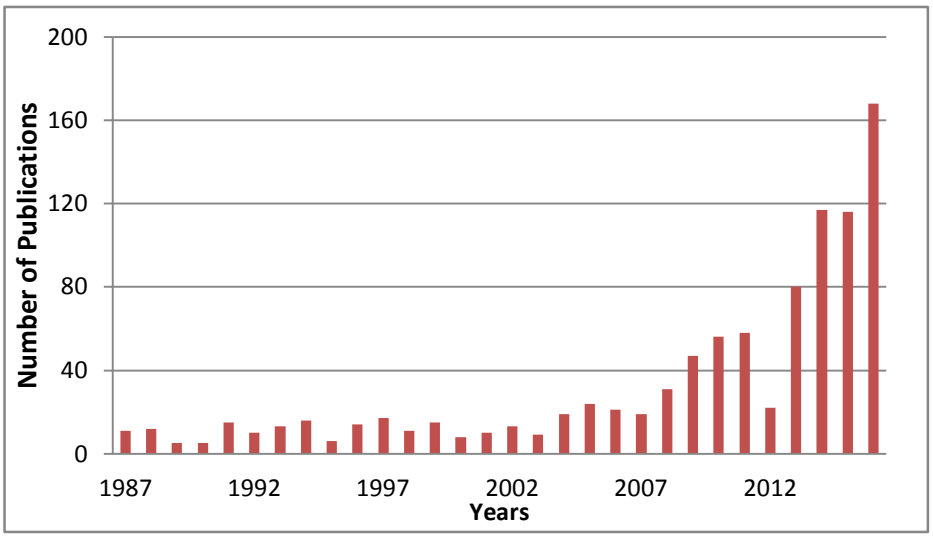

Figure 2: Documents published about 'CO_2 methanation' by year [41].

Recently, CO_2 methanation has gained a considerable attraction in research and development; Figure 2 shows the burgeoning number of publications dealing with CO_2 methanation for the last three decades. Advances have been

performed specifically about hydrogenation of CO_2 with the use of heterogeneous catalysts. However, methane production from CO_2 has been studied both via biological or catalytic methanation which will be described in following sub-sections.

2.1.1. Biological Methanation

Biological methanation proceeds in aqueous solutions at low temperatures and pressures (20-70 ^{o} C, 1-10 bar) in reactors such as stirred tank, membrane, trickle bed or fixed bed reactors [1, 21]. Since the reaction medium is an aqueous solution and the solubility of the gaseous reactants in liquid is very low, specific microorganisms such as methanogens are required as biocatalysts [13, 42, 43]. Recently, the reactor performance and operation conditions of many previous studies on biological methanation were reviewed in terms of various parameters in order to evaluate the efficiency and final methane content in the product [1]. The limiting steps of the methanogenesis process were observed as the internal diffusion of hydrogen from gas to liquid phase and the amount of energy consumed while pumping the reactants inside and the stirring.

The effective reaction rate was reported to be increased by an increase in pressure following enhancement of solubilities or in mass transfer coefficient by enhanced stirring. The influence of agitation on mass transfer coefficient was studied and found that an improvement in stirring rate increased the number of hydrogen molecules reach the liquid phase to react with carbon dioxide [44]. Furthermore pH of the solution, the pressure and stoichiometric ratio of gas mixture (H_2/CO_2) were the other parameters affecting the rate of methanation reaction. Biological methanation has advantages such as proceeding at low temperatures and having a high tolerance for the various impurities including sulphur and ammonia whose sources can be CO_2 as well as oxygen coming from electrolysis of water [13]. Due to having low reaction rates biological methanation has been investigated mostly in laboratory scale.

2.1.2. Catalytic Methanation

Catalytic methanation of CO_2 reaction which is shown in Eq. 1 was discovered by Paul Sabatier in the beginning of 20th century [14]. The reaction which is a reversible, exothermic process utilises carbon dioxide and hydrogen as reactants for the catalytic production of methane as well as water with the typical operating conditions of 300-550 ^{o}C from 1 to 100 bar [1, 10, 13]. The reaction is thermodynamically favourable with a negative change in Gibbs free energy ($\Delta G_{298\,K} = -130.8\,\mathrm{kJ/mol}$), however due to being highly exothermic, a complete reduction of carbon dioxide to methane requires low temperature. According to Le Chatelier's principle, low temperatures and high pressures shift the equilibrium to the product side. Besides the reduction of CO_2 is an eight-electron process with significant kinetic limitations. As a result a proper catalyst is needed to achieve high reaction rates with high methane selectivity [10].

$$CO_2 + 4H_2 \leftrightarrow CH_4 + 2H_2O \qquad \Delta H_{298\,K} = -165.0\,kJ/mol \qquad (1)$$

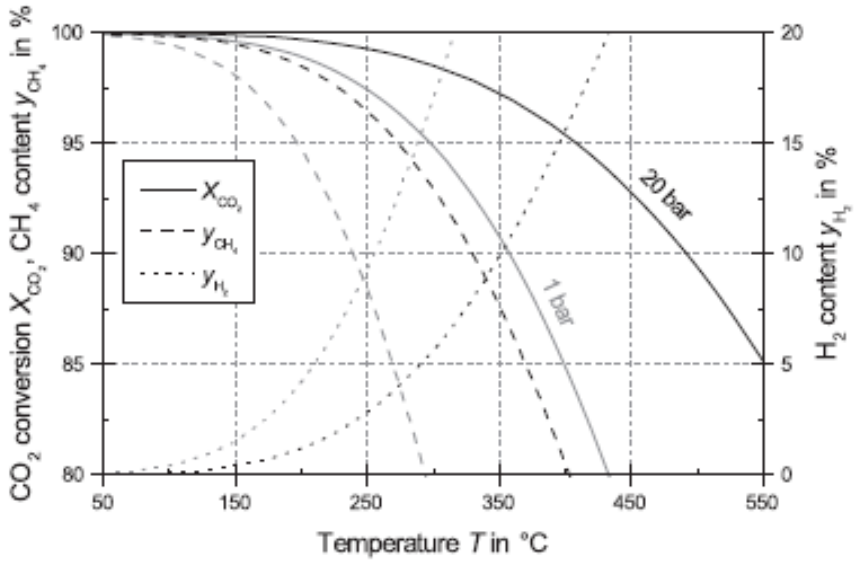

Figure 3: Thermodynamic equilibrium of CO_2 methanation (feed gas: $H_2/CO_2/CH_4$ = 4/1/1) [1].

Figure 3 presents the thermodynamic equilibrium of CO_2 methanation reaction. It is clear from the figure that, high CH_4 yields are limited by the equilibrium at temperatures above 225 ^{o}C for 1 bar and 300 ^{o}C for 20 bar [1]. Therefore, low reaction temperature, high pressure and properly selected H_2/CO_2 ratio are

required to optimize the process. Last but not least, with the help of an active catalyst it is possible to transform carbon dioxide into methane under ambient conditions (room temperature and atmospheric pressure) with high CH_4 yields.

The reactor concepts that have been used for catalytic methanation reaction including fixed-, fluidized-bed and structured reactors will be described in following sections. Furthermore, the reaction mechanisms and the types of solid catalysts utilized for this reaction will be reviewed.

2.1.3. Methanation Reactor Technologies

Catalytic methanation reaction has been studied and realized for various process concepts including different reactor types and operating conditions [45]. The development of catalytic methanation concepts from 1960s to 1970s and over the last 50 years were reviewed recently [45, 21]. Figure 4 represents the overview of different methanation concepts in terms of reactor aspects and the state of development. Furthermore an overview of established catalytic methanation concepts was also reported through the examples of many companies commercially performing catalytic methanation [45]. These commercially available methanation processes are mostly based on methanation of CO; however, any of the technologies reported for CO methanation can be applied for hydrogenation of CO_2, as well, due to the similarity in the thermochemistry of CO and CO_2 methanation processes [21].

As shown in Figure 4, the catalytic methanation concepts are indicated in terms of number of phases and different reactor concepts. State of developments in each case is defined by the help of a letter such as c, d and r, referring to commercial, demonstration scale and research, respectively. The colour of the boxes relates to severity of the hot spots created inside the reactors. The fixed bed reactors with two phases have been employed commercially while fluidized bed are in demonstration scales; besides, slurry and structured reactors including microreactors as well as sorption enhanced reactors are focus of research activities. A list of research group working on the different reactor

concepts was given as a list in which more than 30 groups worldwide showed interest in methanation reaction and more specifically the reactor concepts in order to enhance the temperature control in methanation reaction [1].

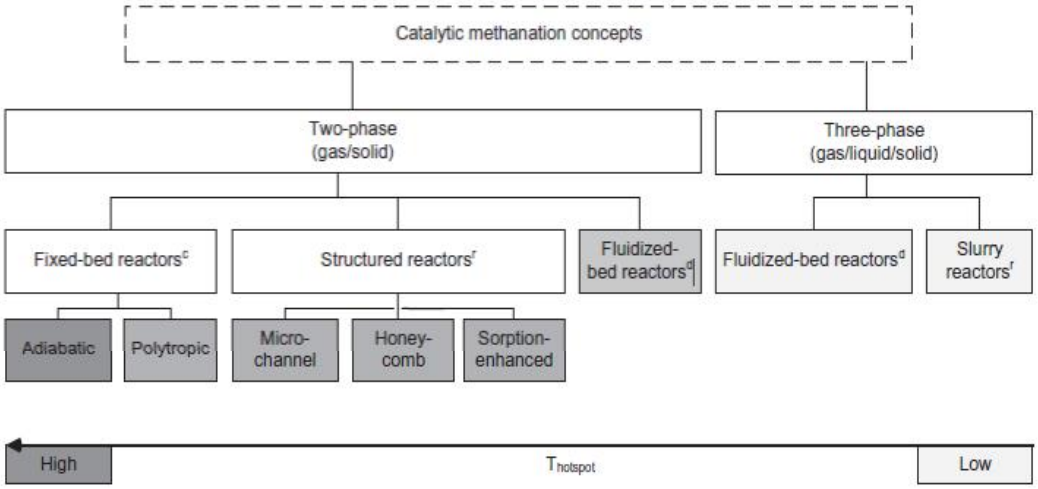

Figure 4: Overview of different methanation concepts; State of development: c – commercial, d -demonstration scale, r – research [21].

2.1.3.1. Fixed-bed methanation

Fixed-bed reactors are tubular reactors which are packed with a solid catalyst that comprises a bed in a fixed position [46]. Currently, fixed-bed reactors are used in adiabatic or polytrophic conditions for catalytic methanation and adiabatic fixed-bed methanation has been the most widely adopted method [45, 13, 21]. The challenge in using an adiabatic fixed bed reactor is the temperature control owing to high amount of heat release during the methanation reaction. One solution approach is to decrease the volume of reactors and employ a series of adiabatic reactors with intercooling systems and sometimes with a cooling gas circulation [13]. Furthermore adiabatic mode of operation requires a catalyst which is active for a broad range of temperature 250-700 ^{o}C. Typical reaction temperatures for fixed bed reactors are between 300-500 ^{o}C while temperatures above 550 ^{o}C cause deactivation of catalysts by sintering [13].

An example of an approach to prevent the hot spots and related sintering effects on catalyst particles, NiO catalyst with the average grain size of 0.15 up to 0.25 mm was distributed in a bed of quartz sand which had the same average grain

size [17]. The mixture of catalysts and the sand was filled into a metallic reactor tube of 8 mm in diameter and 100 mm in length. The reactor was placed inside an oven in order to maintain an isothermal condition. The conclusion was conducted from the experiment that the performance of the catalyst was not influenced by dilution effects and the long term stability of the catalyst was sustained as shown in Figure 5. A similar dilution example to prevent the hot spots was carried out with the help of silica glass particles having similar mesh sizes [27].

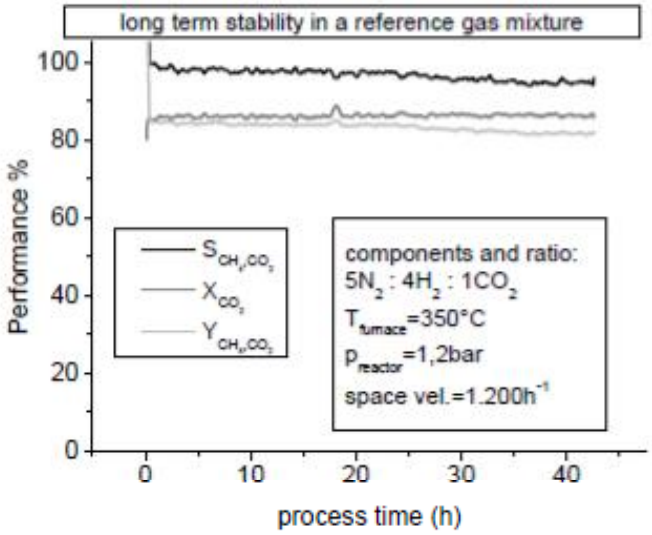

Figure 5: Catalytic performance of Ni based catalysts diluted in quartz sand with similar average grain size [17].

2.1.3.2. Fluidized-bed methanation

Fluidized bed reactors can accomplish multiphase reactions, in which reactants in gas phase fluidizes the solid catalyst particles inside the reactor [46]. The fluidized-bed reactors generate uniform mixing, enhance the mass transfer of gas molecules through the pores of fine catalysts particles, and thus create almost isothermal conditions in the reactor [13]. Heat removal is more effective in the reactor compared to fixed-bed reactors enabling the use of a single reactor with a rather simple design; however, catalyst particles can be damaged due to strong collisions as well as the walls of the reactor. Furthermore, the superficial gas velocity requires to be optimized in order to have a fluidized medium but not to

lose particles. Due to the possibility to achieve higher mass and heat transfer rates in fluidized-bed reactors, they have been utilized efficiently for methanation reactions [15]. For instance, a fluidized bed reactor was used to investigate the characteristics of the RWGS reaction with Fe/Cu/K/Al catalyst; CO_2 conversion in the fluidized bed reactor (46.8%) was higher than that in the fixed bed reactor (32.3%) [47].

2.1.3.3. Structured reactors

Structured reactors have been promising equipment especially for research activities in laboratory scale, due to having many advantages compared to the drawbacks of fixed-bed reactors. The drawbacks include the hot spots and high pressure drops due to catalyst loading as well as the particle size of catalysts [21]. The structured reactors such as microreactors, which are special concepts having a high surface to volume ratio, have been developed for various applications. Microreactors consist of microchannels coated with prepared catalysts have been used for methanation reactions, as well [23, 48-50]. A microreactor was fabricated for utilization of CO_2 to produce fuel on Mars for space habitat [49]. Ru/TiO_2-based catalyst was prepared and loaded as porous-metal-felt placed into each channel in which it was possible to control the temperature efficiently. Figure 6 represents a drawing of this microreactor and its sections; an active side-wall cooling was supplied with controlling the oil flow, which was used as a coolant. The reactor consisted of two columns of 15 microchannels, inlets and outlets for reactants/products as well as cooling oil, having a total volume of 40.8 cm^3. The counter flow of oil and reactant streams was claimed to be helpful for the control of the temperature throughout the reactor while a complete conversion of CO_2 into methane at around 330 ^oC was achieved.

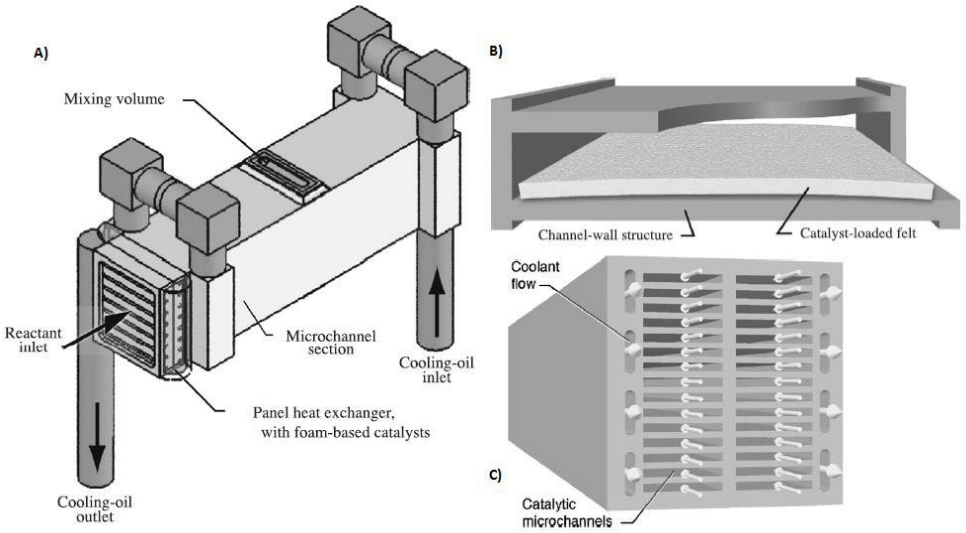

Figure 6: Illustrations of microreactor A) Sabatier microreactor, B) Single channel with an interior catalyst-loaded porous metal felt, C) A section of microreactor with cooling and microchannels [49].

2.1.4. Reaction mechanism of CO_2 Methanation

Even though the methanation reaction has been known for a long time, the exact reaction mechanism for CO_2 methanation is still subject to debates [40]. Even the mechanism of CO methanation still hasn't been in consensus, yet for over a hundred years. Different mechanisms for methanation of CO_2 have been proposed as two main divisions [10, 16, 40]. The first one starts with the dissociative adsorption of CO_2 to form CO and O, namely reverse water gas shift reaction, on the surface of the catalyst prior to methanation. Afterward, it follows the same steps with the CO methanation process [24, 26, 28, 51, 52]. However, according to another proposed mechanism, reaction proceeds by the direct hydrogenation of CO_2 to methane via carbonate or formate intermediates without the formation of CO [22, 25, 53].

Figure 7 demonstrates one of the proposed mechanisms which involve a reaction intermediate of CO_{ads} referring the adsorbed CO species on the surface of the catalysts. This intermediate is considered to be a side product due to having strong bonds with the support material. Subsequently, the formate species reacts with six adsorbed hydrogens which is not an elementary reaction. Another

pathway included to this proposal is the formation of intermediate formate species as hydrocarbons [54, 15, 10, 16].

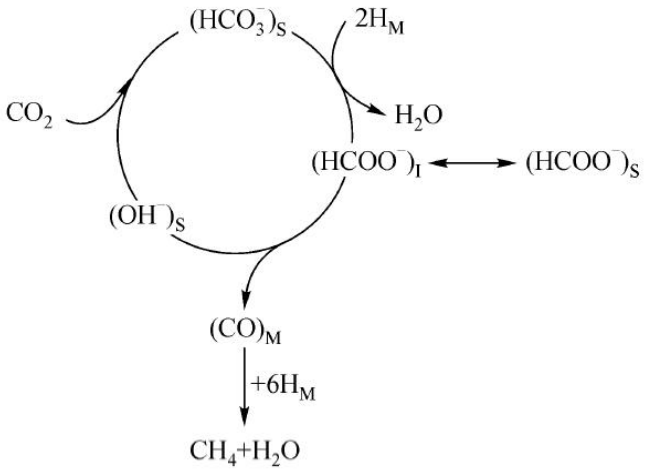

Figure 7: Proposed mechanism for CO_2 methanation process; where S, M and I refer to the support, metal and metal-support interface [54].

The rate determining step in hydrogenation of CO_2 was proposed to be either the dissociation of CO as C species and its hydrogenation or the formation of the intermediates CH_xO and their interaction with hydrogen. Elementary reaction steps of CO_2 methanation on Ni (111) catalysts was studied using Atom Superposition and Electron Delocalization-Molecular Orbital theory [29]. The following steps were considered to have two main parts, firstly the formation of C species adsorbed on the surface of the catalysts and secondly the methanation of C species. Activation energies of each step were listed next to the step number in terms of electron volts (eV), indicating that the rate determining step as step 3 with the highest activation energy, CO dissociation to C and O.

$CO_{2\,ads} \rightarrow CO_{ads} + O_{ads}$ $Step\ 1$ - 1.27 eV

$CO_{ads} \rightarrow C_{ads} + O_{ads}$ $Step\ 2$ - 2.97 eV

$2CO_{ads} \rightarrow C_{ads} + CO_{2\,gas}$ $Step\ 3$ - 1.93 eV

$C_{ads} + H_{ads} \rightarrow CH_{ads}$ $Step\ 4$ - 0.72 eV

$CH_{ads} + H_{ads} \rightarrow CH_{2\,ads}$ $Step\ 5$ - 0.52 eV

$CH_{2\,ads} + 2H_{ads} \rightarrow CH_{4\,gas}$ $Step\ 6$ - 0.50 eV

However, another study reported that prior to all of the steps mentioned above; chemisorption of CO_2 on the catalyst was needed [20]. The dissociative adsorption of carbon dioxide to form CO and oxygen on the catalyst surface was proved using in situ diffuse reflectance infrared Fourier transform spectroscopy (DRIFTS) experiments (Fig. 8). In general, by utilizing this technique it is possible to identify active adsorbates and follow the surface site occupancy over the reaction. A chromatogram is further generated showing the interaction between the catalysts and the compounds with the help of bands. Each band corresponds to a specific interaction with respect to the value of wavenumbers and the absorbance [55]. CO_2 dissociation on the catalyst surface was proved by the presence of the bands, which refer to the interactions between the catalyst ($Rh/\gamma\text{-}Al_2O_3$) and CO_2 as well as CO, without having any CO as one of the reactants.

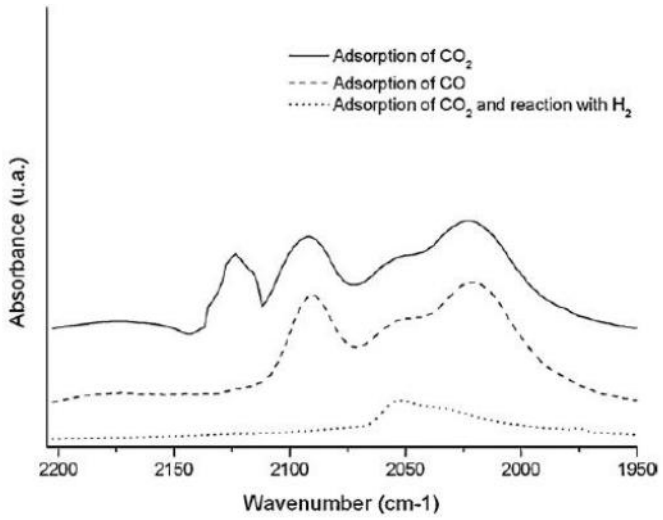

Figure 8: The results of DRIFT analysis for dissociative adsorption of CO_2 [20].

2.1.5. CO_2 Methanation over Solid Catalysts

As CO_2 methanation studied first by Sabatier and Senderens, many metals were employed as active materials such as Cu, Co, Pt, Pd and Ni in their early work, but it was reported that Ni was the best metal to catalyse the methanation reaction [14]. Subsequently, a number of compounds have been studied as heterogeneous catalysts for hydrogenation of CO_2 [15, 18, 19, 56].

Heterogeneous catalytic reactions, in which a mixture of gaseous or liquid compounds reacts on a solid catalyst surface, have been used in almost all processes in energy and chemical industries [57-59]. Heterogeneous catalysts should be prepared to meet many requirements due to the enormous market demand. The first curial requirement is to be active and selective with respect to the reactants and the desired products. Secondly, catalysts should accommodate the large differences in operating conditions (e.g. temperatures), products and the feedstocks. Furthermore the catalysts should be stable for long hours and should prevent the active sites to be poisoned irreversibly by impurities or some side products [57, 60].

As heterogeneous catalysts, many metals especially in groups 8 to 10, such as Ni, Pd, Pt, Co, Rh, Fe and Ru have been reported as active for methanation reaction [16, 21]. Ru and Rh-based catalysts have attracted significant interests due to their high activity and selectivity in CO_2 methanation reactions especially at low temperatures [22]. However, owing to the price of Ru which is 120 times of Ni, Ni still is the most widely used catalyst for CO_2 methanation, although it can be deactivated due to sintering at higher temperatures [19]. The activity and selectivity of the metal catalysts have been evaluated in various methanation studies and hence many rankings with respect to performance of the catalysts have been proposed. One of the rankings proposed in terms of activity and selectivity [61] given as follows:

Activity: Ru>Fe>Ni>Co>Mo
Selectivity: Ni>Co>Fe>Ru

The performance of catalysts, such as the activity and selectivity, depends on various parameters including the choice of supporting materials, loading of active materials, employing a second metal, preparation methods, calcination and reduction processes. The effect of supports, loading of active materials, calcination and reduction processes on the reaction of CO_2 methanation will be further reviewed.

2.1.5.1. Effect of supports

Support is a material, generally a solid with a high surface area, on which a catalyst is deposited. Support materials mainly determine the density, nature and the accessibility of the active sites [58]. The requirements for an excellent support are included but not limited to the high purity, well-defined porosity, pore size distribution and pore volume [62]. The nature of the supports has a pivotal role due to affecting the interaction between the active metal and support itself, and hence governs the performance of catalysts by conditioning the activity and selectivity of the catalysts [10, 16, 53]. The main idea is to create a better dispersion of active phase on the support materials, which needs focus on preparation of highly dispersed metal supported catalysts with controlled crystallite sizes. A direct measurement of the crystallite size and the dispersion of the active metals are necessary for this purpose. The two common methods to measure the supported crystallite size are transmission electron microscopy (TEM) which is excellent for imaging the crystallites and X-ray diffraction line broadening analysis (XRD) [58, 63]. Besides, the active metal dispersion can be characterized by chemisorption analysis.

Metal catalysts have been supported by various oxides such as TiO_2, Al_2O_3, SiO_2, CeO_2, ZrO_2 as well as zeolites and reported that support materials influenced the activity and selectivity of the catalysts for methanation reaction [10, 16]. Ni catalyst supported on both silica gel and amorphous silica prepared by different methods were compared in methanation in terms of turnover frequency (TOF) of methane (amount of methane produced per number of nickel sites per second) [15]. It was proved that high dispersion of nickel nanoparticles obtained for the samples on amorphous silica which further had better TOF results than those on silica gel. Both unsupported and supported Ni nanoparticles on Al_2O_3 were studied with a high Ni loading (125% Ni/Al_2O_3). It was reported that Ni/Al_2O_3 had been more active than Ni nanoparticles without a support materials, while CO_2 conversion and CH_4 selectivity at 500 ^oC were recorded as 71-86% and 50-50%, respectively [27]. The reason was explained as the support might actively

participate the adsorption process of CO_2 on its surface as it was previously proposed by Busca et al. [64].

Another research evaluated the effect of different supporting materials on catalytic properties of Ru and resulted that the activities of catalysts were dependent on the Ru dispersion as well as the type of support materials [65]. The performance of supported Ru catalysts on CO_2 methanation reaction was given in an order as Ru/Al_2O_3>$Ru/MgAl_2O_4$>Ru/MgO>Ru/C. Alumina supported Ru had the highest performance while the carbon supported Ru had the lowest activity due to covering all the active surface which is called site blocking effect.

Furthermore, loading of active metal was declared to influence both the interaction of metal with the support and the dispersion of metal particles [16, 27, 35, 66]. Highly dispersed metals were analysed at low metal loadings, whereas with highly loaded catalysts metal aggregates were observed. Considering that the reaction taking place on the surface of the catalysts, the dispersion of the metallic nickel might have predominant importance on the catalytic activity.

2.1.5.2. Effect of calcination

Calcination is a thermal treatment of a material in oxidizing atmosphere for a few hours at temperatures slightly higher than the operating temperature for the catalysts [59]. The aim of calcination process is stabilization of physical and chemical properties of the prepared catalysts. A calciner is employed which is a steel cylinder rotates inside a heated furnace with a temperature range of 550-1150 ^{o}C through a controlled air or oxygen atmosphere. The treatment stabilizes the thermally unstable compounds such as hydroxides, carbonates or organic compounds and transforms them into oxide forms, while it is possible to produce new species at higher temperatures. Furthermore, pore features and crystal structures are subjected to a change subsequent to calcination process.

The effect of calcination on catalysts activity and selectivity in methanation were reported for various catalysts. $Ru/Ce_{0.8}Zr_{0.2}O_2$ catalysts were calcined at different temperatures and their catalytic properties were tested in a continuous fixed-bed reactor [30]. The prepared catalyst samples by various methods were characterized and tested in order to understand the influence of calcination temperatures on the structure of catalysts and subsequently to the activity. The results regarding to the characterization of textural properties of catalysts and H_2-TPR experiments were reported. It was concluded that an increase in calcination temperature decreased the surface area and pore volume while increasing the pore diameter. Another study using Ni supported by Zr-Sm oxide catalysts for various temperatures from 800 to 1000^{o}C, claimed that as the calcination temperature got higher the conversion increased accordingly. However, the highest conversion was obtained at 800 ^{o}C, as further temperature was proved to be deleterious [31]. Higher calcination temperature proved to cause a change in textural properties of catalysts by agglomerations consequently the Brunauer-Emmett-Teller (BET) surface area of the catalysts and the metal dispersion got smaller.

2.1.5.3. Effect of reduction

Reduction of a catalyst material is performed in a hydrogen atmosphere to activate or regenerate the catalysts by forming active sites; prior to reduction processes, the reduction temperature of the metal of interest should be decided via temperature programmed reduction (TPR) analysis [16, 21]. The influence of reduction process on the performance of catalyst samples have been emphasised in various studies. For instance, Jacquemin et al. proved the effect of reduction on samples for methanation reaction, performing CO_2 chemisorption measurements on a Micromeritics ASAP2010Chemi apparatus while employing a catalyst Rh supported on Al_2O_3 [20]. Figure 9 shows the results of the measurements showing the volume of CO_2 chemisorbed per gram of catalyst with respect to pressure for both reduced and fresh catalyst samples. The fresh catalyst, which referred to the samples employed before reduction, showed no

production of methane due to having in almost no active sites where CO_2 molecules chemisorbed on [20]. However, the reduced catalyst samples were reported to have a significantly higher number of adsorbed CO_2 molecules leading a major conversion to methane. Besides it was claimed that, pressure has an augment effect on the volume of chemisorbed CO_2, specifically for the reduced catalyst sample.

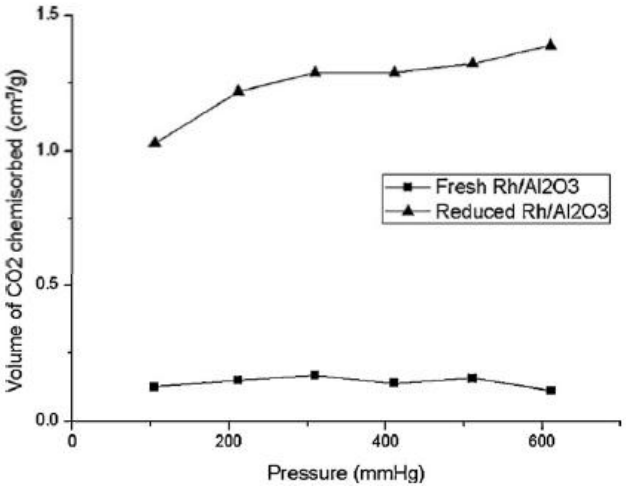

Figure 9: Chemisorption of CO_2 on the catalyst with and without reduction process [20].

On the other hand, recently, HTs which are also called as LDHs or anionic clays have received considerable attention as a choice of catalyst or catalyst supports for CO_2 methanation due to their various properties. HTs have a complex layered structure, high ion exchange capacity, ability for absorption of CO_2 and the basicity [32-36, 38, 39]. Promising results for activity and selectivity toward CO_2 methanation reactions make HTs attracting materials as catalyst, yet few studies have been done so far. Since CO_2 methanation will be catalyzed in this thesis using hydrotalcites-based nickel catalysts, the next section will discuss the definition, the important features, preparation techniques and applications of HTs.

2.2. Hydrotalcites

LDHs are a group of minerals that have multi layers of structures. LDHs can be divided into different classes with respect to containing compounds and molecular structures. Being one of LDHs, HTs, whose name was derived from its similarity to talc and its high water content, are naturally occurring anionic clays [67]. HTs were the first type of LDH that was discovered in Snarum, Norway and was described as white pearly lustres [68]. A map showing the distribution profile for the sources of HTs worldwide is depicted in Figure 10 [69]. As shown in figure, HTs can, in addition to the Snarum area of Norway, be also mined in almost every continent including the Ural area of Russia and Somerville, New York [70]. Early studies about HTs were confusing due to the large number of structures shared by other related minerals. For this reason, HTs were initially believed to be a mixture of other compounds [71]. However, HTs were eventually accepted as a valid species after Manasse characterized HTs using analytical, thermal and optical techniques.

Figure 10: Localities for Hydrotalcites [69].

The current general formula of HTs was derived by Manasse and later confirmed by Foshag [71, 72] while the types of occurrences of HTs were not proposed until much later [73]. The results showed that all the samples of HTs from different areas had mainly mixture phases of hexagonal and rhombohedral types. The

rhombohedral phases were classified as Hydrotalcite, while the hexagonal phases are commonly known as manasseite. On the other hand, they are commonly referred as 'hydrotalcites', 'hydrotalcite-like compounds' or the 'hydrotalcite group' of minerals [70]. Recently, the nomenclature of the HT supergroup of minerals has been described by Mills, while reviewing the chemistry, polytypic variations and the structure of HTs.

Since HT based Ni catalysts will be utilized in this thesis, the next sub-sections will discuss the important features including unique layered structures, preparation techniques and applications of HTs.

2.3.1. Important features of HTs

The attractive features of both natural and synthetic HTs are the unique layered structure, basicity, ability to capture organic and inorganic anions, biomolecules and genes, tendency to protect intercalated anions from physicochemical degradation, memory effect as well as relative ease of synthesis [74, 75, 76, 77]. Furthermore HTs are usually chosen over other compounds due to the versatility, simplicity, easily tailored properties and low cost of the materials [78]. These features of HTs will be explained in detail through following sections.

2.3.1.1. Layered structure

HTs have a unique layered structure (Figure 11a) consisting of brucite-like layers which are positively charged and compensating anions that are intercalated between the layers [79-83]. The brucite ($Mg(OH)_2$) structure (Figure 11b) consists of two adjacent arrays of closely-packed hydroxide anions containing octahedral spaces between OH^- layers which is filled by Mg^{2+} cations. HTs are differed from brucite-like structure which is electrostatically neutral, replacing M^{2+} octahedral cations with M^{3+} ions which lead positive charged layers. This positive charge is balanced by anions which are intercalated between the layers. Intercalated molecules, water typically, provides hydrogen bonding between the brucite layers.

HTs have the general formula of $\mathbf{[M^{2+}_{1-x}\ M^{3+}_{x}\ (OH)_2]\ [\ A^{n-}_{x/n}\cdot mH_2O]}$ where, M^{2+} represents divalent cations among which most commonly used ones are Mg, Co, Cu, Ni, Ca, Zn, Mn, Fe, whereas M^{3+} denotes for trivalent cations such as Al, Fe, Cr . A in the formula shows the anions located in the interlayers with a charge 'n' the most common anions are NO_3^- , Cl^-, SO_4^-, OH^- , and water molecules fill the remaining space between layers. The value of x is equal to the molar ratio of $M^{2+}/(M^{2+} + M^{3+})$ and m shows the water amount [79, 84, 85]. Furthermore, employing monovalent (Li^+) and tetravalent cations such as Zr_4^+, Sn_4^+, Ti_4^+, Si_4^+ have been also reported as possible synthesis approach [79].

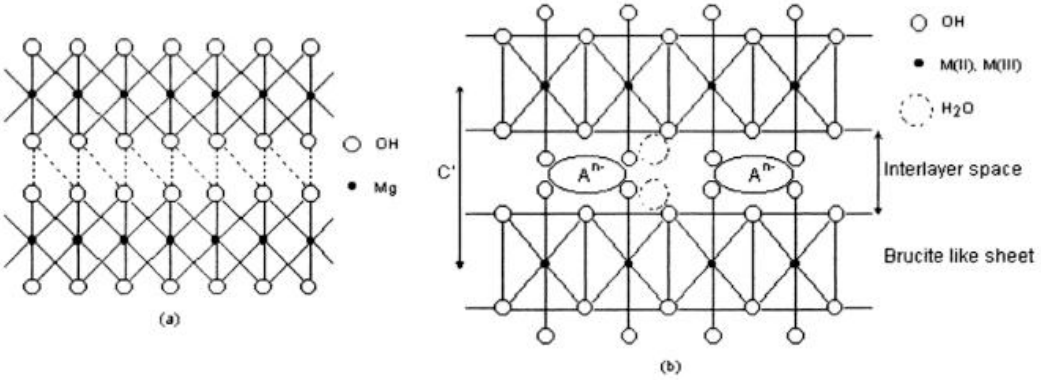

Figure 11: Schematic representation of Brucite and Hydrotalcite structure [85].

As many parameters have been found to affect the general formula of the HTs with widely varied physicochemical properties can be obtained by changing the nature of the metal cations, the molar ratios of M^{2+}/M^{3+} as well as the type of interlayer charge balancing anions [86, 87]. Besides, the unique structure of HTs has been proposed to contribute to the basicity, the sorption and ion exchange capacity of compounds.

2.3.1.2. Basicity

HTs can be used as such or after thermal treatment which is called calcination. Calcined HTs have been widely used as solid base catalysts for various heterogeneous reactions [79, 88]. Calcination of HTs increases not only the surface area but also the number of defects in the material structure which causes higher density of basic sites [89-91].

HTs with highest basicity were found to have highest catalytic activity [89, 92]. Several different preparation techniques were employed to synthesize HTs and the effects of these methods on the crystal size and textural properties of HTs were reported. Furthermore the ratio of divalent to trivalent cations (M^{II}/M^{III}), the crystallite size of HTs and the nature of intercalated anions were early reported as important parameters to control the basicity of the catalyst, and hence the activity and the reaction rate [91, 93]. Basicity of the catalysts can be quantitatively determined by CO_2-TPD measurements.

2.3.1.3. Ability to capture and exchange compounds

HTs have the ability to capture various compounds due to its structure and the interactions between the layers, between the intermaller anions and the positively charged layers, as well as the space between these layers [79, 74].

HTs have been reported to be used as effective adsorbents for capturing CO_2 [94-100]. Capturing CO_2 from flue gas has been mostly processed by pressure swing adsorption in which a proper adsorbent with the properties of high selectivity and adsorption capacity for CO_2 at high temperatures, stable capacity for repeated adsorption/desorption cycles as well as adequate mechanical strength after high pressure exposures are required. It has been claimed that HTs could meet these requirements. The adsorbent capacity of commercial HTs was tested while the main factors affecting the adsorption capacity were studied at high temperatures [94]. It was claimed that HTs met the criteria with an adsorption capacity greater than 0.30mmol/g at 300^{o}C and 1 bar. For lower temperatures the adsorption capacity of HTs was reported to be up to 2.5 mmol/g [100]. The type of anion and cation, the calcination process, addition of another species as promoters reported as the effecting parameters of adsorption of CO_2 [98, 101, 100].

HTs have been further utilized as an ideal material for the removal of toxic materials from water, soil as well as atmosphere [102]. They have been used as such or as calcined products to treat high concentrated solutions in order to

remove excess amount of various compounds such as chromium [103-105], phosphate, chlorinated organic pollutants [106], fluoride [107], boron [108], arsenic [109, 110], cadmium, lead [109], SO_x [111, 112] and several dyes [113-115]. These treatments reported as experimental studies in which kinetics and equilibrium parameters were determined while evaluating the effect of different parameters, including agitation speed, temperature, pH and concentration of the solution for different types and charge densities of used HTs [111, 116, 117]. Furthermore the sorption capacities, sorption affinity and efficiency of the HTs as sorbents were calculated. Several kinetic models were evaluated to fit the experimental data adsorption isotherm were used accordingly [103, 108]. Moreover, the structural characteristics of HTs such as degree of layer substitution, interlayer anion and crystallinity, the basal spacing and the orientation of interlayer molecules were proved to affect the removal processes [118]. Furthermore, removal of halides as pollutants with high concentrations in natural waters was performed using HTs. The use of HTs as soil conditioner for decreasing nitrate leaching, as a slow release nitrate fertilizer, and for purification of wastewater was patented in various countries [119, 120].

HTs are excellent anion exchangers due to their lamellar structure in which anions are trapped by the positively charged host sheets and swellable interlayer space is highly favourable for anion diffusion [121]. The interactions between the interlayers in LDHs are mediated by two forces: the Coulombic forces between the positively charged layers and the intercalated anions, and secondly the hydrogen bonds between the hydroxyl anions and the water molecules in the interlayer [122, 123]. The anion exchange capacity of LDHs has been claimed to be affected by these forces, and the ratio of metal cations, whereas not influenced by the molecular compositions, crystallinity or particle size of the material [124].

Furthermore, it is also possible to replace small interlayer anions such as NO_3^- and Cl^- with larger ones in order to get an expanded layer structure [84, 125, 126]. A three dimensional structure is declared to be applicable, as zeolites, if

permanent porosities can be obtained within the interlayer space of HTs, then the new materials can be considered as pillared anionic clays (PILACs) [84,87]. To prepare PILACs highly charged and large anions were reported to be required in order to create an interlayer with a negative charge as well as an expanded interlayer space. Besides, highly charged anions were used to decrease the population between the layers which make easier to find a space for guest species [87].

2.3.2. Preparation Techniques of Hydrotalcites

HTs commercially produced by first Kyowa Chemical Industry and then Kisuma Chemicals, and Sasol. In recent years, synthesizing techniques of HTs have received people's attention due to their various aforementioned properties. HTs can be tailored by varying the types and relative proportions of the di- and trivalent cations as well as the identity of the interlayer anions [127]. HTs can be synthesized directly with a number of different techniques. The most common preparation technique is simple co-precipitation method; however ion exchange processes are widely employed for preparing HTs, as well. Furthermore, other studied methods [128] include sol-gel, hydrothermal synthesis, microwave irradiation and electrochemical methods.

All of these methods used for the preparation of HTs have been reviewed with different aspects [129]. The method of choice is depend on the purpose of usage, in other words, the required properties are well determinative while selecting the preparation method; for instance if HTs would be used as a catalyst, catalyst support or precursor than high surface area as well as small particle size, presence of structural defects and well defined composition of specific compounds would be crucial.

Mainly methods to be employed are chosen depending on the specific application requirements, thus desired properties of the compounds can vary such as catalytic activity, adsorptive affinity to definite particles and surface chemistry, furthermore cost effective, nature friendly and easy to up-scale

methods should be used [130]. The most common preparation techniques of HTs will be mentioned in following sub-sections.

2.3.2.1. Co-precipitation methods

The mostly employed technique to prepare HTs is co-precipitation method which can be applied under constant or variable pH depending on the conditions [129]. During this method a mixed solution of di- and trivalent metal salts is slowly charged into a reactor which contains distilled water, while keeping the pH of the solution at desired values by controlling the addition of an alkaline solution to the reactor. The interlayer anions can either originate as OH^- or as CO_3^-. The source of OH^- can be the alkaline solution itself when the pH is too high or the solution of metallic salts if they are the counter-anions of these metals. CO_3^- moves to interlayer if the alkaline solution is selected as potassium or sodium carbonate [79]. An example of automated experimental set-up for co-precipitation method is presented in Figure 12. As can be seen in the figure, setup includes a pH meter and pH controller which make easy to create a constant-pH solution, while addition of alkaline and metal solutions.

Many researches have used co-precipitation methods to synthesize HTs, and further comparative studies on the effect of different parameters and variables have been carried out as well, to understand the relationship between the parameters and resulting structures as well as the specifications of HTs. These properties are crystallinity, thermal stability, purity of the phase, particle size distribution, average pore diameter and textural properties. For instance, HTs were used as soil conditioner which could adsorb excess nitrate from the soil and allow plants to take up required amount of N, reversibly. In order to optimize the experimental conditions to prepare materials with best anion exchange properties HTs were synthesized via co-precipitation methods [120].

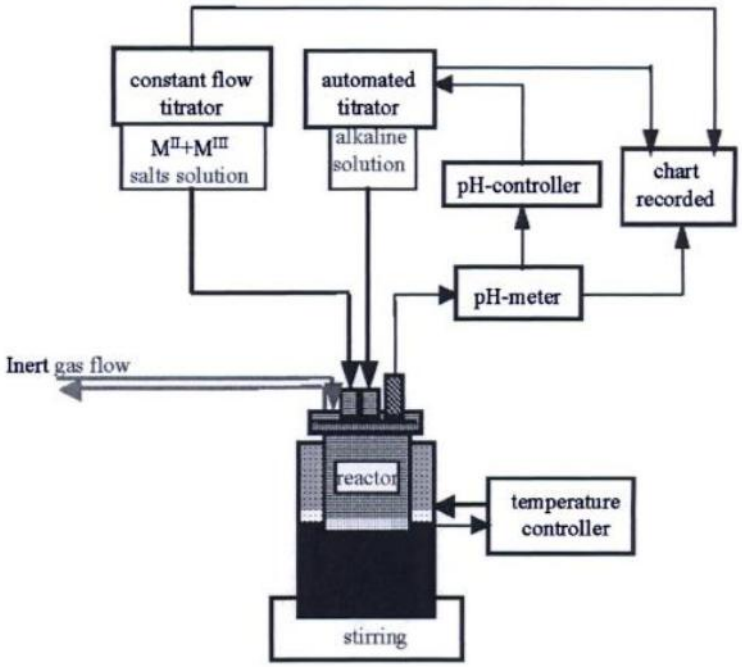

Figure 12: Experimental set-up for the preparation of LDHs by the co-precipitation method [79].

It has been extensively reported in the literature that pH is one of the determinant factor on the properties of HTs for co-precipitation methods due to its influence on mostly the crystallinity as well as phase purity [127] while other factors being the temperature in the reactor, aging of precipitate, flow rate and concentrations of both alkaline and metal solutions [79]. A thermal treatment which refers to calcination is often employed following the co-precipitation method in order to enhance the crystallinity of the materials. However for specific conditions while keeping the pH constant during precipitation, Valim et al. proposed that the prepared samples without thermal treatment were less influenced by the thermal treatment and showed the same stability with the other thermally treated samples [127]. Thermal treatment of the prepared HTs is the most energy consuming and the longest step in the preparation process. Although the co-precipitation method is most widely used for synthesize of catalysts, many drawbacks of this method have been reported. The method proceeds as a very long procedure with many parameters need to be controlled such as pH of the solutions. Furthermore this method results in a catalyst that has a wide particle size distribution [131].

2.3.2.2. Ion-exchange methods

Ion exchange which has been also widely used, as a method for synthesizing LDHs has been successfully deployed for the intercalation of various anions for different applications such as the inorganic anions (Cl^- , NO_3^- , SO_4^{2-} , CO_3^{2-}) and organic ions e.g. dicarboxylic acid, pharmaceutical agents like para-amino salicylic acid, and cetirizine [77, 79, 129]. This method is also referred to an indirect method where firstly LDHs are prepared with host anions such as carbonate, nitrate or chloride ions. Subsequently, guest species which are the desired anions are exchanged with the host anions. The ion exchange method is mostly employed when it is preferable to exchange the inter anions with the guest species and when the di- and trivalent cations or the anions in the alkaline solutions are not stable [77].

Ion exchange method is a reversible process during which ions are exchanged between an electrolyte solution and a complex material. It is a form of sorption along with adsorption and absorption processes [79]. LDHs are widely used as ion exchangers among others such as zeolites, montmorillonite and clays, due to their anion exchange capacity by the inorganic as well as the organic anions, as it was explained in detailed within Section 2.1.3. A typical example of ion exchange process is schematized in Figure 13 where H is hydrogen, M^{2+} and M^{3+} used to indicate di and tri-valent cations, respectively.

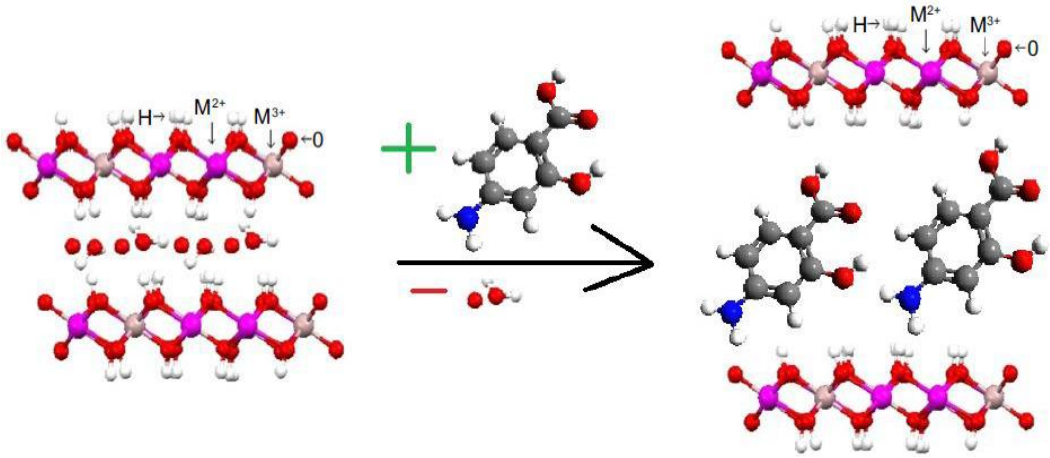

Figure 13: Ion-exchange process [77].

The anion exchange reactions in equilibrium can be described with two possible reactions given below where X is the host anions and Y is the guest species. Exchange of anions thermodynamically depend mainly on the electrostatic interactions between the anions and the positively charged host sheets of LDHs as well as the free energy involved in the changes of hydration [129]. As shown in Equation 2 the anions are univalent such as NO_3^- or Cl^- in which the interactions between anions and the layers are weak, therefore it is easy to exchange the ions, whereas the interaction in Equation 3 is strong since the anions are highly charged (CO_3^{2-} or carboxylate) but an acidic medium helps anions to be deintercalated easily [77].

$$[M^{2+}\ M^{3+}\ X^{m-}] + Y^{n-} \leftrightarrow [M^{2+}\ M^{3+}(Y^{n-})_{m/n}] + X^{m-} \quad (2)$$

$$[M^{2+}\ M^{3+}\ X^{m-}] + Y^{n-} + mH^{+} \leftrightarrow M^{2+} - M^{3+} - (Y^{n-})_{m/n}] + H_mX \quad (3)$$

On the other hand the expansion of the space between the layers, which is possible using a proper medium, may favour the ion exchange process due to weakening the interactions. An organic medium for example can enhance the exchange by organic anions, whereas an aqueous solution can favour the exchange by inorganic anions. Exchange of interlamaller anions by organic ions such as dicarboxylic acid anions was first reported by Kumura and Miyata who initiated the development of industrial production methods for synthetic hydrotalcite-like materials in the 1970's [128].

Furthermore many other parameters can either enhance or slow down the rate of ion exchange reactions including, pH of the electrolyte solutions, type of the exchange medium, and chemical composition of the layers, washing and drying processes. For instance higher pH values can enhance intercalation of carbonate while a CO_2-free atmosphere is constantly supplied for the process, however in any case pH should not be kept below 4.0 which causes for basic LDH layers themselves begin to dissolve [129].

2.3.2.3. Hydrothermal methods

Hydrothermal methods as material preparation techniques are generally preferred when co-precipitation or ion exchange methods are not applicable for guest anions which have a low affinity to be intercalated while producing new LDHs [77, 79, 129]. Employing this method can lead many features such as a controllable particle size distribution of produced LDHs. The hydrothermal temperature has been proposed as an affecting parameter for crystal structure while pressure and the contact time have also effect on the properties of LDHs [129].

The experimental procedure for hydrothermal methods as follows: Metal solutions are mixed with the anion solution and the pH of the solution is maintained at usually between 9 and 10 for Mg/Al LDHs. Next, the prepared solution with the specific pH is placed in a stainless steel autoclave, and warmed up to a temperature level or rotated simultaneously [79, 129].

By hydrothermal methods very fine Ni/Al LDHs were produced in the form of one-dimensional nanorods at 180°C and pH of 10.0 for 12 h–18 h in a 50mL stainless Teflon-lined autoclave while the effect of pH and the reaction time were evaluated [132]. It is reported that as the time proceeded to 18 h the nanorods became longer and wider with a diameter of 30–70 nm and a length of 1–3 μm. Another study was conducted for a wide range of temperature and pressure values, using continuous-flow hydrothermal method to produce nanoplate shaped LDHs with very fine and controllable particle size and shape [131]. The new preparation method was proposed to complete the production of LDHs within a few minutes being very rapid compare to coprecipitation methods lasting for 10-20 hours. With a feed rate of solutions 20ml/min, it was found out that temperature has much more influence on the products than pressure.

2.3.2.4. Sol-Gel methods

Sol-gel method has been employed for various studies due to its cost effectiveness and high product purity which are mostly required for sustainable production of new materials to be suitable for large-scale applications [130, 78]. A sol is a dispersion of the solid particles which is also known as colloidal suspension with particles size of 1-1000 nm in a liquid where gravitational forces are negligible, yet only Brownian motions suspend the particles. A gel is a state where both liquid and solid are dispersed in each other, presenting a solid network containing liquid components [133, 134]. There are two distinct reactions in the sol-gel process which are presented in the following equations: hydrolysis of the alkoxides (Eq. 4)/alcohol groups (Eq. 5) and condensation of the resulting hydroxyl groups (Eq. 6).

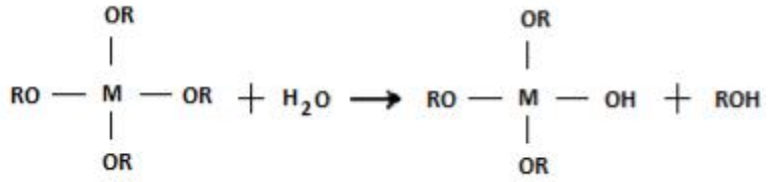

(4)

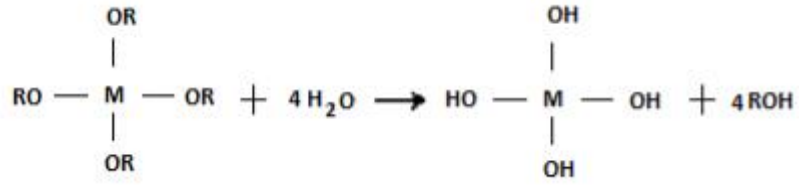

(5)

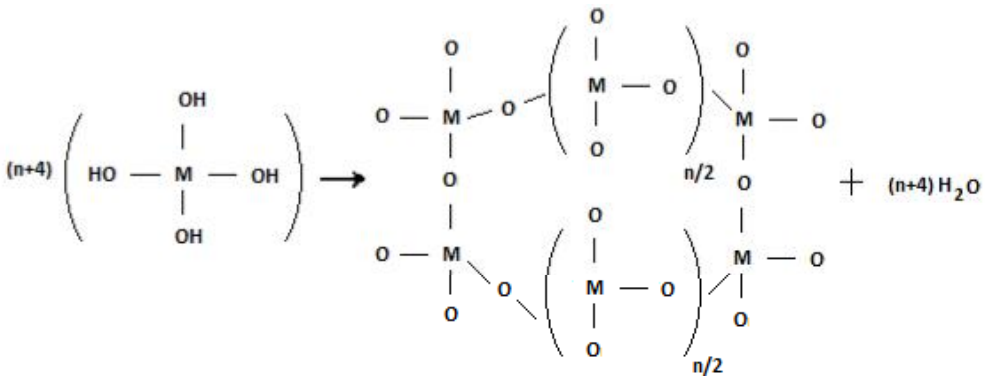

(6)

Sol-gel process consists of many steps to produce different end products for various applications as shown in Figure 14 [134]. First of all, colloidal particles or

a liquid alkoxide precursor is mixed with water to be hydrolysed as shown in Eqs. 4 and 5, partial and complete hydrolysis, respectively. The hydrated metal compound interacts with the similar species in a condensation reaction forming M-O-M bonds (Eq. 3). Further polycondensation reactions take place to create a gel formation. Different drying processes such as solvent extraction, evaporation or gelation, result in divergent material structures. Densification is the last step in which final dense materials are produced by heating the porous gel or film at high temperatures. This method has gained an increasing interest in synthesizing hydrotalcite-like materials [135-137] for different purposes such as obtaining materials with different sorption properties [130], as drug carriers with high purities [138], as thin films in catalytic membrane reactions and separation technologies.

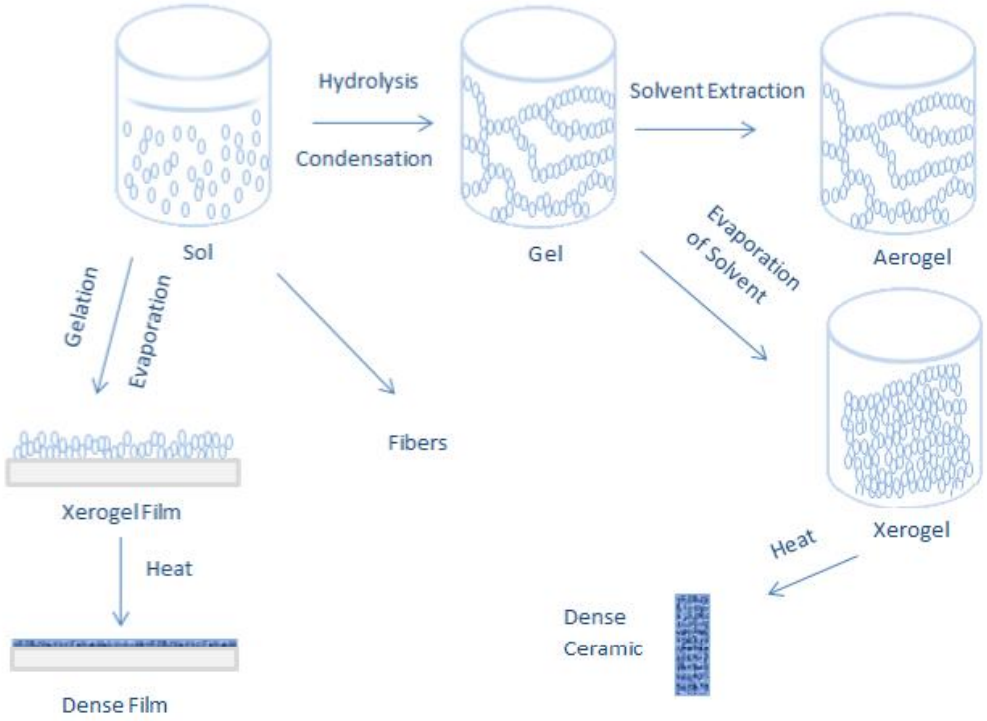

Figure 14: Sol-Gel process [133].

Mg-Al HTs were synthesized by sol-gel method to analyse the effect of parameters to final structure and texture of materials using different aluminium precursors (aluminium alkoxide and aluminium acetylacetonate) and higher Mg/Al ratios which were limited to the range of 1.5-3.0 [139]. Further studies

were conducted using variable aluminium sources in order to see the effects of these different sources to the crystallinity of materials [136]. A correlation between the aluminium precursors and the crystallinity was reported for increasing crystal sizes with the order of aluminum acetylacetonate>aluminium chloride>aluminum nitrate>aluminum sulfate.

Ni-Al HTs synthesis by sol-gel method was studied and the resulting material properties were compared with previously prepared HTs by co-precipitation method [137]. Crystal sizes and surface areas were reported to be affected as a function of the preparation method. The samples prepared by sol-gel method were found to display higher BET surface areas and lower crystals sizes comparing to co-precipitated samples. The reactivity of the samples obtained after calcination of the HT precursors at different temperatures was investigated as well. A higher reactivity of the sol-gel oxides was concluded due to a higher dispersion of the cations and low dimension of the crystallites. Another study, reported the occurring reactions and production steps during synthesis of HTs by sol-gel method while providing detailed information relating to the effect of process parameters and the conversion energy from sol to gel [140].

2.3.3. Applications of Hydrotalcites

HTs are promising materials for a large number of applications in catalysis (as catalysts or catalyst supports), medical science (as drug or bioactive molecule carrier), cosmetics (as carriers for pigments), anion exchangers (mainly the removal of toxic anions), adsorption (CO_2 capturing), photochemistry, electrochemistry, neutralizers (antacids), polymer stabilizers (heat stabilization in PVC), optics and nanocomposite material engineering due to their various unique properties [79, 74, 130]. Main applications of HTs are given in Figure 15. HTs have been exploited aforementioned applications due to their complex layered structure, high ion exchange capacity, variable layered charge densities, wide range of chemical compositions, large reactive surface areas and the interlayer space as well as the stability and homogeneity of the materials [77, 81, 82, 138].

Furthermore HTs are known to show biodegradability which is required in pharmaceutic applications and many of these properties can be tailored easily for different end uses.

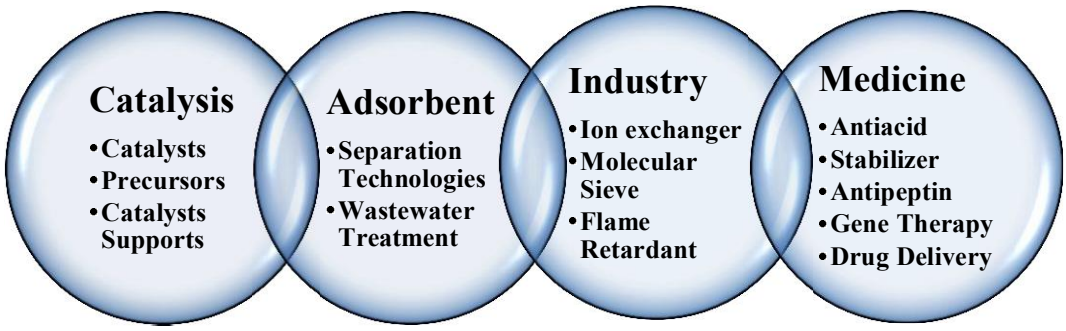

Figure 15: Main applications of HTs.

The most significant attention on HTs is to conduct research on the preparation and characterization techniques for synthetic HT-like compounds to be used in various applications. Figure 16 represents the trend of published scientific documents relating to HTs by year from late 1960s, while Figure 17 reviews the portion of the documents by subject areas [141]. Figures indicate that HTs have attracted a gradually increased interest in many different fields.

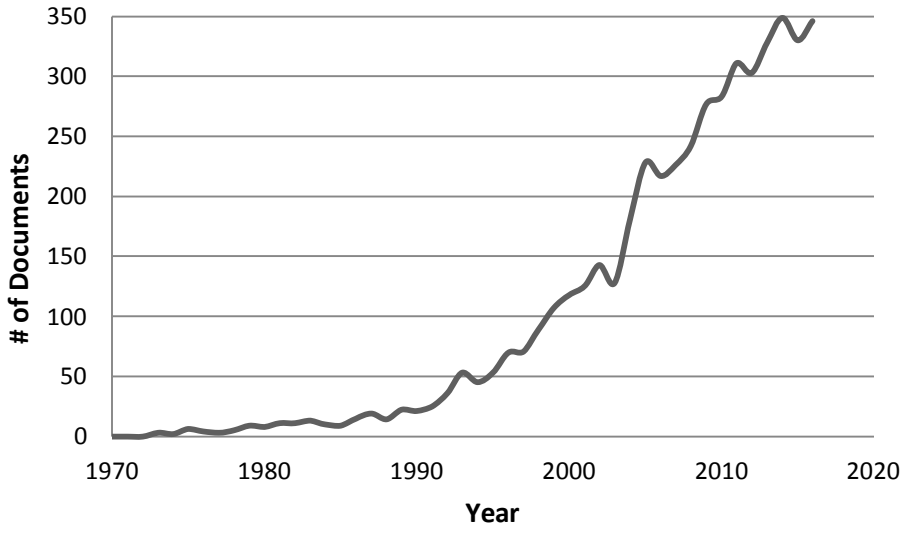

Figure 16: Documents published about 'HTs' by year [141].

The related published documents include mainly journal articles (83.4%), conference papers (11.5%) and reviews (2.1%). Chemistry and Chemical

Engineering have been the leading fields being interested in HTs, so far. Besides, many works based on HTs have been patented and the patents related to health were listed while emphasizing the importance of HTs in health applications as drug carriers for controlled release and biosensors [142].

Utilizing HTs for synthesis of new materials with low dimensions has gained tremendous interests in fundamental material science and in many applications for various fields, including electronics, mechanical and biomedical [77, 138, 142, 143]. Low dimensioning requires a process to slice or peel of the laminated layers into individual sheets which is called delamination or exfoliation [75, 143]. However, the high charge density and consequently strong electrostatic interactions between layers and interlayer anions as well as solvation molecules make slicing individual layers challenging.

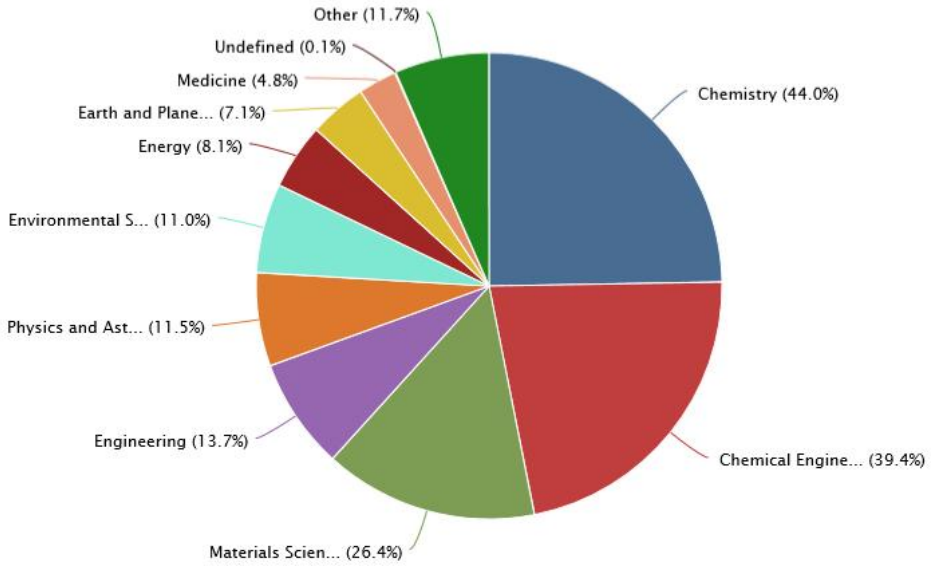

Figure 17: Documents published about 'HTs' by subject area [141].

HTs have been employed as catalysts in aldol condensation [89-91, 144], oxidation of many compounds such as ethanol, methanol, selective oxidation of glycerol, selective oxidative halogenations, and oxidation of water for oxygen production and several other applications [89, 145, 146]. Furthermore, HTs have been also utilised as catalyst supports [146-148] as well as precursors [149] due to small crystallite size and high resistance to coke formation.

2.3. Methanation of CO_2 over Hydrotalcites

Hydrotalcites have been utilized for various applications one of which is the methanation reaction, due to their unique structures and many properties. The applications of HTs were described in detail within Section 2.3. However, few research has been done regarding to CO_2 methanation over HTs, so far. Main inferences out of recent studies and their claims are crucial prior to decide the approach of this study. Therefore, they will be reviewed in this section.

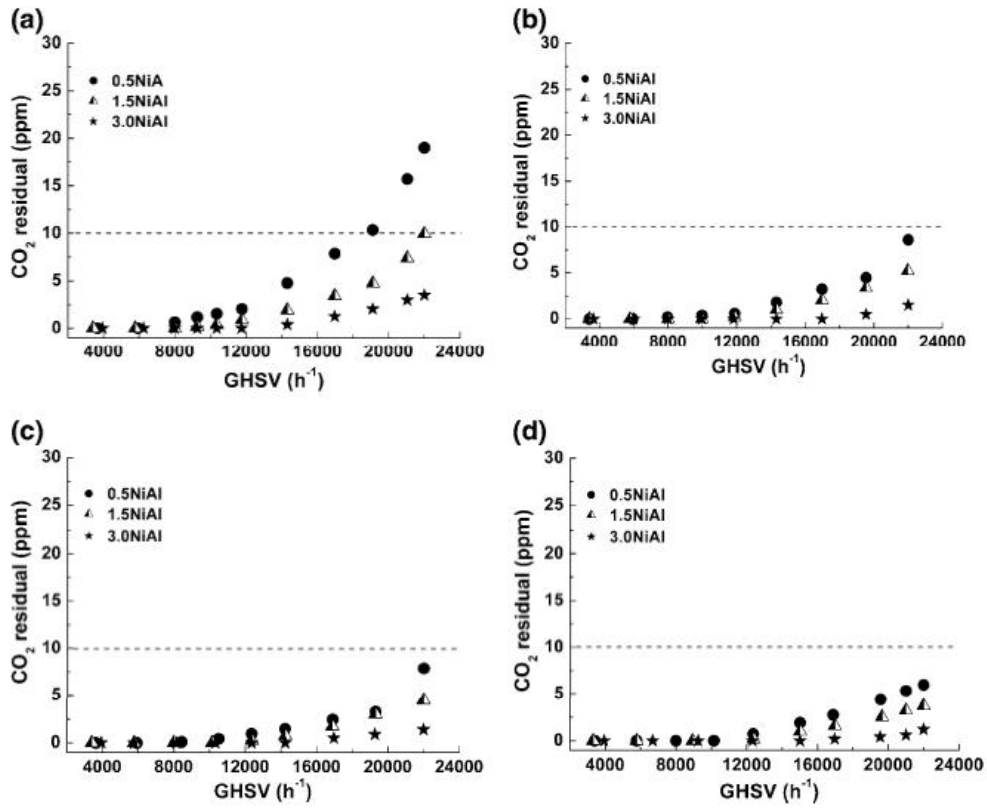

Figure 18: Activity of catalysts at 300°C subsequent to reduction processed at ambient pressure and different temperatures: a)400 °C, b)450 °C, c)530 °C and d)600 °C [35].

Methanation of CO_2 at low temperatures was studied by utilizing co-precipitated Ni–Al HTs based catalyst for CO_2 methanation [35]. A variety of cation ratios (Ni^{2+}/Al^{3+}: 3.0, 1.5, 0.5), reduction and reaction temperatures were chosen to evaluate the effect of Ni content on the structure as well as the activity of catalysts. Many analyses for characterization and catalyst testing experiments were reported in detail. For instance, amount of residual CO_2 was determined in

order to test the catalytic activity of the catalysts prepared with different cation ratios as well as reduced at different temperatures, and the results with respect to GHSV were reported as shown in Figure 18 which indicates a low residual concentration of CO_2 and thus high conversion of CO_2. Reduction temperature claimed to have no effect on the catalyst with highest Ni/Al ratio 3.0; however, as the cation ratio decreased the conversion value diminished accordingly indicating a decrease in catalytic activity. The greatest activity of catalyst was obtained at highest reduction temperature 600 ^{o}C, resulting an order of activity 3.0NiAl>1.5NiAl>0.5NiAl. Higher reduction temperatures were shown as causes to a change in the crystallinity and an increase in the nickel specific surface area. Besides reduced Ni–Al LDHs based catalyst was found to have good methanation activity at low reaction temperatures between 220-400 ^{o}C.

A similar study was recently published utilizing a catalyst derived from Ni–Mg–Al HTs precursors by constant-pH co-precipitation method [34]. Catalyst testing was performed at temperatures starting from 220 ^{o}C, and proposed enhanced conversion values. However comparing to the results that Gabrovska et al. reported, no significant change in activity was noticed [35]. Nevertheless, it was reported with the help of SEM images exhibiting the platelet-like crystals (Fig.19a) that this morphology remained intact after calcination at 600^{o}C [34].

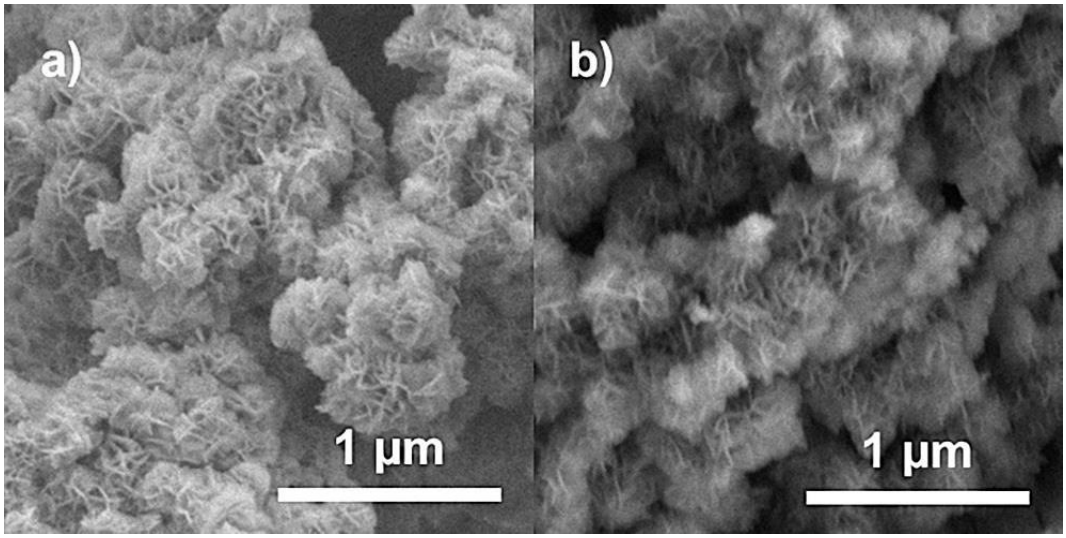

Figure 19: SEM images of a) the HT-like precursor with 50 mol% Ni and b) the sample calcined at 6008C in air [34].

Another catalyst sample, Ni-Al_2O_3-HT was synthesized using Ni-Al hydrotalcite as a precursor and employed for methanation of CO_2 [36]. Another catalyst sample Ni supported on γ-Al_2O_3 was further prepared by wet impregnation method in order to compare the properties, activity and stability of the catalysts. CO_2 conversions were recorded higher for HT based catalyst than for the catalyst Ni supported by alumina at low reaction temperatures. It was proposed that, the existence of strong basic sites could activate CO_2 and well-dispersed as well as highly-stable nickel nanoparticles with a narrow size distribution enhanced the methanation activity. In another study, lanthanum was employed to synthesize a La promoted Ni-Mg-Al HT derived catalyst by co-precipitation method for methanation reaction. The idea of utilizing La was explained as La can modify the redox properties of a catalytic material [39]. Prepared catalyst samples with various compositions were tested in terms of their catalytic activities towards methanation of CO_2. Figure 20 shows the conversion values reported by Wierzbicki et al. with respect to reaction temperature for different catalyst samples, having the thermodynamic equilibrium behaviour in bold continuous line. The conversion values calculated for lower temperatures were distant from equilibrium predictions, nevertheless addition of La reported to enhance the basicity and the activity of catalysts.

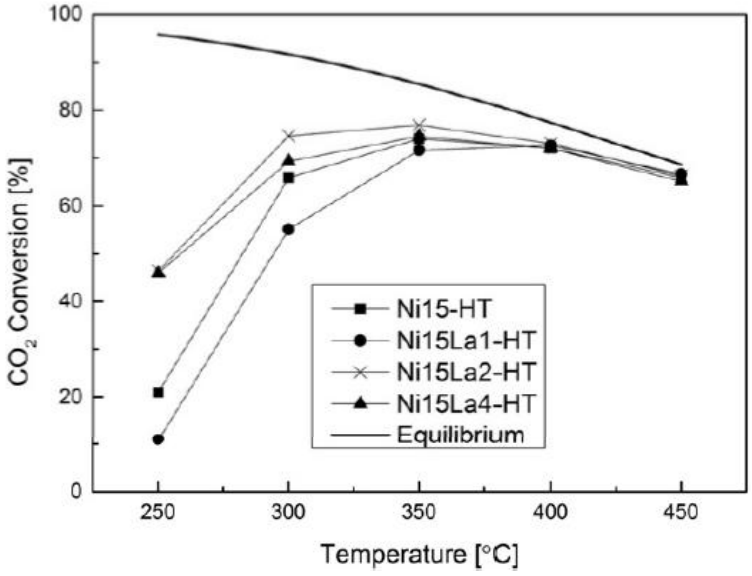

Figure 20: CO_2 Conversion versus reaction temperature for prepared catalyst samples (numbers indicating the weight percentage of compounds (wt. %)) [39].

With the aim of further modifying the basicity of catalysts used in methanation reaction, Ce and/or Zr promotors employed while synthesizing Ni-Mg-Al-HT derived catalysts. These catalysts were tested at low reaction temperatures in the presence of hybrid plasma [38]. Methanation reactions were carried at temperature range between 110-430 ^{o}C, in a dielectric barrier discharge (DBD) plasma reactor operating at atmospheric pressure with on and off plasma mode. They claimed to get higher conversion values up to 80% in the presence of DBD plasma even at very low temperatures, such as 110 ^{o}C while having almost complete CH_4 selectivity (Fig. 21). However, addition of Ce and Zr reported to show no influence on the catalytic activity.

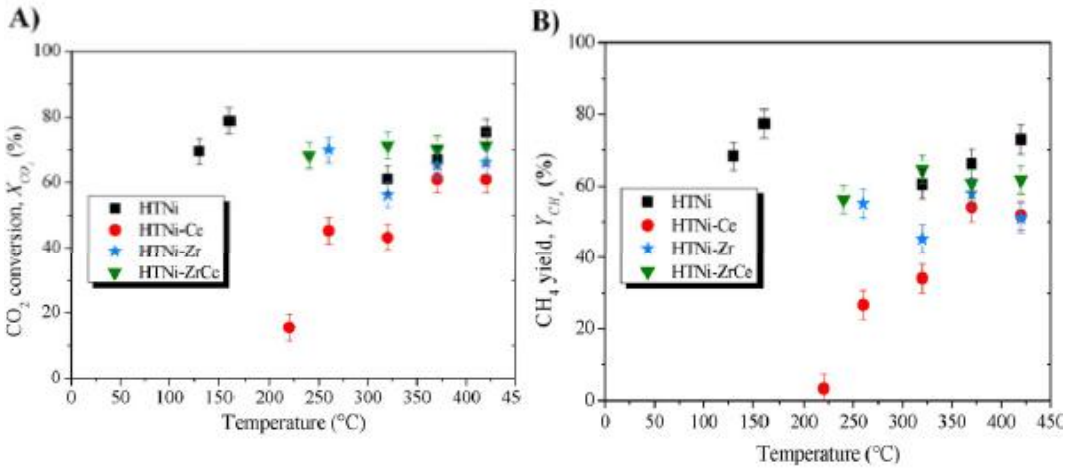

Figure 21: CO_2 methanation in the presence of DBD plasma A) CO_2 conversion, B) CH_4 yield [38].

As the pH values during co-precipitation influences the resulting catalyst properties, two different pH values 8.7 and 12 were adjusted while synthesizing Ni-Al-HT derived catalysts with high Ni content [33]. Besides a commercial Ni catalyst supported on γ-Al_2O_3 was compared with the new prepared catalysts. The XRD patterns of the HT-derived catalysts were determined for dry and calcined catalysts to clarify the effect of calcination on bulk features as given in Figure 22.

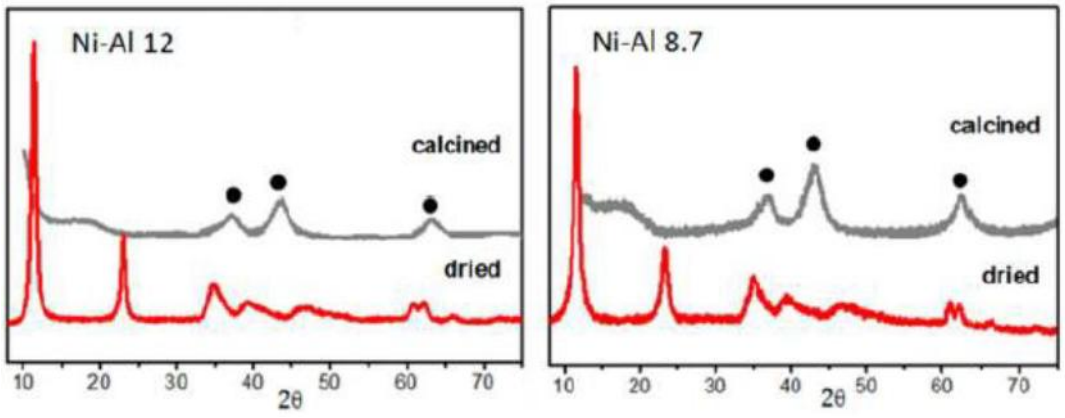

Figure 22: XRD patterns of the HT-derived catalysts [33].

Significant differences in their XRD profiles were obtained between dried and calcined catalysts, while dried HT-derived catalysts showed the typical profiles for HTs: narrow symmetric and intense reflections of the basal (003), (006) and (009) were observed from left to right at low 2θ angles, whereas for higher 2θ angles broader, small reflections of non-basal (012), (015) and (018) planes were seen.

CHAPTER 3 EXPERIMENTAL PART

3.1. Materials

Table 1: List of materials used in catalyst preparation.

Materials name	Details
Aluminum oxide	**γ-Al_2O_3 (**SBET = 200 $m^2 \cdot g^{-1}$, porosity = 0.979 cm^3/g=
Nickel nitrate hexahydrate	**$Ni(NO_3)_2 6H_2O$** (>97.0%,Sigma Aldrich)
Magnesium nitrate hexahydrate	**$Mg(NO_3)_2 6H_2O$** (>99.0%, Merck)
Aluminum nitrate nonahydrate	**$Al(NO_3)_3 9H_2O$** (>98.5%, Riedel-de Haen)
Sodium carbonate	**Na_2CO_3** (>99.5%, Merck)
Magnesium ethoxide	**$C_4H_{10}MgO_2$** (98.0%, Sigma Aldrich)
Nickel (II) acetylacetonate	**$C_{10}H_{14}NiO_4$** (95.0%, Sigma Aldrich)
Aluminum (III) acetylacetonate	**$C_{15}H_{21}AlO_6$** (99.0%, Sigma Aldrich)

A list of materials used for the preparation of catalysts is given in Table 1, which includes some details about the materials. All of these materials were used without further purification.

3.2. Catalyst Preparation

Catalysts used throughout this thesis were synthesized by different preparation methods including wet impregnation, co-precipitation and sol-gel. Subsequently, slurries were prepared using synthesized catalysts, and they were wash-coated to the inner surface of the reactor tubes. This chapter will describe and illustrate these procedures including the specifications of the materials.

3.1.1. Ni/Al_2O_3 by the incipient wetness impregnation method

Ni/Al_2O_3 catalyst was prepared by the incipient wetness impregnation of γ-Al_2O_3 support using $Ni(NO_3)_2 6H_2O$ solution as a precursor. Two batches were produced and the targeted Ni loadings were 17.75 wt% and 25 wt%. About 30 g of support material was weighed and dried at 150 ^oC for two hours while generating below

15 mbar vacuum inside the flask. Nickel nitrate solution was prepared with the calculated amount of precursor and ion-exchanged water which was calculated taking into account the pore volume of the support materials. Precursor solution was poured onto the dried support material and ensured that all of the support material was in contact with the precursor before leaving it overnight. Afterward, the precursor with the support was dried under vacuum in a water bath at 80 ^{o}C while rotating the flask, till the material was dried. The resulting material subsequently was taken out from the flask and poured in a quartz tube which was closed from each side with the help of quartz wool, for calcination. The catalyst was calcined under air flow at 550 ^{o}C for two hours, with a heating rate of 5^{o}C/min. The synthesized catalysts were named as 17.75 wt% Ni/Al_2O_3 and 25 wt% Ni/Al_2O_3, respectively.

3.1.2. Ni/Mg/Al HTs by the co-precipitation method

Ni/Mg/Al hydrotalcite catalyst was prepared by the co-precipitation method as described by Mette et al. using a setup shown in Figure 23 [150]. Two batches of HT-based Ni catalysts were synthesized following one-pot synthesis approach. The Ni^{2+} loadings were 0.5 and 0.17 mol% where the total amount of cations was 1 mol. The materials included metal nitrates: $Ni(NO_3)_26H_2O$, $Mg(NO_3)_26H_2O$ and $Al(NO_3)_39H_2O$ as cation sources, Na_2CO_3 as carbonate source and NaOH was used for adjusting the pH. 0.4 M aqueous metal nitrate solution (0.5Ni^{2+}/0.17 Mg^{2+}/0.33Al^{3+}) and a precipitating agent solution with 0.6M NaOH/0.09M Na_2CO_3 were prepared.

As shown in Figure 23, 200ml of distilled water was poured into a three-neck flask which was placed in a water bath and heated to 50 ^{o}C. Both of the solutions were introduced dropwise simultaneously and controlled manually to keep the pH constant at 8.5 while mixing the solution vigorously. Afterward, the resulting solution was filtered off and washed with distilled water until the pH of the remaining water was 7. Finally, the filtered catalyst was ground finely and calcined in air at 550^{o}C for four hours.

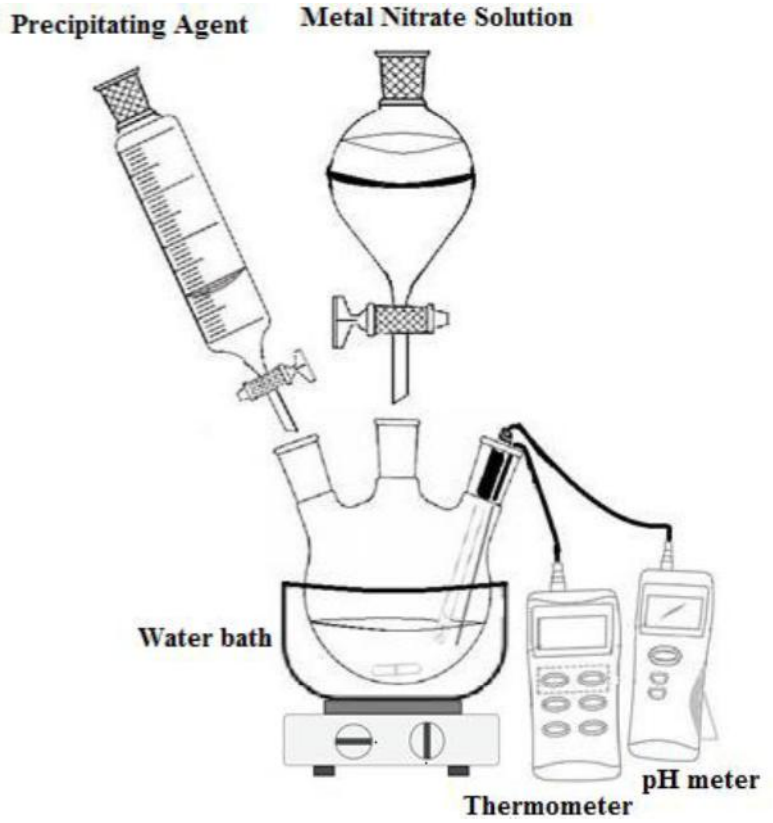

Figure 23: Setup for catalysts preparation by co-precipitation.

3.1.3. Ni/Mg/Al HTs by the sol-gel method

Ni/Mg/Al hydrotalcite catalysts were prepared by the sol-gel method as follows: Two batches of HT catalysts were synthesized and the Ni^{2+} loadings were 0.5 and 0.17 mol% where the total amount of cations was 1 mol. However, the targeted nickel loadings as weight percentages were calculated to be 15 and ~5 w%, respectively. Figure 24 illustrates the setup used for preparation HT-based Ni catalysts by the sol-gel method.

Magnesium ethoxide was dissolved in 200 ml of ethanol and pH of the solution was adjusted to 3 by addition of minute amount of 35% HCl. Further, the solution was refluxed for about 3 hours with the help of a condenser circulating cooling water (Fig.24). Nickel (II) acetylacetonate, and Aluminum (III) acetylacetonate were dissolved in 200 ml of acetone and mixed with the first solution. Subsequently, pH of the solution was raised to 10 with 33% ammonia solution and left under mixing under reflux till a gel was formed. The gel was filtered off, dried at room temperature and crushed into small particles prior to be dried in

oven at 110^{o}C for 2 hours. A solution was prepared with 250 ml of distilled water and calculated amount of Na_2CO_3 for ion-exchange of dried HTs and heated to 100^{o}C. The dried catalyst was added and mixed vigorously for 2 hours. Finally the excess amount of water was evaporated; the catalyst was dried under vacuum in a water bath at 80 ^{o}C and calcined in air at 550^{o}C for four hours.

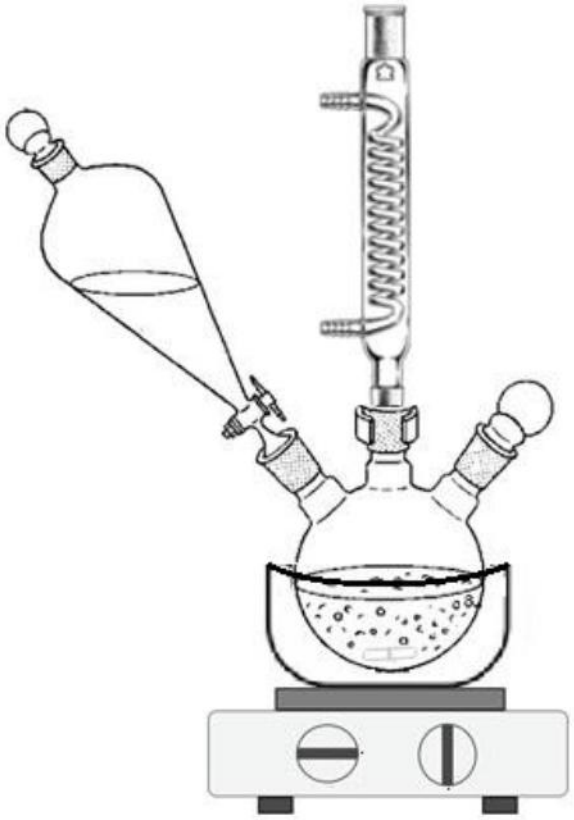

Figure 24: Setup for catalysts preparation by sol-gel.

The catalysts prepared by the co-precipitation and sol-gel method were named for instance 15 w% Ni/Mg/Al_co-prec_packed indicated the targeted weight percentage of Ni, preparation method (e.g. co-prec. or sol-gel) and the way of catalyst utilization such as packed-bed or wash-coated.

3.1.4. Ni-loaded Ce- or Zr-doped HTs by wet impregnation

Commercially available Ce- and Zr-doped HTs were used as catalyst support to produce two catalyst batches having 5 and 15 w% Ni loadings, respectively. Since no information such as pore volumes was available related to these materials, the wet impregnation method was applied for the nickel deposition.

An excess amount of distilled water was used for ion-exchange. The rest of the preparation procedure was similar with that for Ni/Al_2O_3; however, final catalysts were calcined in air at 550^oC for four hours.

3.3. Slurry Preparation

The slurries of all catalysts were prepared following the procedure that was developed at VTT. A mixture was prepared including the catalyst, aluminasol, nitric acid and ion-exchanged water . The slurries were first mixed with the help of a spoon and they were left overnight under mixing.

3.4. Wash Coating the Reactor Tubes

The reactor tubes (Inconel tubes with an inner diameter of 4mm) were cut into pieces of 17.5 cm long, and the inlet as well as the outlet of the tubes were drilled in order to create smooth surfaces. Every one of the tubes was named with the help of a marker showing a letter and a number e.g. A-01. Subsequently, they were heat-treated to create a rough surface on the inner side of the tubes which allowed a well-coated catalyst surface. After the treatment, the masses of the tubes were noted. The reactor tubes were wash coated as shown in Figure 25 utilizing the slurry of a catalyst.

A syringe was used to suck the slurry through the length of the tube. The slurry was kept inside the tube for a few seconds and blew back to the beaker. The sucking, keeping the slurry inside and blowing it back was repeated three times in order to have enough amounts of catalysts. Then, the tube was dried. The catalyst amount for the first coating was noted and if the catalyst loading was not enough another cycle including coating and drying was repeated. After each cycle, the weight of the tubes was noted. Finally the coated tubes were calcined, and weighed again after leaving them to cool down to room temperature.

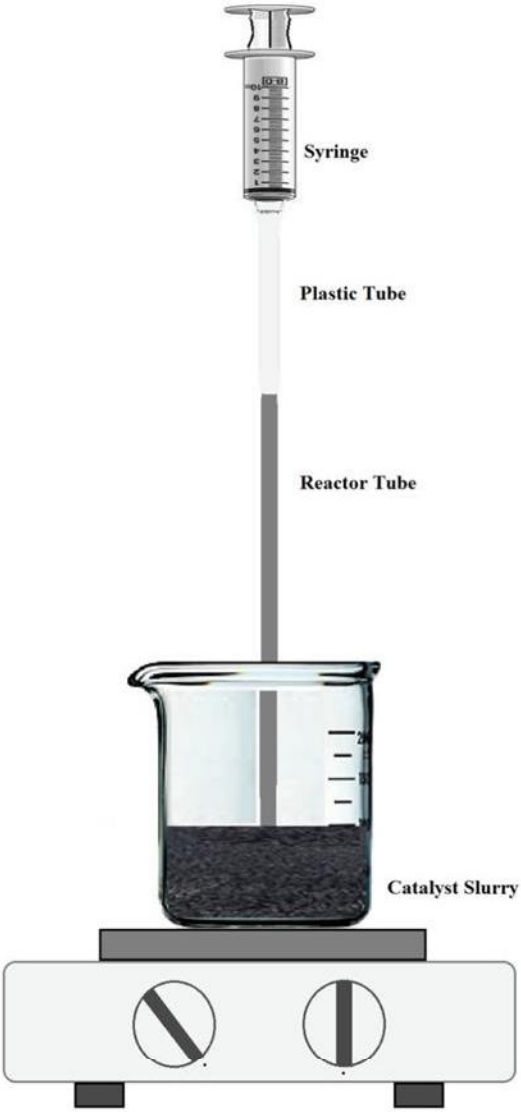

Figure 25: Setup for wash coating the reactor tubes.

3.5. Description of Catalysts Testing Setup and Activity Tests

The catalyst testing setup used throughout this thesis and the procedure followed for performance test runs will be explained in detail within the following sections. Furthermore equations for calculation of conversion, selectivity and yield will be given.

3.5.1. Description of Catalysts Testing Setup

A scheme of the reactor system is shown in Figure 26 including inlet lines of the reactant gases, a by-pass line to preheat the reactants, two places for reactor tubes, cooling trap for the water vapour to be cooled, a gas flow meter and an

online gas analyser. Three mass flow meters were employed and calibrated for reactant gases which were H_2, CO_2, and N_2, while the flow rate of the gases was adjusted by a readout system. A pressure indicator (max: 2.5 barg) was used to measure the pressure inside the lines and reactors. Pressure test was performed using N_2 just after packing new reactors to test the tightness of the system and to find the points of leakage with the help of a liquid leak detector solution. Pressure tests were considered to succeed if the pressure was constant in a range of ±0.003 bar for 30 seconds, otherwise the joints were tightened and pressure test was repeated.

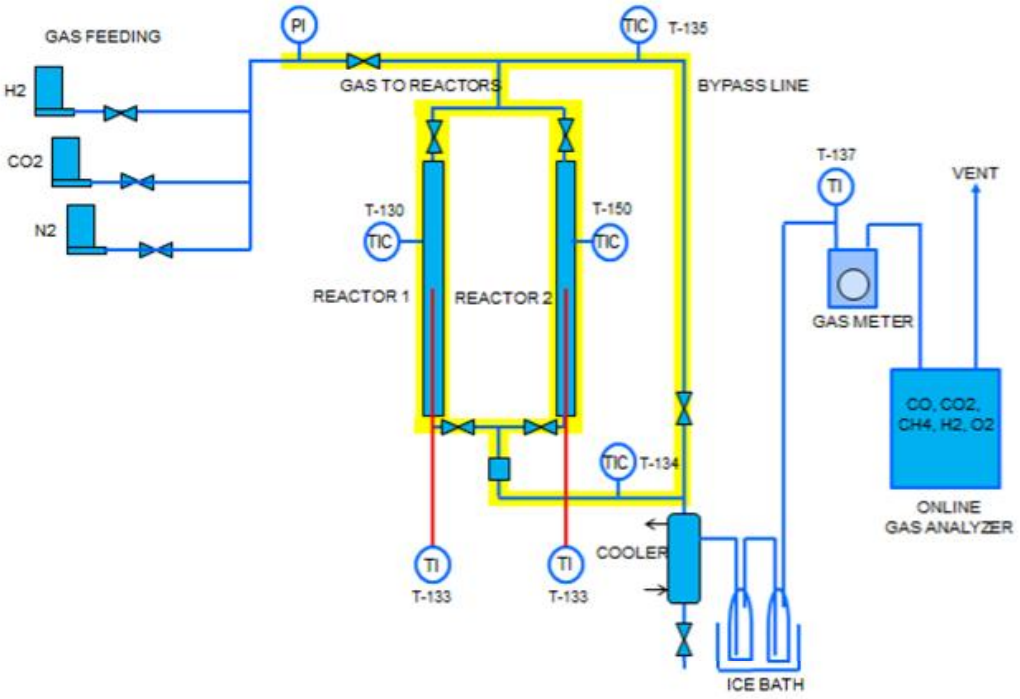

Figure 26: Experimental Setup for performance tests.

Two temperature resistances were fixed onto the by-pass line and the cooling line and two more were placed and tightened with a wire onto the reactor tubes. These resistances were controlled via an ABB temperature controller unit. K-type thermocouples were placed inside the reactor tubes and to the line just before a gas flow meter, as well.

Reaction mixtures with various compositions of H_2, CO_2, and N_2 were properly mixed using calibrated mass flow meters whose performances were cross-checked with the gas flow meter at the beginning and in the end of each test run.

The outlet gas mixtures were cooled down through the cooling system and only dry gas compositions were measured by the online gas analyser. The online analyser consisted of three detectors; Uras14 measuring CO, CO_2 and CH_4 by an infrared photometer, Caldos17 measuring H_2 in N_2 using a thermal conductivity detector and a Magnos106 oxygen analyser. The gas analyser was calibrated to 0 vol% for all of the gases feeding pure nitrogen in. A gas standard from AGA Gas, a mixture of CO_2 (10%), H_2 (30%), CH_4 (45%), CO (5%) and N_2 (10%), was used for calibration to certain values. The data from the online gas analyser and the temperature control unit was acquired via an external storage device.

Figure 27: Picture of a) reactors with and without fittings and b) test setup.

Packing of reactor tubes required proper fittings; hence the coated reactor tubes had been assembled with the fittings prior to be placed to the testing setup as shown in Figure 27a. All of the fittings were tightened up, and aforementioned pressure test was performed in advance of packing the temperature resistances and insulating the reactor tubes. Finally, the reactor tubes were packed first by a thick insulator and multilayer of packing materials which were made of quartz wool (Fig.27b).

3.5.2. Reduction of the Catalysts

The reactor tubes coated with catalysts were reduced prior to test runs. For the reduction of catalysts a gas mixture of 10vol% H_2/ 90vol%N_2 with a feed flow rate of 0.3 L/min was used. Reduction was performed at 450^{o}C for Ni/Al_2O_3 catalysts for two hours and at a temperature chosen from the range of 500-650^{o}C for the HT-based Ni catalysts for two hours. The difference in temperature was due to the strength of Ni-Al-O bonds in catalysts, as claimed in many studies [33-39]. Different reduction temperatures were employed to determine the effect of reduction temperature on the performance of catalysts for HT-based Ni catalysts. Related results will be reported and discussed in Chapter 4.

3.5.3. Activity Tests

The performance of the catalysts was evaluated for gas-phase hydrogenation of carbon dioxide to methane in a continuous plug flow reactor operating at atmospheric pressure. The catalytic activity measurements were performed by means of gaseous mixtures of $CO_2/H_2/N_2$ with different volumetric ratios in a temperature range 250-500^{o}C and GHSV from 8185 to 20463 h^{-1}. Prior to the activity tests the catalysts were reduced following the procedure described in the previous section.

The activity tests are also called as test runs. Every test run started with setting the temperature, feeding the appropriate composition of reactant gases into the bypass line, measuring the gas flow rates with the mass flow meter and noting the initial gas compositions as well as the temperature inside the reactor tubes. Subsequently, the feed gas mixture was directed to the inlet of the reactor tube. The instant composition of the gases and temperature values were recorded for 5 minutes interval. The test runs were terminated subsequent to observing the equilibrium compositions for at least 20 minutes. The final mass flow rate was measured and gases were flushed with the help of pure nitrogen flow. The duration of a single test run could take up to two hours in total. Any change in composition, feeding flow rates or the reaction temperature corresponded to a

new test run. The performance of the catalysts was evaluated in terms of CO_2 conversion, CH_4 yield or CH_4/CO selectivity. These values were calculated by the equations given as Equation 7, 8 and 9, respectively. While calculating and evaluating the results, it was assumed that the experimental setup was a closed system having no leakage. The reactor was assumed as a plug flow reactor and the catalyst coating was assumed to be uniform along the reactor tube. A sample sheet showing the recordings of an activity test run, a list of all test runs and a list of reactor tubes are given in the Appendix 1, 2 and 3, respectively.

$$X_{CO_2}(\%) = \frac{F_{CO_2\,in} - F_{CO_2\,out}}{F_{CO_2\,in}} * 100 \quad (7)$$

$$Y_{CH_4}(\%) = \frac{F_{CH_4\,out}}{F_{CO_2\,in}} * 100 \quad (8)$$

$$S_{CH_4/CO}(\%) = \frac{F_{CH_4/CO\,out}}{\sum F_{out}} * 100 \quad (9)$$

3.6. Catalysts Characterizations

X-ray diffraction (XRD) analysis of the samples in the 2θ range of 5–80° was performed by using a PANalytical X'Pert PRO MPD α-1 powder diffractometer operating with CuKα-1 radiation (1.54056Å). The average crystallite size was calculated by X-ray diffraction line broadening using the Scherrer formula which is given in equation 10. The Scherrer constant was taken as 0.89 [33].

$$L = \frac{k*\lambda}{\beta*cos\,\theta} \quad (10)$$

The total surface area of the catalysts was determined for dried and calcined samples calculated from BET equation following the adsorption isotherms. Micromeritics TriStar 3000 equipment was used to obtain the adsorption isotherms under a nitrogen gas at the liquid nitrogen temperature. Before the measurements, the samples were dried at 100°C in He-flow.

CHAPTER 4 RESULTS AND DISCUSSIONS

In order to determine the performance of HT-based Ni catalysts in the CO_2 methanation reaction, this chapter presents and discusses the results of the catalyst characterizations and activity test runs. Firstly, the characterization results will be given. Furthermore, the results will be reported confirming the effect of feed composition, GHSV, catalysts amount and the reduction temperature on the conversion of CO_2 into methane. Stability of the catalysts will be evaluated based on the long term test runs.

4.1. Characterization results of the HT-based Ni catalysts

The specific surface area of the materials was calculated from their respective N_2 adsorption isotherms, and XRD patterns were recorded as described in Section 3.6. Table 2 lists the results for the dried and calcined samples of the HT-based Ni catalysts prepared by the co-precipitation and sol-gel methods. A clear difference was observed between the specific surface of the dried and calcined catalysts. This enhancement in the specific surface area after the calcination process agrees well with those proposed by Mette et al. and explained by the loss of materials during calcination and shrinkage of the platelets [37].

Table 2: The specific surface area and particle size of the catalysts.

Catalyst Name	Specific surface area (m2/g) BET	Particle size (nm)[a]
5 w% Ni/Mg/Al HT_co-prec_dried	63	1.1
5 w% Ni/Mg/Al HT_co-prec_calcined	145	13.7
15 w% Ni/Mg/Al HT_co-prec_dried	1	29.2
15 w% Ni/Mg/Al HT_co-prec_calcined	119	0.9
5 w% Ni/Mg/Al HT_sol-gel_ dried	61	-
5 w% Ni/Mg/Al HT_sol-gel_calcined	65	3
15 w% Ni/Mg/Al HT_sol-gel_ dried	32	-
15 w% Ni/Mg/Al HT_sol-gel_calcined	49	4

a: calculated from the Scherrer formula

Figure 28 shows the XRD patterns of the catalysts listed in Table 2. The dried catalysts matched with a magnesium-aluminium-carbonate-hydroxide-hydrate structure, while calcined catalysts matched with the nickel oxide structure. Lower Ni content exhibited more crystalline structure in the dried catalysts, as the peaks were sharper and stronger. In contrast, higher Ni content enhanced the crystallinity for calcined catalysts. The XRD patterns match with those reported previously for HT-based catalysts [34, 35, 37, 137].The particle size of these catalysts were calculated using Equation 10, and they reported in Table 2. The particle size of the catalysts varied in all samples, showing maximum 29 nm size. However, these results corresponded to only one portion of the samples detected during XRD measurements. A particle size distribution would allow for more discussions that could have been obtained by TEM analysis.

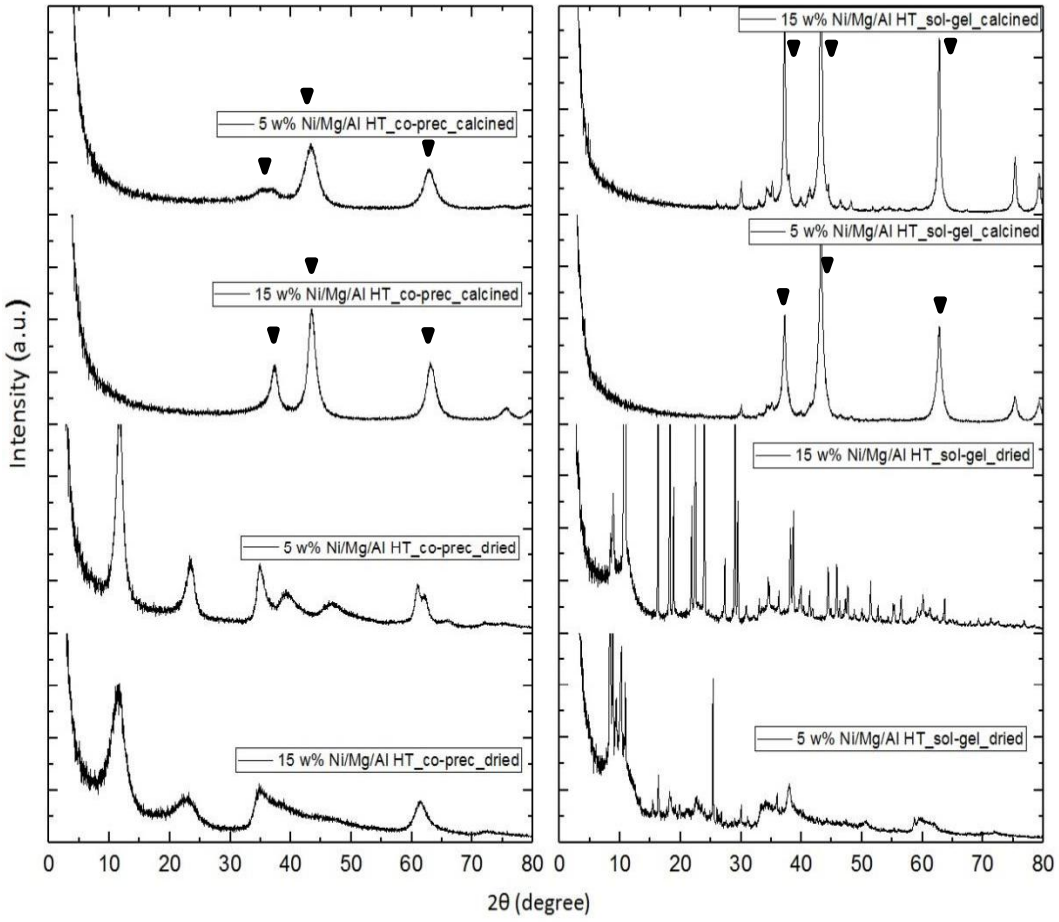

Figure 28: Powder diffraction patterns of the catalysts prepared by the a)Co-precipitation and b)Sol-gel method. (▼ : NiO)

4.2. Temperature profile inside the empty reactor tube

As presented in Section 3.5., thermocouples were placed inside the reactor tubes to verify that the temperature was maintained as close as possible to the set point temperature. In order to establish the location for the thermocouples, a temperature profile was plotted by measuring the temperature along the length of the reactor tube starting from the inlet of the tube. For this purpose, an empty tube, without catalyst coating, was chosen while having only nitrogen flow being preheated to 200^{o}C. The temperature inside the tube was set to 300, 400 and 500^{o}C. Measurements were started from the top (the inlet) of the reactor, and changed for every 1 cm. The results are plotted in Figure 29. The figure clearly shows that along the 17.5 cm-length of the tube, the temperatures measured after 7 cm from the inlet of the reactor tube were close to the set point temperatures in each case. As shown in the figure, the set point temperature was achieved along only 3-4 cm of the reactor tube.

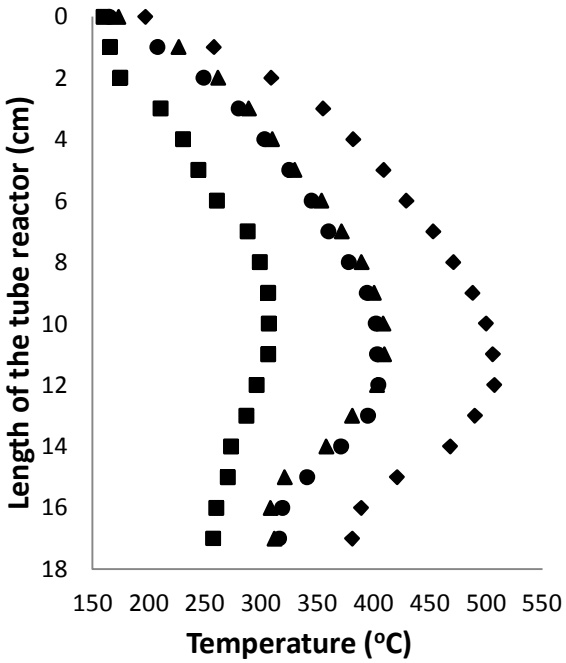

Figure 29: Temperature Profile inside the empty reactor tube (■:300^{o}C, ▲:400^{o}C, ● :400^{o}C [preheated to 250^{o}C], ◆ :500^{o}C).

Furthermore, changing the preheating temperature of the feeding gas from 200^{o}C to 250^{o}C had no influence on the temperature distribution inside the tube.

However, in order to avoid an unwanted reaction of the feeding gas mixture before the inlet of the reactor tube, a further increase in the preheating temperature was avoided. For this reason, during performance test runs, 250^{o}C was chosen as the preheating temperature. Knowledge of this temperature gradient along the reactor tubes was thereafter used to determine the location of the thermocouple in the reactor tubes and will be used while discussing the activity results for the rest of the thesis.

4.3. The effect of feed composition

To study the effect of feed gas compositions, several test runs were performed at 300^{o}C with a feed flow rate of 0.5 L/min by varying only the volume percentages of the reactant gases CO_2 and H_2, as well as the inert gas N_2. A reactor tube coated with 17.75 wt% Ni/Al_2O_3 benchmark catalyst was used during these test runs. CO_2 conversion and CH_4 selectivity results are presented in Table 3. As can be seen from the table, the excess amount of H_2 (ratio 1/6) enhanced CO_2 conversion and the selectivity of CH_4. However, an increase in the reactant ratio (CO_2/H_2) favoured CO formation, since a lower CH_4 selectivity was observed in the case of 1/2 ratio.

Table 3: Feed compositions effect.

Temp (^{o}C)	Feed Flow Rate (L/min)	Feed Compositions (vol %)	CO_2/H_2 ratio	CO_2 Conversion (%)	CH_4 Selectivity (%)
300	0.5	**10**%CO_2:**30**%H_2:**60**%N_2	1/3	21.2	94.6
		10%CO_2:**40**%H_2:**50**%N_2	1/4	25.6	95.7
		10%CO_2:**50**%H_2:**40**%N_2	1/5	27.5	97.0
		10%CO_2:**60**%H_2:**30**%N_2	1/6	31.1	97.0
		20%CO_2:**80**%H_2:**0**%N_2	1/4	13.6	88.8
		25%CO_2:**50**%H_2:**25**%N_2	1/2	32.0	94.2

These results demonstrated that the probability of CO_2 meeting with the other reactant gas H_2 and converting into CH_4 was higher in the presence of an excess amount of hydrogen. Furthermore, the CO_2 conversion increased with a dilution

of feed gas using inert nitrogen. In contrast, higher CO formation showed that with the limited hydrogen amount, methanation reactions remained incomplete. This observation could strengthen the findings of earlier studies proposing two-step reaction mechanism for the dissociation of CO_2 into CO and O prior to further reduction to CH_4 [24, 26, 28, 51, 52]. Previous studies employed various feed gas compositions, yet 1/4 CO_2/H_2 ratio was the mostly chosen inlet compositions as the stoichiometric ratio for the reaction [34-36, 38, 39]. However, for some of the studies, minute CO_2 was fed to methanation reaction while having several times higher H_2 flow [17, 33]. This helped to enhance the conversions and the selectivity results. As the highest conversion of those tested was achieved at a 1/6 ratio, this ratio was used for the rest of the experimental studies.

4.4. The effect of GHSV

The effect of GHSV on the conversion of CO_2 into methane was studied in a reactor coated with 17.75 w% Ni/Al_2O_3, at 300°C with a feed composition of 10%CO_2:60%H_2:30%N_2 while changing the feed flow rate of reactant gases (0.3, 0.5 and 0.75 L/min). Figure 30 indicates clearly that as the gas flow rate increased the conversion decreased.

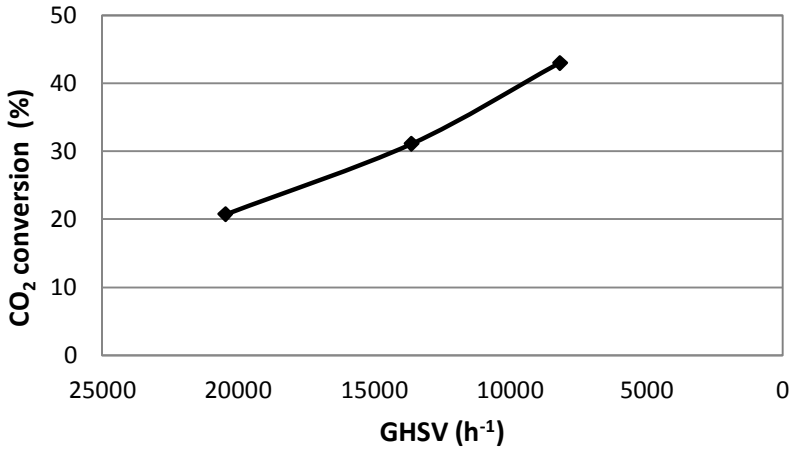

Figure 30: The effect of GHSV to the activity of catalyst (17.75 w% Ni/Al_2O_3, at 300°C with a feed composition of 10%CO_2:60%H_2:30%N_2).

The time for the reactant molecules to spend inside the catalyst coated reactor tube became shorter when the feed flow rate increased, thus having limited

chance of accessibility for the reactants to collide with each other and with the active sites. These results are consistent with previous studies investigating the effect of GHSV [33, 35]. As the temperature was chosen to operate below equilibrium conversion, the effect of GHSV was clear; however, with a further increase in the reaction temperature, the difference in conversion was observed to diminish due to the chemical equilibrium, in a manner identical to that documented in the literature [33, 35]. Thereafter, the feeding flow rate for the reactant gas mixture will be used as 0.3 L/min with a composition of 10%CO_2:60%H_2:30%N_2 if not stated otherwise.

4.5. Performance of catalysts

Performance of catalysts on CO_2 methanation was tested as it was explained in Section 3.5.3. The results for the performance of HT-based Ni catalysts will be reported and compared with the benchmark catalyst. Furthermore, additional effect of utilising Ce- and Zr-doped HTs as catalyst support will be discussed.

4.5.1. Catalysts prepared by different techniques

Throughout this thesis, the employed catalysts were synthesized by various methods, including impregnation, co-precipitation and sol-gel. In order to compare the catalytic activity of the catalysts, targeted Ni loading on catalysts was kept constant around 15 w% of nickel. Figure 31 presents the catalytic activity of these catalysts toward hydrogenation of CO_2 into CH_4 at atmospheric pressure and a temperature range of 220-500^{o}C.

According to the figure, 15 w% Ni/Al/Mg HT prepared by the co-precipitation method showed the highest activity in the CO2 methanation reaction. The CO_2 methanation reaction was already initiated below 220^{o}C (X_{CO2}=10.2 %, S_{CO2}=98.4 %) and reached 80% conversion of CO_2 at 300^{o}C with 99.9 % CH_4 selectivity. With further increment in the temperature at 350^{o}C a complete conversion (99.5 %) of CO_2 was achieved with ~100 % of CH_4 selectivity.

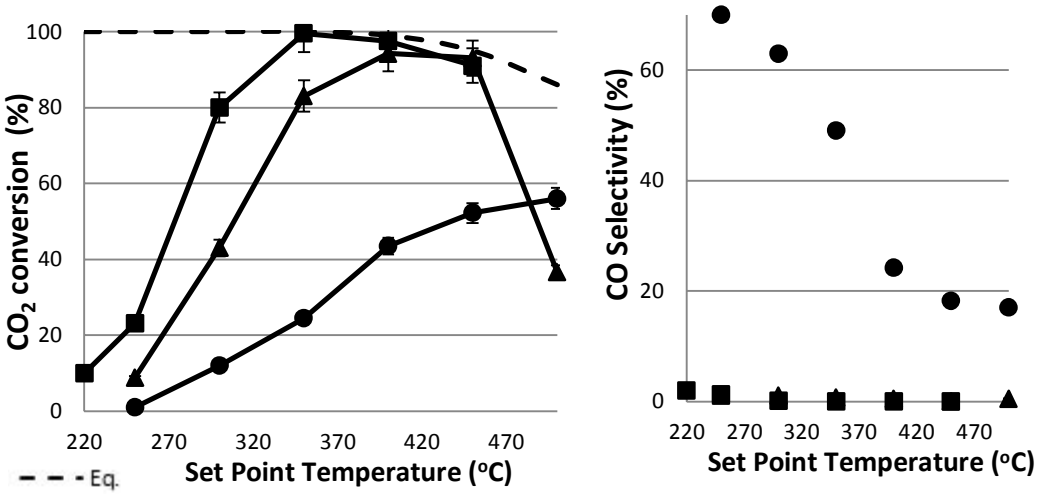

Figure 31: Performance of catalysts prepared with different methods, ■: 15 w% Ni/Mg/Al HT by co-prec., ▲: 17.75 w% Ni/Al_2O_3, ●: 15 w% Ni/Mg/Al HT by sol-gel.

Furthermore, this excellent performance overcame that of Ni/Al_2O_3 prepared as the benchmark catalyst. This higher catalytic activity of the HT-based Ni catalyst could be attributed to the existence of basic sites in HTs which could facilitate the activation of CO_2 and consequently promote the activity toward methane formation. The number of basic sites of the catalysts was reported as the reason of HT-based catalysts for being highly active in the CO_2 methanation reaction [38, 39]. These results are superior to those reported previously for Ni catalysts in CO_2 methanation reactions. He at al. achieved 82.5% conversion of CO_2 at 350°C with 99.4% CH_4 selectivity on Ni-Al_2O_3-HT [36], while Bette at al. reported highest CO_2 conversion of 74% on a similarly prepared Ni/Mg/Al HT catalyst, after reducing the catalyst at 900°C which could enhance the activity of the catalyst [34]. Abate et al. reported the maximum CO_2-to-CH_4 conversion achieved on Ni-Al HT catalyst as 65% at 300°C using a smaller GHSV.

Unfortunately, as illustrated in Figure 31, Ni/Al/Mg HT prepared by sol-gel method showed the lowest activity and selectivity towards CH_4, although higher activity was expected for the catalyst prepared by this method due to the ability of the technique resulting in materials with smaller particle size and a narrow size distribution [137]. Nevertheless, better results obtained with the same catalysts will be reported in the next sections where the catalyst utilized as packed-bed.

The effect of temperature profile on the results should be noted. Recalling the information presented in Figure 29, even though the temperature was set to 300°C, only 4 cm of the reactor tube was about the set temperature, otherwise the temperature varied between 160 and 300°C (average 255°C). For that reason a shift in the catalytic activity towards the lower temperature might expected (~50°C), if one assumes no significant temperature gradient exits in the reactor tube.

The factors that could affect the activity of the catalysts were discussed in Section 2.1.5. Furthermore, the procedures and the important process parameters for different preparation techniques were reported in Section 2.3.2. pH have reported to have a crucial impact on the rate of formation and the crystals growth. During the preparation of HTs by co-precipitation the pH was hardly maintained at a constant value, even though the possible smallest flow rate was chosen for addition of the nitrate solution. Previous studies generally employed automated systems for co-precipitation [34, 35, 38, 39]. The similar importance of pH was valid for the sol-gel synthesis, and since it formed a gel at the end, mixing with a magnetic mixer was not enough for a well-mixed gel. However, since the last step was the ion-exchange and drying of the catalysts by a rotavapor under vacuum conditions, smaller particle sizes with a higher degree of dispersion were expected for the catalysts prepared by sol-gel method. This could have been proved by characterization of the prepared catalysts via different analysis. For instance, H_2 chemisorption could have been performed to investigate active metal dispersion; N_2 physisorption was required to have the morphological information such as the average pore size, particle size distribution and pore volume of the catalysts. This information would have helped to compare the performance results in more detail with the evidences.

Another parameter that could affect the performance of the catalysts was the calcination and reduction temperature. The HT-based Ni catalysts compared in Figure 31 were calcined at 550°C for four hours and reduced at 650°C for two hours. However, no characterization analyses were performed to determine

these conditions. Moreover the reduction temperatures employed in previous research were about 800-900°C due to having very strong interactions between the nickel species and the Al-Mg HT matrix [34, 39]. Higher reduction temperatures could have enhanced the catalytic activity by increasing the number of active metal in metallic state. Thermogravimetric analysis could have been performed in order to see the mass loss through an increase in the temperature for each type of catalysts in order to determine the calcination temperature. Temperature programmed reduction analysis could have been conducted for selecting the reduction temperature with supporting results from XRD analysis. However, the maximum reachable temperature of the available equipment and experimental setup was 650°C. As these analyses determine the number of active material as metal oxides or in metallic state, they are crucial for the performance of the catalysts.

Furthermore, the effect of reduction temperature was studied for these catalysts and the results will be given in Section 4.6. Besides other significant parameters such as active metal loading, catalyst amount and employing the catalysts as packed bed and wash-coated will be discussed accordingly.

4.5.2. Catalysts with different Ni loading

To establish the effect of Ni content on the catalyst performance, the same types of catalysts mentioned in previous section were prepared by two different Ni loading. Ni/Al_2O_3 catalysts, prepared as benchmark, were synthesized by a targeted Ni loading of 17.75 and 25 w%. Subsequent to wash-coating and reduction processes, these catalysts were tested at the same temperature range 250-500°C, under atmospheric pressure. The results are shown in Figure 32. As can be seen from the figure, the highest Ni loading on alumina support indicated lower activity, while the catalysts with a lower Ni content showed higher CO_2 conversions, especially at 350°C, the difference in CO_2 conversion was clearer.

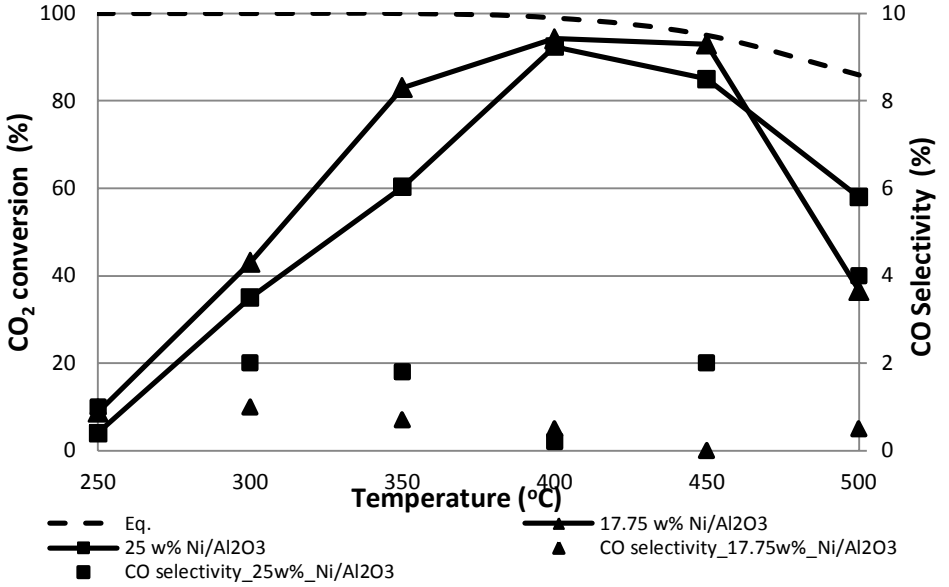

Figure 32: Effect of active metal content for Ni/Al_2O_3.

The Ni content was varied also for Ni/Mg/Al HTs prepared by the co-precipitation and sol-gel method with targeted Ni loadings of 5.0 and 15.0 weight percent. The results for the catalysts prepared by the co-precipitation are given in Figure 33 while the results for the catalysts prepared by the sol-gel method are reported in Figure 34. Furthermore, selectivity results are also plotted within the figures and noted in labels. According to Figure 33, although Ni content was tripled to 15.0 w%, the conversion results improved only slightly.

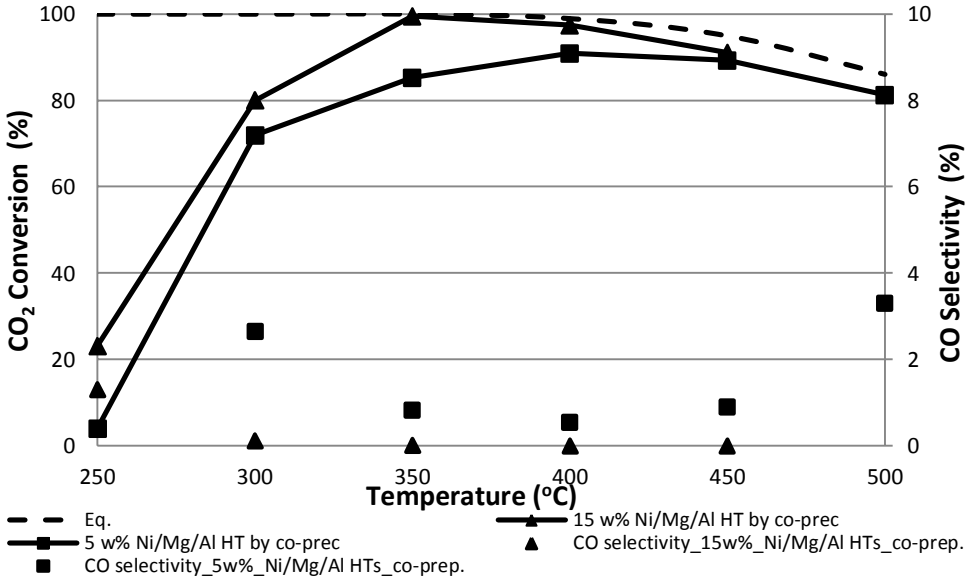

Figure 33: Effect of active metal content for Ni/Mg/Al HT prepared by co-precipitation method.

Analogously, an increment in the content of Ni had no effect on the performance of the hydrotalcite-based Ni catalyst prepared by the sol-gel method, while showing still very low CH_4 selectivity. CO selectivity remained below 5% for the benchmark catalysts (Fig. 32) and the catalyst prepared by co-precipitation (Fig. 33).

It is clear from the figures that, higher Ni content had a minor effect on the performance of catalysts. Moreover, an increase in Ni loading was expected to enhance the activity of the catalysts, if the dispersion of active metal could have been kept high enough, which could have resulted in higher amount of available active sites for the reaction. On the contrary, higher metal loading could possibly create metal agglomerates in these cases, which limited the accessible surface area of active metal. This finding agrees well with that reported for the catalysts prepared by the impregnation method [10]. On the other hand, the result conflicts with that established previously for Ni-Al LDH by Gabrovska et al. where a decrease in the Ni loading resulted in a decrease of the methanation activity [35]. Active metal dispersion of the catalysts could have been analysed by characterization techniques such as, chemisorption and TEM making the discussion more concrete.

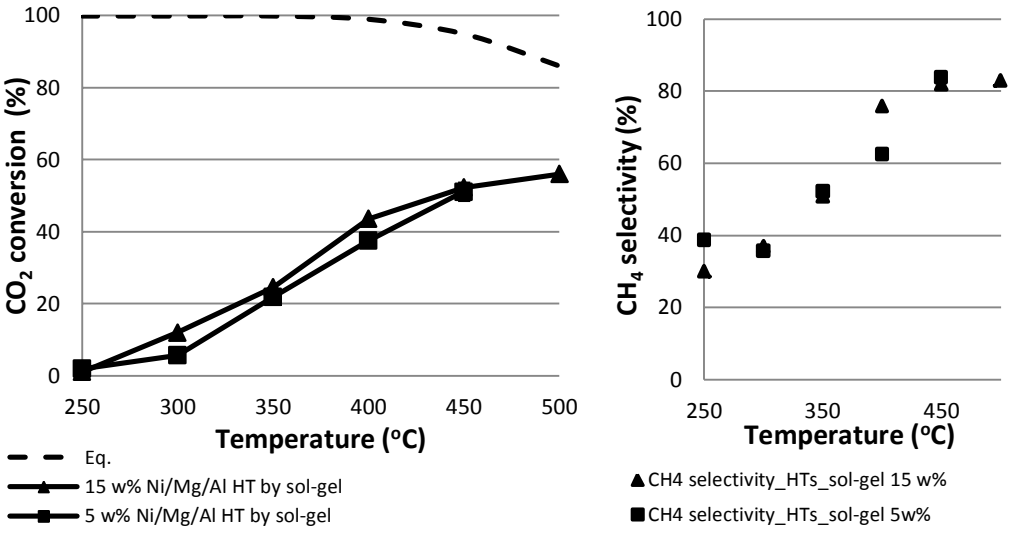

Figure 34: Effect of active metal content for Ni/Mg/Al HT prepared by sol-gel method.

4.5.3. Effect of catalysts amount

To determine the effect of catalyst amount the reactor tubes were coated with several wash-coating cycles, as it was outlined in Section 3.3. The results are shown in Figure 35 in terms of CO_2 conversion at different temperatures. The figure has the results of two different types of catalysts; a) 17.75 w% Ni/Al_2O_3 prepared by incipient wetness impregnation while b) 15 w% Ni/Mg/Al HT prepared by co-precipitation method. The amounts of catalyst coating were noted in the figure. As can be seen from the figure, a significant increase in the CO_2 conversion was achieved for both of the catalyst types. However the increment got smaller as the temperature was risen, while the differences were much more distinguishable at lower temperatures. This could be explained by approaching the equilibrium at higher temperatures.

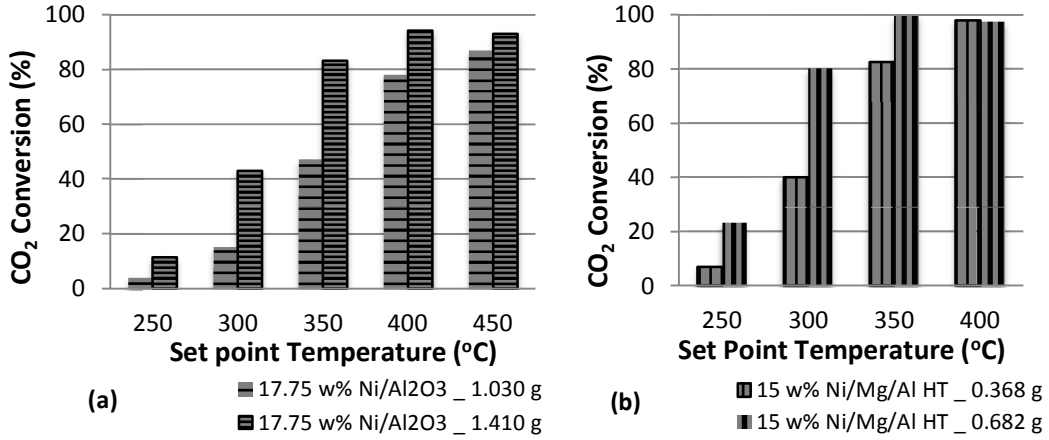

Figure 35: Effect of catalyst amount a)17.75 w% Ni/Al_2O_3, b)15 w% Ni/Mg/Al HT_co-prec.

Furthermore, another conclusion from this study confirms that the active sites available after coating are located not only on the outer surface of the coating but also inside the pores and cracks of the coating which resulted in higher CO_2 conversions with thicker catalyst coating. This could have been proved by characterization of the morphology of the coating; however, the structure of the reactor tube which was a closed stainless steel cylinder with a diameter of 4mm limited any analysis. In order to analyse the morphology of the coating, cutting the reactor tube into two pieces along the length of the tube was discussed,

however it could have damaged the coating structure. On the other hand, analysing a plate-like stainless steel coated with the same catalysts by dip coating could differ too much from the coated tubes to compare with the current results.

4.5.4. Addition of Ce and Zr

One of the targets was to evaluate the effect of addition of Ce and Zr on the activity of HTs for CO_2 methanation reaction. For this purpose, commercially available Ce- and Zr-doped HTs were employed as catalyst supports and Ni loading was deposited on these materials by wet impregnation. The trials of wash-coating of these catalysts, for which the same procedure was used for preparing slurries, were unsuccessful. The slurries had viscous foam-like appearance and adhesion was very poor, after drying and calcination the whole coating peeled off, only one reactor tube which was coated using Ni-loaded Zr-doped HT catalyst remained coated. The reason of this successful coating might have caused by the Ni loading; however, the other catalysts deposited with Ni showed very poor adhesion. For this reason, their performance on the methanation reaction was tested as packed beds created between two layers of quartz wool inside the reactor tubes. The results of CO_2 conversion achieved by testing these catalysts which contained Ce or Zr are reported in Figure 36. As can be seen from the figure, the catalysts showed very low CO_2 conversions at especially lower temperatures in contrast to that plotted for the catalyst prepared by the sol-gel method. Even at higher temperatures the catalysts containing Ce and Zr compounds were unable to reach the equilibrium conversions. Although addition of Ce has previously been reported as beneficial for methanation of CO_2, Ni-loaded Ce-doped HTs remained less active than the Ni-loaded Zr-doped HTs [19, 38]. Moreover, note in the figure that, higher Ni loading on Ce-doped HT had no influence on the activity of the catalyst.

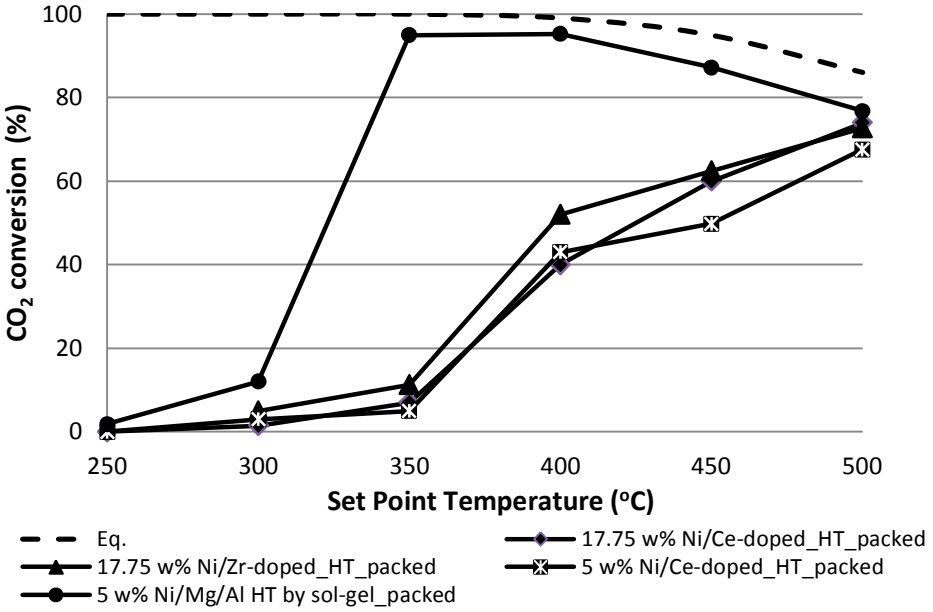

Figure 36: Effect of Ce and Zr addition calcined at 550°C and reduced at 500°C.

There could be two reasons for these catalysts being less active in the CO_2 methanation reaction. The first reason could be the mass and heat transfer limitations inside the packed beds which were observed during long test runs that reached equilibrium slowly. However, the pressure drop remained negligible inside the reactor tubes compared to the test runs with the 5 w% Ni/Mg/Al HT prepared by the sol-gel method. Secondly, the calcination and reduction temperature used for these catalysts might be inappropriately chosen. It was observed after calcination that the colour of the samples was paler than those samples previously calcined without containing Ce and Zr compounds. Moreover, it was reported that calcination and reduction temperatures were chosen as 550°C and 900°C, respectively, for Ni-Ce-Zr hydrotalcite-derived catalysts [38].

4.6. Effect of reduction temperature

Different reduction temperatures were chosen to determine its effect on the performance of catalysts for CO_2 hydrogenation reaction. Reduction procedure was explained in Section 3.4.2. The maximum temperature that could be reached with the existing experimental setup was 650°C. For this reason, reduction temperature was chosen between 500°C and 650°C for each prepared and tested HT-based Ni catalysts. The activity results for these catalysts are plotted as CO_2

conversion versus temperature graphs in Figure 37. The types of catalysts are stated in the description of the figure.

According to the figure, the effect of reduction temperature on the performance of catalysts was distinguishable for each type of catalysts. For 15.0 w% Ni/Mg/Al HT prepared by co-precipitation (Fig.37a) and 17.75 w% Ni/Ce-doped HT (Fig.37c), the higher reduction temperature improved the performance of catalysts on methanation reaction. Once again, the discrepancy was diminished at higher temperatures due to reaching the equilibrium while it was obvious at lower temperatures. On the contrary, for 5 w% Ni/Mg/Al HT prepared by both co-precipitation (Fig.37b) and sol-gel methods (Fig.37d), as the reduction temperature raised reduced CO_2 conversions were reached.

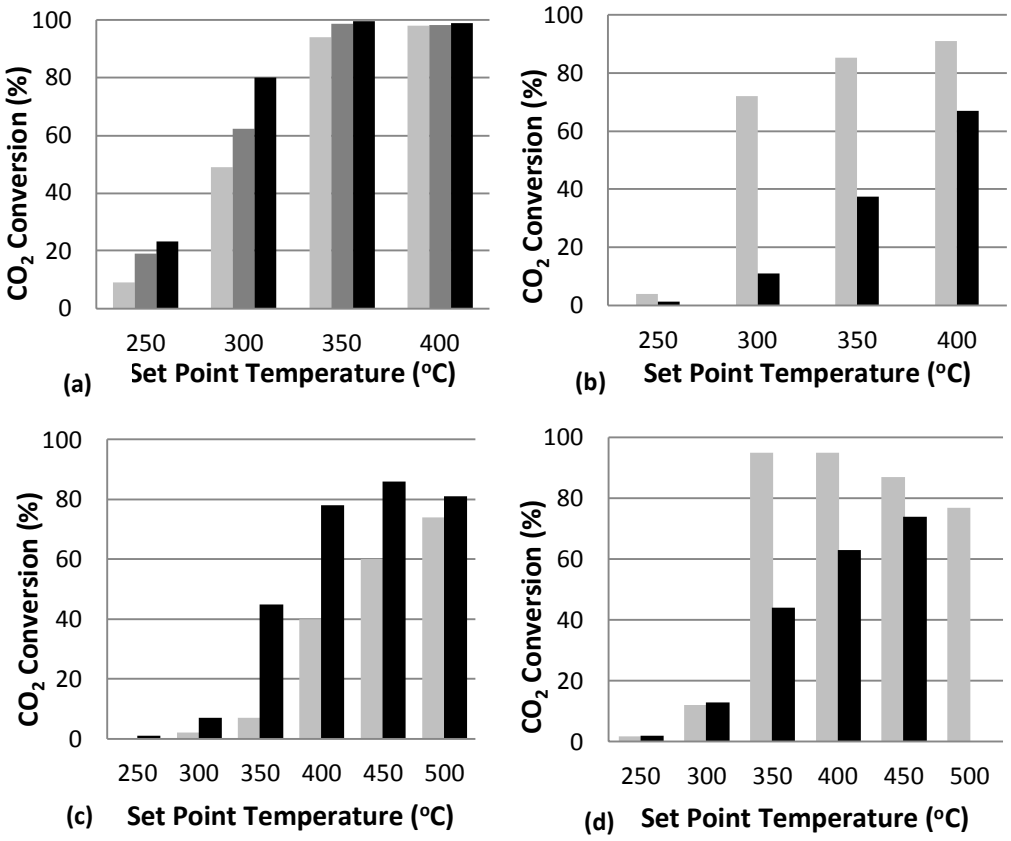

Figure 37: The effect of reduction temperature on the performance of HT-based Ni catalysts: ■:500°C, ■:600°C and ■:650°C a) 15.0 w% Ni/Mg/Al HT_co-prec., b) 5.0 w% Ni/Mg/Al HT_co-prep., c) 17.75 w% Ni/Ce-doped HT and d) 5 w% Ni/Mg/Al HT_sol-gel_packed-bed.

Higher reduction temperature was claimed to enhance the performance of catalysts for CO_2 methanation reaction for each cases that was tested [35]. Although, this proposal was valid for two cases, the results indicated that higher reduction temperature might cause negative effects on the performance of some catalysts. Reasons for the enhanced performances of catalysts after reduction at higher temperatures could be that the number of active metal sites which were in metallic state was intensified by maintaining high temperatures for reduction processes which was stated in previous studies, as well [35].

One reason for the negative effect of the higher reduction temperatures could be the sintering of active metals, which reduce the total surface area of the corresponding metal, consequently results in lower CO_2 conversions. H_2-TPR analysis should have been performed to determine the optimum reduction temperature for each catalyst that could make the highest amount of active sites which were in metallic state available for the reactant gases to react on. However, even though the optimum reduction temperature was known, if the temperature was found above 650^{o}C, which was expected according to previous studies proposing higher reduction temperatures due to the strength of Ni-Al-O bonds in HTs, this higher temperature would have been limited by the current experimental setup. Furthermore, XRD analysis should have been repeated with the reduced catalyst to find out the presence of the metallic states of active metals.

4.7. Stability results

For determining the stability of the catalysts showing the lifetime of catalysts, long-term tests were performed similar to the procedure of activity test runs which was described in Section 3.5.3. The stability results showing the CO_2 conversion and CH_4 selectivity with respect to time are shown in Figure 38. The figure confirms that the HT-based Ni catalysts were stable during 40-hours test run.

First Ni/Al_2O_3 catalyst was left for the stability test over weekend at 450 C in order to evaluate the effect of sintering of Ni catalyst. As can be seen from the figure no distinguishable difference was observed in the activity of the catalyst. However, that might have caused by being near to the equilibrium conditions. For this reason next stability test was performed being away from equilibrium which was achieved setting a lower temperature, 350^{o}C. Moreover, recording of the data corresponding to this test was unsuccessful. Only initial and final compositions could be recorded manually which showed that after 60 hours of operation, the catalyst lost its activity by 15% reduced CO_2 conversion (from 46% to 39%) and 21% reduced CH_4 selectivity.

The next stability test evaluated the life of the 15 w% Ni/Mg/Al HT prepared by the co-precipitation method. A long term experiment at 300^{o}C revealed the remarkably stable performance of the HT-based Ni catalyst under methanation conditions with 78% of CO_2 conversion and 100% of CH_4 selectivity. This excellent stability of HT-based Ni catalyst is consistent with those reported previously for $Ni\text{-}Al_2O_3$-HT catalyst at 350^{o}C for 20 hours [36] and $(Mg,Al)O_x$ supported Ni catalyst at 225^{o}C about 50 hours [34].

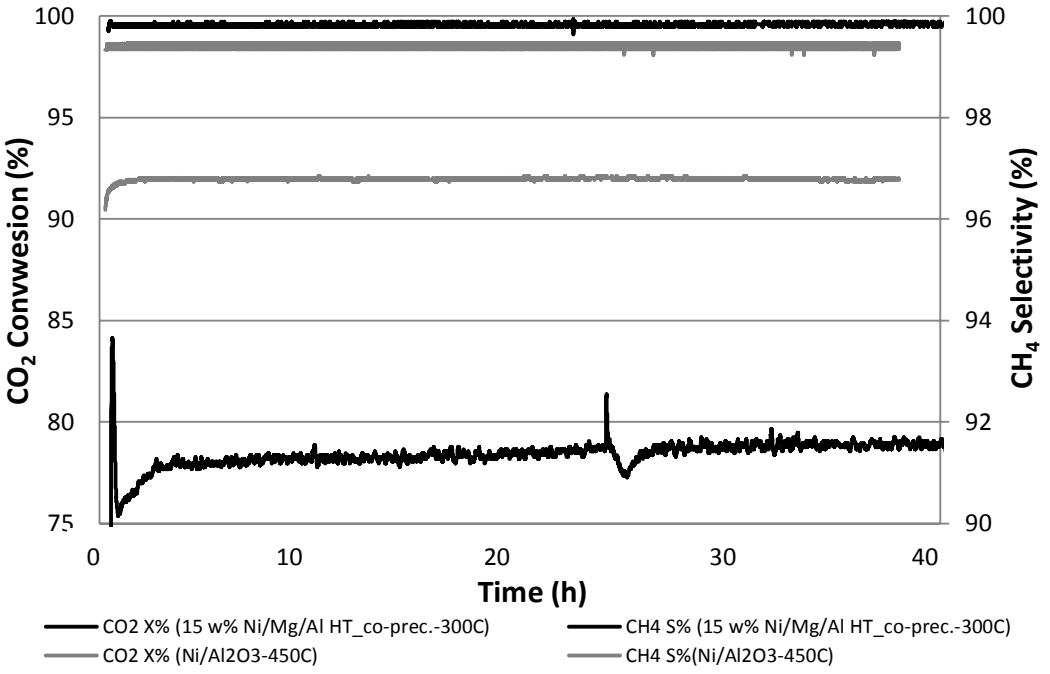

Figure 38: Stability profiles.

4.8. Packed-bed or Wash-coated

The aim for the studies was to wash-coat the reactor tube with the synthesized catalysts and to test them in the CO_2 methanation reaction. However, because of the reasons explained in previous sections, some of the catalysts had to be tested as packed-bed. In order to be able to interpret the results which were reported for packed-bed and wash-coated catalysts a comparison was needed. For this reason, the same catalysts was tested both as packed-bed (~400mg) and wash-coated. Figure 39 provides the results of these experiments done for 5 w% Ni/Mg/Al HTs prepared by co-precipitation and sol-gel, respectively. As can be seen from the figure, the difference in the performance of catalysts is clear. However, the results showed no direct correlation between these two environments with respect to the performance of the catalysts for methanation reaction.

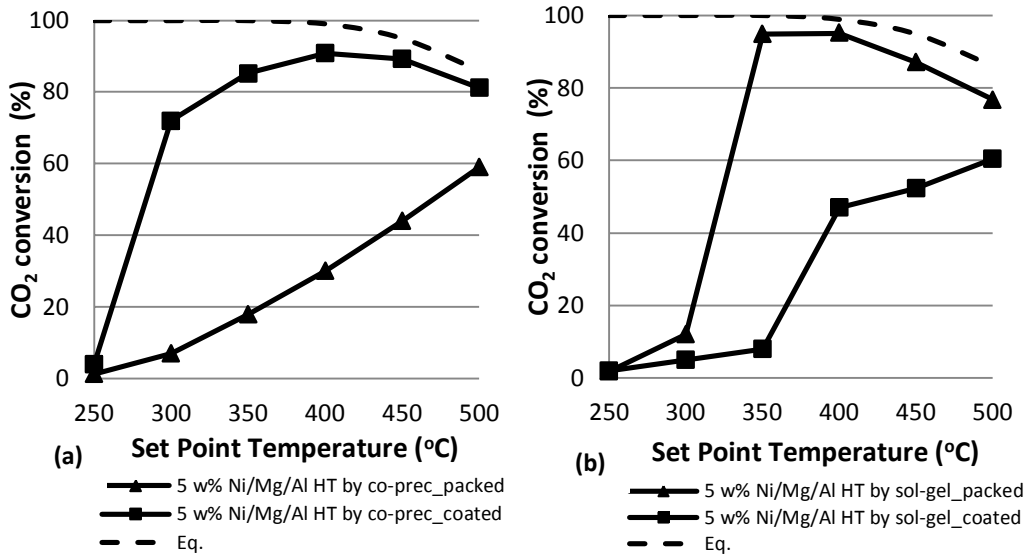

Figure 39: Comparison of packed-bed and wash-coated catalysts performance prepared by the a)co-precipitation and b) sol-gel method.

Unfortunately, the previously reported studies for CO_2 methanation reactions utilized the HT-based catalysts only as packed beds [33-36], thus no comparison between packed bed and wash-coated catalyst was performed before.

In order to be able to compare these two environments, ideal conditions should have been created, which could have avoided heat and mass transfer limitations and pressure drop inside the reactors. The packed-bed reactors tested in the experiments exhibited pressure drop which varied with the particle size of the catalysts and the reaction temperature (max 1 bar). Figure 40 shows a combined plot of temperature profile inside the empty tube and the scheme of a catalyst packed-bed inside the reactor tube. The figure clearly illustrates the temperature variation inside the reactor tube (radial temperature variation was neglected), for instance setting the reaction temperature to 500°C would result in a temperature range of 250-450°C. This confirms that the results of the performance tests revealed shifted conversion values towards higher temperatures.

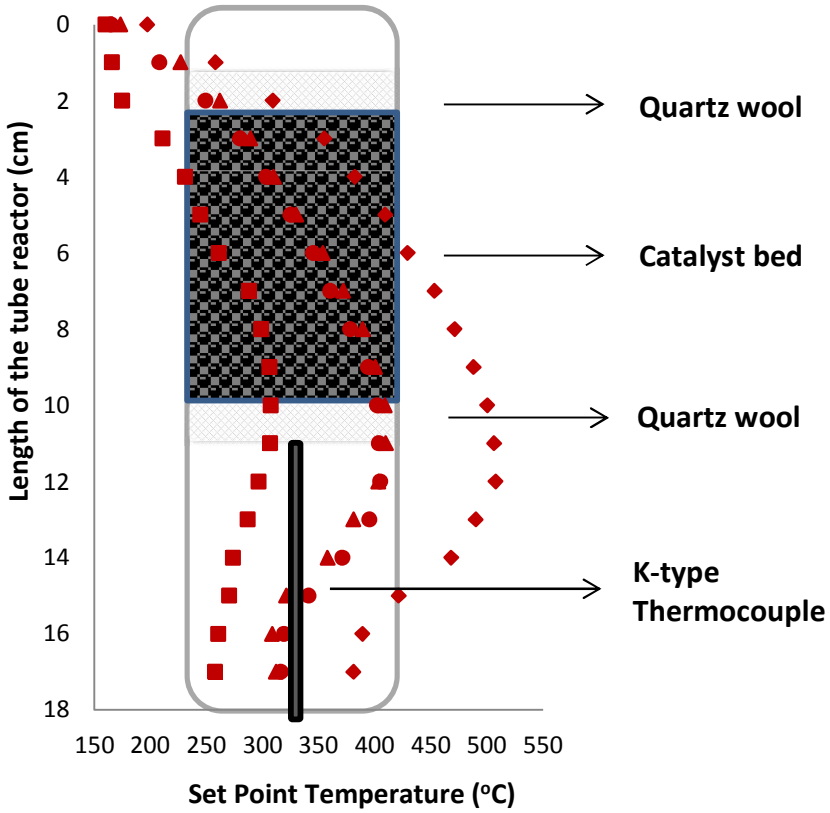

Figure 40: Temperature Profile inside the empty reactor tube (■:300°C, ▲:400°C, ●:400°C [preheated to 250°C], ◆:500°C).

4.9. Error estimation

This thesis presented the conversion and selectivity results of the compounds which were calculated from the readings of the online gas analyser. The reaction temperature was set to a certain value and the temperature inside the reactor was recorded using the ABB temperature controller unit. The possible error could originate from improper calibrations and the limitations of measurement equipment including temperature indicators and the gas analyser.

The calibrations were performed for three mass flow meters once in the beginning and the online gas analyser for once in a month. Since the gas flow rate used during the experiment was rather slow it is likely to have error. The total gas flow rate was double checked by a mass flow meter which could also be a source of error. However, since the same feeding gas composition was employed for all test runs, no significant difference was observed in the initial gas compositions.

The online gas analyser ABB AO2020 was a combination of three different modules. Uras14 measuring CO, CO_2 and CH_4 by an infrared photometer, Caldos17 measuring H_2 in N_2 using a thermal conductivity detector and Magnos106 was an oxygen analyser with an accuracy of ±0.05%. The analyser was calibrated with pure nitrogen and a gas standard. The equipment itself had limitations and calibrations could also cause some errors.

The temperature measurements and adjustments were done using the controller unit. Unfortunately, the data was unstable in a range of $\pm 3^{o}C$. Nevertheless, after setting the temperature, settling of the new temperature was waited before any measurement. In addition, the placement of the temperature indicators was always done appropriately. The variation of temperature inside the reactor tube was already discussed which could cause errors in CO_2 conversions.

Finally, errors could occur due simply to mistakes on the part of the person performing the work such as misreading the values on the temperature and gas

compositions, making calculation mistakes during preparation of the catalysts. However while recording the gas compositions and temperatures during the test runs, a template was used including a graph of CH_4 production which helped to observe any wrong data. Furthermore, atom and mol balances were performed in order to obtain the CO_2 conversion and CO/CH_4 selectivity values. One example of this excel sheet is shown in Appendix 1.

CHAPTER 5 CONCLUSIONS AND OUTLOOKS

With the aim of evaluating the catalytic performance of the catalysts for gas-phase hydrogenation of carbon dioxide into methane, this thesis has successfully synthesized several hydrotalcite-based Ni catalysts based on a one-pot synthesis approach. These catalysts were prepared with different nickel contents through various methods, including impregnation, co-precipitation and sol-gel. Furthermore, two batches of the Ni/Al_2O_3 catalyst were synthesized as benchmarks by wetness incipient impregnation using two different nickel loadings. These catalysts were calcined and coated to the inner side of the reactor tubes which were made of stainless steel, 17.5 cm in length and 0.4 cm in diameter. The reactor tubes had been previously calcined at 800^{o}C for four hours in order to create a rough inner surface that could enhance the adhesion of the coating. One procedure was utilized to prepare slurries for coating the reactor tubes; however, the procedure resulted in a foam-like slurry for the samples containing Ce and Zr. For this reason, their performance on the methanation reaction was tested as packed beds created between two layers of quartz wool inside the reactor tubes.

The catalytic performance of the wash-coated catalysts for carbon dioxide methanation was evaluated in a continuous plug flow reactor operating at atmospheric pressure. The catalytic activity measurements were performed by means of a gaseous mixture of $CO_2/H_2/N_2$ at different volumetric ratios in a temperature range of 250-500^{o}C and GHSV from 8185 to 20463 h^{-1}. The performance of the catalysts was evaluated in terms of CO_2 conversion, CH_4 yield and CH_4/CO selectivity.

Throughout this study, numerous test runs were performed in order to identify the effect of various factors on the performance of catalysts prepared for the CO_2 methanation reaction. The effect of feed gas composition was studied in order to establish the optimum composition. An excess amount of H_2 was found

to be beneficial for CO_2 conversion and CH_4 selectivity. A diluted mixture of the same composition, CO_2/H_2 ratio of 1/6, revealed the best results in terms of CO_2 conversion and CH_4 selectivity. As a result, 10%CO_2:60%H_2:30%N_2 was chosen to be used as the feed gas mixture composition. The effect of GHSV of the feed gas mixture was varied to maximize the conversions. As the probability of CO_2 meeting the other reactant gas, H_2, increases at a lower GHSV, the lowest feed flow rate (0.3 L/min) was chosen for the reactant gases.

The performance of hydrotalcite-based Ni catalysts synthesized using the preparation methods described in Section 3.1 was compared with that of the benchmark Ni/Al_2O_3 catalyst in terms of CO_2 conversion and CH_4 selectivity. This comparison revealed that the 15 w% Ni/Mg/Al HT prepared by the co-precipitation method exhibited the best activity in the CO_2 methanation reaction. With this catalyst, the CO_2 methanation reaction was already initiated below 220^{o}C (X_{CO2}=10.2 %, S_{CO2}=98.4 %) and reached 80% conversion of CO_2 at 300^{o}C with 99.9 % selectivity towards CH_4. However, using higher Ni loading showed no significant influence on CO_2 conversion. Nevertheless, enhanced CO_2 conversions were achieved at a higher catalyst loading by repeating the washcoating procedure several times, thus confirming that the reaction had occurred not only on the outer surface of the coating but also inside the pores and cracks of the coating. The catalysts were also utilised as packed beds. Of these, the 5 w% Ni/Mg/Al HT prepared by the sol-gel method showed the highest activity at 300^{o}C, with 95.0% conversion of CO_2 and 99.8% CH_4 selectivity. These results are superior to those reported previously for Ni catalysts in CO_2 methanation reactions. The higher catalytic activity of the HT-based Ni catalysts could be attributed to the existence of basic sites of HTs and the dispersion of Ni particles on this basic support.

Reduction temperature has been earlier reported to be an important parameter for determining the number of active sites in metallic states. However, due to the limitations of the existing experimental setup, the maximum achievable reduction temperature remained as 650^{o}C, which was well below temperatures

as high as ~800^{o}C reported previously. This lower reduction temperature reduced the probability of achieving higher CO_2 conversions at lower temperatures.

The presence of Ce and Zr was studied by loading Ni on the commercially available Ce- and Zr-doped HTs. Although addition of Ce has previously been reported as beneficial for methanation of CO_2, Ni-loaded Ce-doped HTs remained less active than the Ni-loaded Zr-doped HTs. Final test runs were performed to compare the performance of the catalysts in packed-bed or washcoated reactors tubes. However, the results showed clear difference in experiments applying packed beds and washcoated tubes resulting in no direct correlation between these two environments.

In order to optimize working conditions for achieving the best activity and selectivity in the CO_2 methanation reactions, the reaction temperature, feed composition as well as the feed flow rate of the reactants were adjusted during the test runs. Both the co-precipitation and sol-gel methods were found to yield the highest conversion of CO_2. The best results were achieved when initiating the conversion of CO_2 into CH_4 at a temperature ~100^{o}C lower than the conditions currently reported. The greatest challenge directly affecting the results was the temperature variation along the reactor tube, which caused a shift in the conversion of CO_2 to higher temperatures. Therefore, future work should focus on developing the current setup by placing the reactor tube in either an oven or a molten salt bath, as well as increasing the length of tubes where the feeding gas mixture is preheated.

One limitation of this study is that it was unable to exploit common techniques for characterizing the catalyst samples. Such characterization is crucial for heterogeneous catalysis, in order to be able to discuss the obtained results; the different features of the samples should be identified using various techniques.

Furthermore, for improving dispersion of the active metals and controlling the particle size of the synthesized catalysts, future studies could utilize advanced

synthesis methods and other active site engineering techniques [151-153]. These techniques would enable the active sites of the catalysts to be adjusted, thus offering a breakthrough in the field of heterogeneous catalysis, since an incremental increase in the efficiency of production processes is able to make a tremendous change in the bigger picture. Finally, one promising direction for future research would be to employ light sources for initiating reactions using e.g. Ce and Zr compounds, as these compounds have been highly utilized in photocatalytic reactions in order to convert captured CO_2 into methane by the aid of sun lights.

REFERENCES

[1] M. Götz, J. M. F. Lefebvre, A. M. Koch, F. Graf, S. Bajohr, R. Rainer and T. Kolb, "Renewable Power-to-Gas: A technological and economic review," *Renewable Energy,* vol. 85, pp. 1371-1390, 2016.

[2] P. Nema, S. Nema and P. Roya, "An overview of global climate changing in current scenario and mitigation action," *Renewable and Sustainable Energy Reviews,* vol. 16, no. 4, p. 2329–2336, 2012.

[3] M. R. Raupach, G. Marland, P. Ciais, C. L. Quere, J. G. Canadell and G. Klepper, "Global and regional drivers of accelerating CO2 emissions," *Proceedings of the National Academy of Sciences of the United States of America,* vol. 104, p. 10288–10293, 2007.

[4] M. Mikkelsen, M. Jørgensen and F. C. Krebs, "The teraton challenge. A review of fixation and transformation of carbon dioxide," *Energy & Environmental Science,* vol. 3, p. 43–81, 2010.

[5] X. Xiaoding ja J. A. Moulijn, "Mitigation of CO2 by Chemical Conversion: Plausible Chemical Reactions and Promising Products," *Energy Fuels,* osa/vuosik. 10, nro 2, p. 305–325, 1996.

[6] D. M. Alessandro, B. Smit and J. R. Long, "Carbon Dioxide Capture: Prospects for New Materials," *Angewandte Chemie,* vol. 49, p. 6058 – 6082, 2010.

[7] Y. Ding and E. Alpay, "High Temperature Recovery of CO2 from Flue Gases Using Hydrotalcite Adsorbent," *Process Safety and Environmental Protection,* vol. 79, no. 1, pp. 45-51, 2001.

[8] G. Centi ja S. Perathonera, "Opportunities and prospects in the chemical recycling of carbon dioxide to fuels," *Catalysis Today,* osa/vuosik. 148, p. 191–205, 2009.

[9] "http://co2chem.co.uk/," [Online]. Available: http://co2chem.co.uk/. [Accessed 10 January 2017].

[10] W. Wang and J. Gong, "Methanation of carbon dioxide: an overview," *Front. Chem. Sci. Eng,* vol. 5, pp. 2-10, 2011.

[11] S. Sahebdelfar and M. T. Ravanchi, "Carbon dioxide utilization for methane production: A thermodynamic analysis," *Journal of Petroleum Science and Engineering,* vol. 134, p. 14–22, 2015.

[12] C. Song, “Global challenges and strategies for control, conversion and utilization of CO2 for sustainable development involving energy, catalysis, adsorption and chemical processing,” *Catalysis Today,* vol. 115, p. 2–32, 2006.

[13] M. Götz, A. M. Koch and F. Graf, “State of the Art and Perspectives of CO2 Methanation Process Concepts for Power-to-Gas Applications,” Copenhagen, 2014.

[14] P. Sabatier and J.-B. Senderens, “Direct Hydrogenation of Oxides of Carbon in Presence of Various Finely Divided Metals,” *Jour. Chem. Soc.,* vol. 82, no. 2, p. 317, 1902.

[15] W. Wang, S. Wang, X. Ma and J. Gong, “Recent advances in catalytic hydrogenation of carbon dioxide,” *Chem. Soc. Rev.,* vol. 40, pp. 3703-3727, 2011.

[16] M. A. A. Aziz, A. A. Jalil, S. Triwahyono and A. Ahmad, “CO2 methanation over heterogeneous catalysts: recent progress and future prospects,” *Green Chemistry,* vol. 17, pp. 2647-2663, 2015.

[17] K. Müller, M. Fleige, F. Rachow and D. Schmeißer, “Sabatier based CO2-methanation of flue gas emitted by conventional power plants,” *Energy Procedia,* vol. 40, pp. 240-248, 2013.

[18] I. Omae, “Aspects of carbon dioxide utilization,” *Catalysis Today,* vol. 115, pp. 33-52, 2006.

[19] S. Tada, T. Shimizu, H. Kameyama, T. Haneda and R. Kikuchi, “Ni/CeO2 catalysts with high CO2 methanation activity and high CH4 selectivity at low temperatures,” *International Journal of Hydrogen Energy,* vol. 37, no. 7, pp. 5527-5531, 2012.

[20] M. Jacquemin, A. Beuls and P. Ruiz, “Catalytic production of methane from CO2 and H2 at low temperature: Insight on the reaction mechanism,” *Catalysis Today,* vol. 157, pp. 462-466, 2010.

[21] S. Rönsch, J. Schneider, S. Matthischke, M. Schlüter, M. Götz, J. Lefebvre, P. Prabhakaran and S. Bajohr, “Review on methanation – From fundamentals to current projects,” *Fuel,* vol. 166, pp. 276-296, 2016.

[22] Y. J. Lim, J. McGregor, A. J. Sederman and J. Dennis, “Kinetic studies of CO2 methanation over a Ni/γ-Al2O3 catalyst using a batch reactor,” *Chemical Engineering Science,* vol. 141, pp. 28-45, 2016.

[23] Z. Liu, Z. X. Bozhao Chu, Y. Jin and Y. Cheng, “Total methanation of syngas to synthetic natural gas over Ni catalyst in a micro-channel reactor,” *Fuel,* vol. 95, pp.

599-605, 2012.

[24] G. D. Weatherbee and C. H. Bartholomew, “Hydrogenation of CO2 on group VIII metals: I. Specific activity of NiSiO2,” *Journal of Catalysis,* vol. 68, pp. 67-76, 1981.

[25] S. Sharma, Z. Hu, P. Zhang, E. W. McFarland and H. Metiu, “CO2 methanation on Ru-doped ceria,” *Journal of Catalysis,* vol. 278, no. 2, pp. 297-309, 2011.

[26] J. L. Falconer and E. A. Zağli, “Adsorption and methanation of carbon dioxide on a nickel/silica catalyst,” *Journal of Catalysis,* vol. 62, no. 2, pp. 280-285, 1980.

[27] P. Riani, G. Garbarino, M. A. Lucchini, F. Canepa and G. Busca, “Unsupported versus alumina-supported Ni nanoparticles as catalysts for steam/ethanol conversion and CO2 methanation,” *Journal of Molecular Catalysis A: Chemical,* Vols. 383-384, pp. 10-16, 2014.

[28] A. Borgschulte, N. Gallandat, B. Probst, R. Suter, E. Callini, D. Ferri, Y. Arroyo, R. Erni, H. Geerlings and A. Züttel, “Sorption enhanced CO2 Methanation,” *Physical Chemistry Chemical Physics,* vol. 15, pp. 9620-9625, 2013.

[29] S. J. Choe, H. J. Kang, S.-J. Kim, S.-B. Park, D. H. Park and D. S. Huh, “Adsorbed Carbon Formation and Carbon Hydrogenation for CO2 Methanation on the Ni(111) Surface: ASED-MO Study,” *Bulletin of the Korean Chemical Society,* vol. 26, no. 11, pp. 1682-1688, 2005.

[30] L. Tao, S. Wang, D.-n. Gao and S.-d. Wang, “Effect of support calcination temperature on the catalytic properties of Ru/Ce0.8Zr0.2O2 for methanation of carbon dioxide,” *Journal of Fuel Chemistry and Technology,* vol. 42, no. 12, pp. 1440-1446, 2014.

[31] H. Takano, K. Izumiya, N. Kumagai and K. Hashimoto, “The effect of heat treatment on the performance of the Ni/(Zr-Sm oxide) catalysts for carbon dioxide methanation,” *Applied Surface Science,* vol. 257, no. 19, pp. 8171-8176, 2011.

[32] J.-T. Feng, Y.-J. Lin, D. G. Evans, X. Duan and D.-Q. Li, “Enhanced metal dispersion and hydrodechlorination properties of a Ni/Al2O3 catalyst derived from layered double hydroxides,” *Journal of Catalysis,* vol. 266, no. 2, pp. 351-358, 2009.

[33] S. Abate, B. Katia, G. Emanuele, D. Fabio, B. Samir, P. Siglinda, P. Raffaele and C. Gabriele, “Synthesis, Characterization, and Activity Pattern of Ni−Al Hydrotalcite Catalysts in CO2 Methanation,” *Industrial Engineering Chemistry Research,* vol. 55, pp. 8299-8308, 2016.

[34] N. Bette, J. Thielemann, M. Schreiner ja F. Mertens, ”Methanation of CO2 over a (Mg,Al)Ox Supported Nickel Catalyst Derived from a (Ni,Mg,Al)-Hydrotalcite-like

Precursor," *ChemCatChem,* osa/vuosik. 8, pp. 2903-2906, 2016.

[35] M. Gabrovska, R. Edreva-Kardjieva, D. Crisan, P. Tzvetkov, M. Shopska and I. Shtereva, "Ni–Al layered double hydroxides as catalyst precursors for CO2 removal by methanation," *Reaction Kinetics, Mechanisms and Catalysis,* vol. 105, no. 1, pp. 79-99, 2012.

[36] L. He, Q. Lin, Y. Liu and Y. Huang, "Unique catalysis of Ni-Al hydrotalcite derived catalyst in CO2 methanation: cooperative effect between Ni nanoparticles and a basic support," *Journal of Energy Chemistry,* vol. 23, pp. 587-592, 2014.

[37] K. Mette, S. Kuhl, H. Dudder, K. Kähler and A. Tarasov, "Stable Performance of Ni Catalysts in the Dry Reforming of Methane at High Temperatures for the Efficient Conversion of CO2 into Syngas," *CHEMCATCHEM Communications,* vol. 6, p. 100 – 104, 2014.

[38] M. Nizio, R. Benrabbah, M. Krzak, R. Debek, M. Motak, S. Cavadias, M. E. Gálvez and P. Costa, "Low temperature hybrid plasma-catalytic methanation over Ni-Ce-Zr hydrotalcite-derived catalysts," *Catalysis Communications,* vol. 83, pp. 14-17, 2016.

[39] D. Wierzbicki, R. Debek, M. Motak, T. Grzybek, M. E. Gálvez and P. Costa, "Novel Ni-La-hydrotalcite derived catalysts for CO2 methanation," *Catalysis Communications,* vol. 83, pp. 5-8, 2016.

[40] E. Baraj, S. Vagaský, T. Hlinčík, K. Ciahotný and V. Tekáč, "Reaction mechanisms of carbon dioxide methanation," *Chemical Papers,* vol. 70, no. 4, p. 395–403, 2016.

[41] Scopus, "Scopus, CO2 Methanation," 31 December 2016. [Online]. Available: https://www.scopus.com/term/analyzer.uri?sid=B290C8964F6A1FF2A177C742DDF0B12C.wsnAw8kcdt7IPYLO0V48gA%3a20&origin=resultslist&src=s&s=TITLE-ABS-KEY%28CO2+methanation%29&sort=plf-f&sdt=b&sot=b&sl=30&count=1057&analyzeResults=Analyze+results&txGid=B290C8964F. [Accessed 5 January 2017].

[42] M. Burkhardt and G. Busch, "Methanation of hydrogen and carbon dioxide," *Applied Energy,* vol. 111, pp. 74-79, 2013.

[43] B. Demirel and P. Scherer, "The roles of acetotrophic and hydrogenotrophic methanogens during anaerobic conversion of biomass to methane: a review," *Reviews in Environmental Science and Bio/Technology,* vol. 7, no. 2, pp. 173-190, 2008.

[44] J.-P. Peillex, M.-L. Fardeau, R. Boussand, J.-M. Navarro and J.-P. Belaich, "Growth of Methanococcus thermolithotrophicus in batch and continuous culture on H2

and CO2: influence of agitation," *Applied Microbiology and Biotechnology,* vol. 29, no. 6, pp. 560-564, 1988.

[45] J. Kopyscinski, T. J. Schildhauer and S. M. Biollaz, "Production of synthetic natural gas (SNG) from coal and dry biomass – A technology review from 1950 to 2009," *Fuel,* vol. 89, pp. 1763-1783, 2010.

[46] M. E. Davis and R. J. Davis, Fundamentals of Chemical Reaction Engineering, 1st ed., Boston: Mc Graw Hill, 2003.

[47] J. S. Kim, H. K. Kim, S. B. Lee, M. J. Choi, K. W. Lee and Y. Kang, "Characteristics of carbon dioxide hydrogenation in a fluidized bed reactor," *Korean Journal of Chemical Engineering,* vol. 18, no. 4, p. 463–467, 2011.

[48] O. Görke, P. Pfeifer and K. Schubert, "Highly selective methanation by the use of a microchannel reactor," *Catalysis Today,* vol. 110, pp. 132-139, 2005.

[49] K. P. Brooks, J. Z. H. Hu and K. R. J, "Methanation of carbon dioxide by hydrogen reduction using the Sabatier process in microchannel reactors," *Chemical Engineering Science,* vol. 62, pp. 1161-1170, 2007.

[50] I. C. Martin, "Carbon Dioxide Methanation for Intensified Reactors," Aalto University School of Chemical Technology, Espoo, 2015.

[51] S.-i. Fujita, M. Nakamura, T. Doi and N. Takezawa, "Mechanisms of methanation of carbon dioxide and carbon monoxide over nickel/alumina catalysts," *Applied Catalysis A: General,* vol. 104, no. 1, pp. 87-100, 1993.

[52] S. Eckle, H.-G. Anfang and J. R. Behm, "Reaction intermediates and side products in the methanation of CO and CO2 over supported Ru catalysts in H2-rich reformate gases," *The Journal of Physical Chemistry C,* vol. 115, no. 4, pp. 1361-1367, 2011.

[53] P. U. Aldana, F. Ocampo, K. Kobl, B. Louis, F. Thibault-Starzyk, M. Daturi, P. Bazin, S. Thomas and A. Roger, "Catalytic CO2 valorization into CH4 on Nibased ceria-zirconia. Reaction mechanism by operando IR spectroscopy," *Catalysis Today,* vol. 215, pp. 201-207, 2013.

[54] M. Marwood, R. Doepper and A. Renken, "In-situ surface and gas phase analysis for kinetic studies under transient conditions The catalytic hydrogenation of CO2," *Applied Catalysis A: General,* vol. 151, no. 1, pp. 223-246, 1997.

[55] A. Drochner and H. G. Vogel, "Diffuse Reflectance Infrared Fourier Transform Spectroscopy: an In situ Method for the Study of the Nature and Dynamics of Surface Intermediates," in *Methods in Physical Chemistry*, R. S. a. P. C. Schmidt,

Ed., Weinheim, Wiley-VCH Verlag GmbH & Co. KGaA, 2012, pp. 445-475.

[56] P. G. Jessop, F. Joó and C.-C. Tai, "Recent advances in the homogeneous hydrogenation of carbon dioxide," *Coordination Chemistry Reviews,* vol. 248, pp. 2425-2442, 2004.

[57] P. Munnik, P. E. Jongh and K. P. Jong, "Recent Developments in the Synthesis of Supported Catalysts," *Chemical Reviews,* vol. 115, pp. 6687-6718, 2015.

[58] M. E. Davis and R. J. Davis, "Heterogeneous Catalysis," in *Fundamentals of Chemical Reaction Engineering*, M. E. Davis and R. J. Davis, Ed., Boston, Mc Graw Hill, 2003, pp. 133-183.

[59] O. Deutschmann, H. Knözinger, K. Kochloefl and T. Turek, "Heterogeneous Catalysis and Solid Catalysts," in *Ullmann's Encyclopedia of Industrial Chemistry*, Weinheim, Wiley-VCH Verlag GmbH & Co. KGaA, 2009, pp. 1-110.

[60] C. H. Bartholomew, "Mechanisms of catalyst deactivation," *Applied Catalysis A: General,* vol. 212, pp. 17-60, 2001.

[61] A. G. Mills and F. W. Steffgen, "Catalytic Methanation," *Catalysis Reviews,* vol. 8, no. 1, pp. 159-210, 1974.

[62] J. Regalbuto, Catalyst Preparation Science and Engineering, 1 ed., New York: CRC Press Taylor & Francis Group, 2007.

[63] R. Schäfer and P. C. Schmidt, Methods in Physical Chemistry, 1st ed., Weinheim: Wiley-VCH Verlag GmbH & Co. KGaA, 2012.

[64] G. Busca, U. Costantino, F. Marmottini, T. Montanari, P. Patrono, F. Pinzari and G. Ramis, "Methanol steam reforming over ex-hydrotalcite Cu–Zn–Al catalysts," *Applied Catalysis A: General,* vol. 310, pp. 70-78, 2006.

[65] Z. Kowalczyk, K. Stolecki, W. Rarńg-Pilecka, E. Miśkiewicz, E. Wilczkowska and Z. Karpiński, "Supported ruthenium catalysts for selective methanation of carbon oxides at very low COx/H2 ratios," *Applied Catalysis A: General,* vol. 342, pp. 35-39, 2008.

[66] S. Abelló, B. César and M. Daniel, "High-loaded nickel–alumina catalyst for direct CO hydrogenation into synthetic natural gas (SNG)," *Fuel,* vol. 113, pp. 598-609, 2013.

[67] D. G. Evans and R. C. T. Slade, "Structural Aspects of Layered Double Hydroxides," in *Layered Double Hydroxides*, X. Duan and D. G. Evans, Ed., Berlin, Springer Berlin Heidelberg, 2006, pp. 1-87.

[68] C. C. Hochstetter, ”Untersuchung über die zusammensetzung einiger mineralien,,” *Journal für Praktische Chemie,* osa/vuosik. 27, pp. 375-378, 1842.

[69] H. I. o. Mineralogy, “Mineral Database,” 2016. [Online]. Available: http://www.mindat.org/min-1987.html. [Accessed 04 10 2016].

[70] S. J. Mills, A. G. Christy, J.-M. R. Genin, T. Kameda and F. Colombo, “Nomenclature of the hydrotalcite supergroup: natural layered double hydroxides,” *Mineralogical Magazine,* vol. 76, no. 5, pp. 1289-1336, 2012.

[71] S. J. Mills, A. G. Christy, J.-M. R. Génin, T. Kameda and F. Colombo, ”Nomenclature of the hydrotalcite supergroup: natural layered double hydroxides,” *Mineralogical Magazine,* Osa %1/%2Vol. 76(5), pp. 1289–1336, pp. Vol.76(5), pp.1289-1336, 2012.

[72] W. F. Foshag, “The Chemical Composition of Hydrotalcite and the Hydrotalcite Group of Material,” in *U.S. National Museum*, 1920.

[73] C. Frondel, “Constitution and polymorphism of the pyroaurite and sjögrenite groups,” *American Mineralogist,* pp. 26, 295-315, 1951.

[74] F. Li and X. Duan, “Applications of Layered Double Hydroxides,” in *Layered Double Hydroxides*, X. D. a. D. G. Evans, Ed., Berlin, Springer, 2006, pp. 193-223.

[75] C. A. Antonyraj, P. Koilraj and S. Kannan, “Delamination of Layered Double Hydroxides: Methodologies, Characterization and Applications,” in *Hydroxides: Synthesis, Types and Applications*, C. C. Abejundio and D. A. Griego, Ed., New York, Nova Science Publishers, Inc., 2012, pp. 105-140.

[76] I. T. Sherman, Layered Double Hydroxides (LDHs): Synthesis, Characterization and Applications, 1st ed., New York: Nova Science Publishers, Inc., 2015.

[77] B. Saifullah and M. Z. Hussein, “Inorganic nanolayers: structure, preparation, and biomedical applications,” *International Journal of Nanomedicine,* vol. 10, pp. 5609-5633, 2015.

[78] M. R. Othman, Z. Helwani, Martunus and W. J. N. Fernando, “Synthetic hydrotalcites from different routes and their application as catalysts and gas adsorbents: a review,” *Appl. Organometal. Chem.,* vol. 23, p. 335–346, 2009.

[79] V. Rives, Layered Double Hydroxides: Present and Future, 1st ed., New York: Nova Science Publishers, Inc., 2001.

[80] D. G. Evans and R. C. T. Slade, “Structural Aspects of Layered Double Hydroxides,” in *Layered Double Hydroxides*, X. Duan and D. G. Evans, Ed., Berlin, Springer Berlin

Heidelberg, 2006, pp. 1-87.

[81] D. X. a. G. D. Evans, Layered Double Hydroxides, 1st ed., Berlin: Springer, 2006.

[82] A. C. C. a. D. A. Griego, Hydroxides: Synthesis, Types and Applications, 1st ed., New York: Nova Science Publishers, Inc., 2012.

[83] I. T. Sherman, Layered Double Hydroxides (LDHs): Synthesis, Characterization and Applications, 1st toim., New York: Nova Science Publishers, Inc., 2015.

[84] D. E. D. V. a. P. A. J. Bert F. Sels, "Hydrotalcite-like anionic clays in catalytic organic reactions," *Catalysis Reviews,* pp. 43, 443-488, 2001.

[85] S. Kannan, "Hydrotalcites as Potential Catalysts for Hydroxylation of Phenol," in *Trends in Catalysis Research*, L. P. Bevy, Ed., New York, Nova Science Publishers, Inc., 2006, pp. 51-101.

[86] F. L. a. X. Duan, "Applications of Layered Double Hydroxides," in *Layered Double Hydroxides*, X. D. a. D. G. Evans, Ed., Berlin, Springer, 2006, pp. 193-223.

[87] A. Vaccari, "Preparation and catalytic properties of cationic and anionic clays," *Catalysis Today,* pp. 41, 53-71, 1998.

[88] B. F. Sels, D. E. D. Vos and P. A. Jacobs, "Hydrotalcite-like anionic clays in catalytic organic reactions," *Catalysis Reviews,* vol. 43, no. 4, pp. 443-488, 2007.

[89] M. Climent, A. Corma, S. Iborra, K. Epping and A. Velty, "Increasing the basicity and catalytic activity of hydrotalcites by different synthesis procedures," *Journal of Catalysis,* vol. 225, pp. 316-326, 2004.

[90] A. Corma, V. Fornés, R. Martín-Aranda and F. Rey, "Determination of base properties of hydrotalcites: Condensation of benzaldehyde with ethyl acetoacetate," *Journal of Catalysis,* vol. 134, no. 1, pp. 58-65, 1992.

[91] W. T. Reichle, "Catalytic reactions by thermally activated, synthetic, anionic clay minerals," *Journal of Catalysis,* vol. 94, no. 2, pp. 547-557, 1985.

[92] W. Xie, H. Peng and L. Chen, "Calcined Mg-Al hydrotalcites as solid base catalysts for methanolysis of soybean oil," *Journal of Molecular Catalysis A: Chemical,* vol. 246, pp. 24-32, 2006.

[93] M. Climent, A. Corma, S. Iborra and J. Primo, "Base Catalysis for Fine Chemicals Production: Claisen-Schmidt Condensation on Zeolites and Hydrotalcites for the Production of Chalcones and Flavanones of Pharmaceutical Interest," *Journal of Catalysis,* vol. 151, no. 1, pp. 60-66, 1995.

[94] Z. Yong, V. Mata and A. E. Rodrigues, "Adsorption of Carbon Dioxide onto Hydrotalcite-like Compounds (HTlcs) at High Temperatures," *Ind. Eng. Chem. Res,* vol. 40, pp. 204-209, 2001.

[95] S. Walspurger, M. S. d. P. D. Cobden, W. Haije, R. v. d. Brink and O. V. Safonova, "Correlation between structural rearrangement of hydrotalcite-type materials and CO2 sorption processes under pre-combustion decarbonisation conditions," *Energy Procedia,* vol. 4, pp. 1162-1167, 2011.

[96] J. Soares, G. L. Casarin, H. J. José, R. D. F. P. M. Moreira and A. E. Rodrigues, "Experimental and Theoretical Analysis for the CO2 Adsorption on Hydrotalcite," *Adsorption,* vol. 11, pp. 237-241, 2005.

[97] Z. Yong and A. E. Rodrigues, "Hydrotalcite-like compounds as adsorbents for carbon dioxide," *Energy Conversion and Management,* vol. 43, no. 14, pp. 1865-1876, 2002.

[98] Z. Yong, V. Mata and A. E. Rodrigues, "Adsorption of carbon dioxide at high temperature—a review," *Separation and Purification Technology,* vol. 26, pp. 195-205, 2002.

[99] Y. Ding and E. Alpay, "Equilibria and kinetics of CO2 adsorption on hydrotalcite adsorbent," *Chemical Engineering Science,* vol. 17, p. 55, 2000.

[100] O. Aschenbrenner, P. McGuire, S. Alsamaq, J. Wang, S. Supasitmongkol, B. Al-Duri, P. Styring and J. Wood, "Adsorption of carbon dioxide on hydrotalcite-like compounds of different compositions," *Chemical Engineering Research and Design,* vol. 89, pp. 1711-1721, 2011.

[101] K. Lee, A. Verdooren, H. Caram and S. Sircar, "Chemisorption of carbon dioxide on potassium-carbonate-promoted hydrotalcite," *Journal of Colloid and Interface Science,* vol. 308, no. 1, pp. 30-39, 2007.

[102] R. Rojas, "Layered Double Hydroxides Applications as Sorbents for Environmental Remediation," in *Hydroxides: Synthesis, Types and Applications*, A. C. C. a. D. A. Griego, Ed., New York, Nova Science Publishers, Inc., 2012, pp. 39-72.

[103] N. Asouhidou and D. Lazaridis, "Kinetics of sorptive removal of chromium(VI) from aqueous solutions by calcined Mg-Al-CO3 hydrotalcite," *Water Research,* vol. 37, pp. 2875-2882, 2003.

[104] E. Alvarez-Avuso and H. W. Nugteren, "Purification of chromium(VI) finishing wastewaters using calcined and uncalcined Mg-Al-CO3-hydrotalcite," *Water Research,* vol. 39, no. 12, pp. 2535-2542, 2005.

[105] W. Wang, J. Zhou, G. Achari, Yu and J. W. Cai, "Cr(VI) removal from aqueous solutions by hydrothermal synthetic layered double hydroxides: Adsorption performance, coexisting anions and regeneration studies," *Colloids and Surfaces A: Physicochemical and Engineering Aspects,* vol. 457, pp. 33-40, 2014.

[106] K. Kuzawa, Y.-J. Jung, Y. Kiso, T. Yamada, M. Nagai and T.-G. Lee, "Phosphate removal and recovery with a synthetic hydrotalcite as an adsorbent," *Chemosphere,* vol. 62, no. 1, pp. 45-52, 2006.

[107] L. Lv, J. He, M. Wei, D. Evans and Z. Zhou, "Treatment of high fluoride concentration water by MgAl-CO3 layered double hydroxides: Kinetic and equilibrium studies," *Water Research,* vol. 41, no. 7, pp. 1534-1542, 2007.

[108] O. P. Ferreira, G. M. Sandra, D. Nelson, C. Lorena and O. L. Alves, "Evaluation of boron removal from water by hydrotalcite-like compounds," *Chemosphere,* vol. 62, no. 1, pp. 80-88, 2006.

[109] S. K. R. Yadanaparthi, D. Graybill and R. v. Wandruszka, "Adsorbents for the removal of arsenic, cadmium, and lead from contaminated waters," *Journal of Hazardous Materials,* vol. 171, pp. 1-15, 2009.

[110] G. P. Gillmann, "A simple technology for arsenic removal from drinking water using hydrotalcite," *Science of the Total Environment,* vol. 366, pp. 926-931, 2006.

[111] M. Cantú, E. López-Salinas and J. S. Valente, "SOx removal by calcined MgAlFe hydrotalcite-like materials: Effect of the chemical composition and the cerium incorporation method," *Environmental Science and Technology,* vol. 39, no. 24, pp. 9715-9720, 2005.

[112] L. M. Rodriguez-Chiang, J. Llorca and O. P. Dahl, "Effect of Fe–Zn–Mg–Al hydrotalcites on the methane potential of synthetic sulfate-containing wastewater," *Journal of Water Process Engineering,* vol. 10, pp. 120-127, 2016.

[113] M. X. Zhu, "Sorption of an anionic dye by uncalcined and calcined layered double hydroxides: A case study," *Journal of Hazardous Materials,* vol. 120, pp. 163-171, 2005.

[114] L. E. Gaini, "Removal of indigo carmine dye from water to Mg-Al-CO3-calcined layered double hydroxides," *Journal of Hazardous Materials,* vol. 161, pp. 627-632, 2009.

[115] M. Bouraada, "Basic dye removal from aqueous solutions by dodecylsulfate- and dodecyl benzene sulfonate-intercalated hydrotalcite," *Journal of Hazardous Materials,* vol. 153, no. 3, pp. 911-918, 2008.

[116] M. Ulibarri, I. Pavlovic, C. Barriga, M. Hermosin and J. Cornejo, "Adsorption of anionic species on hydrotalcite-like compounds: Effect of interlayer anion and crystallinity," *Applied Clay Science,* vol. 18, pp. 17-27, 2001.

[117] M. J. Reis, F. Silvério, J. Tronto and J. B. Valim, "Effects of pH, temperature, and ionic strength on adsorption of sodium dodecylbenzenesulfonate into Mg-Al-CO3 layered double hydroxides," *Journal of Physics and Chemistry of Solids,* vol. 65, pp. 487-492, 2004.

[118] H. Zhao and K. L. Nagy, "Dodecyl sulfate-hydrotalcite nanocomposites for trapping chlorinated organic pollutants in water," *Journal of Colloid and Interface Science,* vol. 274, no. 2, pp. 613-624, 2004.

[119] L. O. T. Dorante, "Evaluation of a Layered Double Hydroxide (LDH) Mineral as a Long-term Nitrate Exchanger in Soil," Gottfried Wilhelm Leibniz Universität Hannover, Hannover, 2007.

[120] H. W. Olfs, L. Torres-Dorante, R. Eckelt and H. Kosslick, "Comparison of different synthesis routes for Mg–Al layered double hydroxides (LDH): Characterization of the structural phases and anion exchange properties," *Applied Clay Science,* vol. 43, pp. 459-464, 2009.

[121] J. H. Lee, S. W. Rhee and D.-Y. Jung, "Step-wise Anion-Exchange in Layered Double Hydroxide Using Solvothermal Treatment," *Bull. Korean Chem. Soc.,* vol. 26, pp. 248-252, 2005.

[122] H. F. W. Taylor, "Crystal Structures of Some Double Hydroxide Minerals," *Mineralogical Magazine,* vol. 39, pp. 377-389, 1973.

[123] A. Radha, P. V. Kamath and C. Shivakumara, "Mechanism of the anion exchange reactions of the layered double hydroxides (LDHs) of Ca and Mg with Al," *Solid State Sciences,* vol. 7, pp. 1180-1187, 2005.

[124] M. R. Kang, H. M. Lim, S. C. Lee, S.-H. Lee and K. J. Kim, "Layered Double Hydroxide and its Anion Exchange Capacity," September 2005. [Online]. Available: http://www.azom.com/article.aspx?ArticleID=2997. [Accessed 15 10 2016].

[125] S. Miyata, "Anion-Exchange Properties of Hydrotalcite-like Compounds," *Clays and Clay Minerals,* pp. 31, 305-311, 1983.

[126] T. Yamaoka, M. Abe and M. Tsuji, "Synthesis of Cu□Al hydrotalcite like compound and its ion exchange property," *Materials Research Bulletin,* pp. 24, 1183-1199, 1989.

[127] J. B. Valim, E. L. Crepaldi and P. C. Pavan, "Comparative Study of the

Coprecipitation Methods for the preparation of Layered Double Hydroxides," *J. Braz. Chem. Soc.,* vol. 11, pp. 64-70, 2000.

[128] S. Miyata and T. Kumura, "Synthesis of New Hydrotalcite-Like Compounds and their Physico-Chemical Properties," *Chemistry Letters,* vol. 10, pp. 843-848, 1973.

[129] J. He, M. Wei, B. Li, Y. Kang, D. G. Evans and X. Duan, "Preparation of Layered Double Hydroxides," in *Layered Double Hydroxides*, X. D. a. D. G. Evans, Ed., Berlin, Springer, 2006, pp. 89-119.

[130] N. Chubar, V. Gerda, O. Megantari, M. Micusik, M. Omastova and K. Heister, "Applications versus properties of Mg–Al layered double hydroxides provided by their syntheses methods: Alkoxide and alkoxide-free sol–gel syntheses and hydrothermal precipitation," *Chemical Engineering Journal,* vol. 234, pp. 284-299, 2013.

[131] Q. Wang, S. V. Tang, E. Lester and D. O'Hare, "Synthesis of ultrafine layered double hydroxide (LDHs) nanoplates using a continuous-flow hydrothermal reactor," *Nanoscale,* vol. 5, pp. 114-117, 2013.

[132] F. X. a. Q. J. Yun Zhao, "Hydrothermal Synthesis of Ni/Al Layered Double Hydroxide Nanorods," *Journal of Nanotechnology,* vol. 2011, p. 646409, 2011.

[133] J. C. Brinker and G. W. Scherer, Sol-Gel Science, 1st ed., Boston: Academic Press, Inc., 1990.

[134] L. L. Hench and J. K. West, "The Sol-Gel Process," *Chemical Reviews,* vol. 90, pp. 33-72, 1990.

[135] M. Craiu, E. Ivana and M. Jitianu, "High-Thermally Stable NiO Phase Obtained from Hydrotalcite-Like Precursors with Different Ni/Al Ratios," Bucharest, 1996.

[136] T. Lopez, E. Ramos, P. Bosch, M. Asomoza and R. Gomez, "Thermal Stability of Sol-Gel Hydrotalcites," *J. Sol-Gel Sci. & Technol.,* vol. 8, pp. 437-442, 1997.

[137] M. Jitianu, M. Balasoiu, M. Zaharescu, A. Jitianu and A. Ivanov, "Comparative Study of Sol-Gel and Coprecipitated Ni-Al Hydrotalcites," *Journal of Sol-Gel Science and Technology,* vol. 19, pp. 453-457, 2000.

[138] W.-F. Lee and Y.-C. Chen, "Effects of intercalated hydrotalcite on drug release behavior for poly(acrylic acid-co-N-isopropyl acrylamide)/intercalated hydrotalcite hydrogels," *European Polymer Journal,* vol. 42, p. 1634–1642, 2006.

[139] T. Lopez, P. Bosch, E. Ramos, R. Gomez, O. Novaro, D. Acosta and F. Figueras, "Synthesis and Characterization of Sol-Gel Hydrotalcites. Structure and Texture,"

Langmuir, vol. 12, pp. 189-192, 1996.

[140] M. R. Othman and J. Kim, "The study of the conversion of intercalated compounds synthesized from a sol-gel procedure," *J Sol-Gel Sci Technol,* vol. 47, p. 274–282, 2008.

[141] Scopus, "Scopus, Hydrotalcites," 2016. [Online]. Available: https://www.scopus.com/term/analyzer.uri?sid=F7B929D6189E63B57768F5DF5055C60C.wsnAw8kcdt7IPYLO0V48gA%3a1640&origin=resultslist&src=s&s=TITLE-ABS-KEY%28hydrotalcite%29+AND+PUBYEAR+%3c+2017&sort=plf-f&sdt=b&sot=b&sl=27&count=4775&analyzeResults=Analyze+resu. [Accessed 5 10 2016].

[142] D. C. Hoyo, "Layered double hydroxides and human health: An overview," *Applied Clay Science,* vol. 36, p. 103–121, 2007.

[143] Q. W. a. D. O'Hare, "Recent Advances in the Synthesis and Application of Layered Double Hydroxide (LDH) Nanosheets," *Chem. Rev.,* vol. 112, p. 4124–4155, 2012.

[144] K. K. Rao, M. Gravelle, J. S. Valente and F. Figueras, "Activation of Mg–Al Hydrotalcite Catalysts for Aldol Condensation Reactions," *Journal of Catalysis,* vol. 173, pp. 115-121, 1998.

[145] B. M. Choudary, L. M. Kantam, A. Rahman, V. Reddy and K. K. Rao, "The first example of activation of molecular oxygen by nickel in ni-al hydrotalcite: A novel protocol for the selective oxidation of alcohols," *Angewandte Chemie - International Edition,* vol. 40, no. 4, pp. 763-766, 2001.

[146] N. Kakiuchi, Y. Maeda, T. Nishimura and S. Uemura, "Pd(II)-hydrotalcite-catalyzed oxidation of alcohols to aldehydes and ketones using atmospheric pressure of air," *Journal of Organic Chemistry,* vol. 66, no. 20, pp. 6620-6625, 2001.

[147] K. Christensen, D. Chen, R. Lødeng and A. Holmen, "Effect of supports and Ni crystal size on carbon formation and sintering during steam methane reforming," *Applied Catalysis A: General,* vol. 314, no. 1, pp. 9-22, 2006.

[148] K. Takehira, T. Shishido, P. Wang, T. Kosaka and K. Takaki, "Autothermal reforming of CH4 over supported Ni catalysts prepared from Mg-Al hydrotalcite-like anionic clay," *Journal of Catalysis,* vol. 221, no. 1, pp. 43-54, 2004.

[149] F. Kovanda and K. Jirátová, "Supported layered double hydroxide-related mixed oxides and their application in the total oxidation of volatile organic compounds," *Applied Clay Science,* vol. 53, no. 2, pp. 305-316, 2011.

[150] K. Mette, S. Kuhl, H. Dudder, K. Kähler ja A. Tarasov, "Stable Performance of Ni

Catalysts in the Dry Reforming of Methane at High Temperatures for the Efficient Conversion of CO2 into Syngas," *CHEMCATCHEM Communications,* osa/vuosik. 6, p. 100 – 104, 2014.

[151] R. Rinaldi, F. Y. Fujiwara, W. Hölderich ja U. Schuchardt, "'Tuning the acidic properties of aluminas via sol-gel synthesis: New findings on the active site of alumina-catalyzed epoxidation with hydrogen peroxide," *Journal of Catalysis,* osa/vuosik. 244, p. 92–101, 2006.

[152] F. Vermoortele, R. Ameloot, L. Alaerts, R. Matthessen, B. Carlier, E. V. R. Fernandez, J. Gascon, F. Kapteijn ja D. E. D. Vos, "Tuning the catalytic performance of metal–organic frameworks in fine chemistry by active site engineering," *J. Mater. Chem.,* osa/vuosik. 22, pp. 10313-10321, 2012.

[153] M. Vandichel, J. Hajek, F. Vermoortele, M. Waroquier, D. E. D. Vos ja V. Speybroeck, "Active site engineering in UiO-66 type metal–organic frameworks by intentional creation of defects: a theoretical rationalization," *CrystEngComm,* osa/vuosik. 17, pp. 395-406, 2015.

APPENDIX 1. Recordings of an Activity Test Run

Date	14.2.2017	V [ln/min]	0,300	Setpoint 3		Time IN	Time OUT
Reactor	B-03_250-350C_0.3-0.5L	T [°C]	300		set-point started	14.2.2017 11:03	
Catalyst	50% Ni/Mg/Al HT by co-p	p [bara]	1,000		set-point ended	14.2.2017 12:15	
		SV [1/h]	8185		set-point total time	1:12	0:00

FLOW OUT

Pressure [mbar]	1024,200		
Stream	IN	OUT	OUT Calc
Flow, beginning	48,4	73,4	
Flow, end	52,2	75,2	
T [°C]	23,6	23,6	23,6
t [min]	11	5	
t [s]	31,91	57,89	
V [ln/min]	0,303	0,302	0,456
mol/min	0,012465	0,012401	0,01874966

[°C]	[ln/min]	vol-%	vol-%	vol-%
T oven	Q	CO2	H2	N2
300	0,3	10	60	30

GAS COMPOSITIONS

Online analyzer	Time	CO	CO2	O2	H2	CH4
		vol-%	vol-%	vol-%	vol-%	vol-%
IN	11:03	0,16	9,90	0,05	59,90	0,00
OUT	11:15	0,01	1,41	0,00	37,60	12,02
2	11:20	0,01	1,10	0,00	36,90	12,47
3	11:25	0,01	1,41	0,00	37,80	11,96
4	11:30	0,01	1,86	0,00	38,90	11,32
5	11:35	0,01	2,09	0,00	39,60	10,96
6	11:40	0,01	2,21	0,00	39,80	10,82
7	11:45	0,01	2,18	0,00	39,80	10,82
8	11:50	0,01	2,15	0,00	39,70	10,86
9	11:55	0,01	2,12	0,00	39,70	10,89
10	12:00	0,01	2,10	0,00	39,60	10,92
11	12:05	0,01	2,10	0,00	39,70	10,91
12	12:10	0,01	2,10	0,00	39,70	10,91
		0,01	1,90	0,00	39,07	11,24

NOTE

after reduction 600 oC for 1h and at 650 C for 2hs HTs had higher activities.

3 ml of water is produced.

REACTOR CONDITIONS

Online analyzer	P	Reactor Bed (T133)	Oven Resistance (T130)
	bar(g)	[°C]	[°C]
IN	0,0	306,0	300,0
OUT	0,0	308,3	300,1
2	0,0	308,8	300,9
3	0,0	309,1	300,6
4	0,0	307,7	298,2
5	0,0	310,4	299,9
6	0,0	311,2	300,4
7	0,0	310,2	300,2
8	0,0	310,7	299,9
9	0,0	310,8	300,5
10	0,0	311,0	300,2
11	0,0	310,8	300,0
12	0,0	310,2	300,0

Online analyzer	CO2 X%	H2 X%	CH4 S%	CO S%	CH4 Y%	mol/min CH4	mol/min C02	mol/min H2	mol/min CO
							IN	IN	
							0,00072	0,00387	
OUT	85,76	37,23	99,92 %	0,08 %	99,87 %	0,00078	0,00014	0,00238	0,00000
2	88,89	38,40	99,92 %	0,08 %	99,96 %	0,00080	0,00011	0,00244	0,00000
3	85,76	36,89	99,92 %	0,08 %	99,81 %	0,00077	0,00014	0,00251	0,00000
4	81,21	35,06	99,91 %	0,09 %	99,80 %	0,00073	0,00018	0,00256	0,00000
5	78,89	33,89	99,91 %	0,09 %	98,76 %	0,00071	0,00020	0,00257	0,00000
6	77,68	33,56	99,91 %	0,09 %	97,50 %	0,00070	0,00021	0,00257	0,00000
7	77,98	33,56	99,91 %	0,09 %	97,50 %	0,00070	0,00021	0,00256	0,00000
8	78,28	33,72	99,91 %	0,09 %	97,86 %	0,00070	0,00021	0,00256	0,00000
9	78,59	33,72	99,91 %	0,09 %	98,13 %	0,00070	0,00021	0,00256	0,00000
10	78,79	33,89	99,91 %	0,09 %	98,40 %	0,00070	0,00020	0,00256	0,00000
11	78,79	33,72	99,91 %	0,09 %	98,31 %	0,00070	0,00020	0,00256	0,00000
12	78,79	33,72	99,91 %	0,09 %	98,31 %	0,00070	0,00020	0,00252	0,00000
	80,78	35,84	99,91 %	0,09 %	99,28 %	0,00	0,00	0,00	0,00

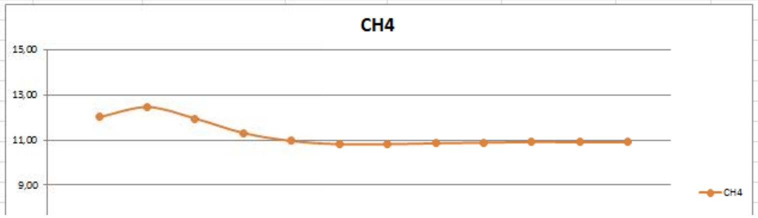

APPENDIX 2. List of Test Runs

GHSV (h^{-1})	Name	# SP	Temp	P	CO2	H2	N2	F (L/min)	X_{CO2} %	S_{CH4} %	Date	Name of the file
13642	A-02	1	300	0	20	80	0	0.5	14	89	23.1.17	A-02_300C_0.5Lmin_ 23012017
13642	A-02	2	300	0	10	40	50	0.5	26	96	23.1.17	
13642	A-02	3	300	0	10	60	30	0.5	31	97	24.1.17	A-02_300C_0.5Lmin_ 4th_ 24012017
13642	A-02	4	300	0	10	50	40	0.5	28	97	24.1.17	
13642	A-02	5	300	0	10	30	60	0.5	21	95	24.1.17	
13642	A-02	6	300	0	25	50	25	0.5	32	97	24.1.17	
8185	A-02	7	300	0	10	60	30	0.3	43	99	25.1.17	A-02_300C_0.3Lmin_ 25012017
8185	A-02	8	300	0	10	40	50	0.3	34	98	25.1.17	
8185	A-02	9	300	0	10	50	40	0.3	39	99	30.1.17	A-02_300-450C_ 0.3Lmin_30012017
8185	A-02	10	350	0	10	40	50	0.3	60	99	26.1.17	A-02_350C_0.3Lmin_ 26012017
8185	A-02	11	350	0	10	60	30	0.3	83	100	26.1.17	
8185	A-02	12	350	0	10	50	40	0.3	75	99	26.1.17	
8185	A-02	13	450	0	10	60	30	0.3	93	100	26.1.17	
8185	A-03	14	450	0	10	60	30	0.3	94	100	27.1.17	A-03_450C_0.3Lmin_ 27012017
8185	A-03	15	450	0	10	40	50	0.3	62	99	27.1.17	
8185	A-02	16	400	0	10	60	30	0.3	94	100	30.1.17	A-02_300-450C_ 0.3Lmin_30012017
8185	A-02	17	400	0	10	40	50	0.3	68	99	30.1.17	
8185	A-02	18	400	0	10	50	40	0.3	86	100	30.1.17	
8185	A-02	19	450	0	10	50	40	0.3	79	99	1.2.17	A-02_450C_0.3Lmin_ 01022017
8185	A-02	20	450	0	10	40	50	0.3	62	98	1.2.17	
20463	A-02	21	300	0	10	60	30	0.75	21	91	1.2.17	
8185	A-02	22	250	0	10	60	30	0.3	9	93	1.2.17	
8185	A-02	23	250	0	10	60	30	0.3	11	96	3.2.17	B-03_300C_0.3Lmin_ 03022017
8185	B-03	24	300	0	10	60	30	0.3	49	98	3.2.17	
8185	B-03	25	350	0	10	60	30	0.3	94	100	3.2.17	
8185	B-12	26	400	0	10	60	30	0.3	98	100	3.2.17	
8185	B-03	27	500	0	10	60	30	0.3	37	96	3.2.17	

GHSV (h^{-1})	Name	# SP	Temp	P	CO2	H2	N2	F (L/min)	X_{CO2} %	S_{CH4} %	Date	Name of the file
8185	B-03	28	250	0	10	60	30	0.3	19		6.2.17	B-03_300C_0.3Lmin_ 06022017
8185	B-03	29	300	0	10	60	30	0.3	62	99	7.2.17	
8185	B-03	30	350	0	10	60	30	0.3	99	100	7.2.17	
8185	B-03	31	350	0	10	60	30	0.5	86	100	7.2.17	B-03_300C_0.3Lmin_ 07022017
8185	B-03	32	250	0	10	60	30	0.5	12	96	7.2.17	
8185	B-03	33	300	0	10	60	30	0.5	54	100	7.2.17	
8185	B-12	36	220	0	10	60	30	0.3	5	96	8.2.17	
8185	B-12	37	300	0	10	60	30	0.3	67	99	8.2.17	B-12_250-350C_0.3Lmin_ 08022017
8185	B-12	38	350	0	10	60	30	0.3	96	100	8.2.17	
8185	B-12	39	350	0	10	60	30	0.5	83	99	8.2.17	
13642	B-12	40	250	0	10	60	30	0.5	12	96	9.2.17	
13642	B-12	41	300	0	10	60	30	0.5	69	98	9.2.17	B-12_250-350C_0.5Lmin_ 09022017
13642	B-12	42	300	0	12.5	25	62.5	0.5	20	89	9.2.17	
13642	B-12	43	250	0	10	60	30	0.3	8	76	10.2.17	
13642	B-12	44	250	0	10	60	30	0.5	11	96	10.2.17	B-12-B03_250-400C_0.3-0.5Lmin_10022017
13642	B-12	45	400	0	10	60	30	0.3	95	100	10.2.17	
13642	B-12	46	400	0	10	60	30	0.5	99	100	10.2.17	
8185	B-03	47	400	0	10	60	30	0.3	98	100	10.2.17	
8185	B-03	48	400	0	10	60	30	0.5	97	100	10.2.17	B03_220-400C_0.3-0.5Lmin_ 13022017
8185	B-03	49	220	0	10	60	30	0.3	5	98	10.2.17	
8185	B-03	50	250	0	10	60	30	0.3	23	99	14.2.17	
8185	B-03	51	300	0	10	60	30	0.3	80	100	14.2.17	
8185	B-03	52	350	0	10	60	30	0.3	100	100	14.2.17	B-03_250-350C_0.3-0.5Lmin_ 14022017
13642	B-03	53	350	0	10	60	30	0.5	95	100	14.2.17	
13642	B-03	54	250	0	10	60	30	0.5	17	97	14.2.17	
13642	B-03	55	300	0	10	60	30	0.5	66	99	15.2.17	

GHSV (h^{-1})	Name	# SP	Temp	P	CO2	H2	N2	F (L/min)	X_{CO2} %	S_{CH4} %	Date	Name of the file
8185	B-12	56	250	0	10	60	30	0.3	20	99	15.2.17	
8185	B-12	57	300	0	10	60	30	0.3	77	99	15.2.17	
8185	B-12	58	350	0	10	60	30	0.3	96	100	15.2.17	B-12_250-350C_0.3-0.5Lmin_ 15022017
13642	B-12	59	350	0	10	60	30	0.5	91	99	15.2.17	
13642	B-12	60	250	0	10	60	30	0.5	15	94	15.2.17	
13642	B-12	61	300	0	10	60	30	0.5	66	99	15.2.17	
8185	B-03	62	220	0	10	60	30	0.3	10	98	16.2.17	B-03_220-400C_0.3-0.5Lmin_ 16022017
13642	B-03	63	400	0	10	60	30	0.5	97	100	16.2.17	
8185	D-01	64	300	0	10	60	30	0.3	11	25	20.2.17	B-01-D01_500C_0.3Lmin_ 20022017_Reduction
8185	B-01	65	250	0	10	60	30	0.3	6	88	21.2.17	
8185	B-01	66	300	0	10	60	30	0.3	25	88	21.2.17	B-01-D01_250-350C_0.3Lmin_ 21022017
8185	D-01	67	250	0	10	60	30	0.3	1	30	21.2.17	
8185	D-01	68	350	0	10	60	30	0.3	37	53	21.2.17	
8185	B-01	69	350	0	10	60	30	0.3	62	96	22.2.17	
8185	B-01	70	400	0	10	60	30	0.3	86	99	22.2.17	B-01-D01_250-400C_0.3Lmin_ 22022017
8185	D-01	71	400	0	10	60	30	0.3	67	93	22.2.17	
8185	D-01	72	250	0	10	60	30	0.3	4	50	27.2.17	
8185	B-01	73	250	0	10	60	30	0.3	7	95	27.2.17	B-01-D01_250-400C_0.3Lmin_ Reduction_27022017
8185	D-01	74	350	0	10	60	30	0.3	85	99	27.2.17	
8185	B-01	75	350	0	10	60	30	0.3	83	100	28.2.17	
8185	D-01	76	300	0	10	60	30	0.3	72	97	28.2.17	
8185	B-01	77	300	0	10	60	30	0.3	40	97	28.2.17	B-01-D01_250-400C_0.3Lmin_ Reduction_28022017
8185	D-01	78	400	0	10	60	30	0.3	91	99	28.2.17	
8185	B-01	79	400	0	10	60	30	0.3	98	100	28.2.17	
8185	D-01	80	450	0	10	60	30	0.3	89	99	1.3..17	D01_500-450C_0.3Lmin_ 01032017
8185	D-01	81	500	0	10	60	30	0.3	81	97	1.3..17	

GHSV (h^{-1})	Name	# SP	Temp	P	CO2	H2	N2	F (L/min)	X_{CO2} %	S_{CH4} %	Date	Name of the file
8185	A-13	82	250	0	10	60	30	0.3	4	99	3.3.17	A-13_D-02_250-500C_ 0.3Lmin_ 03032017
8185	A-13	83	400	0	10	60	30	0.3	92	100	6.3.17	
8185	A-13	84	350	0	10	60	30	0.3	60	98	6.3.17	
8185	A-13	85	500	0	10	60	30	0.3	85	98	6.3.17	A-13_D-02_250-500C_ 0.3Lmin_06032017
8185	D-02	86	250	0	10	60	30	0.3	1	0	6.3.17	
8185	D-02	87	350	0	10	60	30	0.3	18	25	6.3.17	
8185	A-13	88	450	0	10	60	30	0.3	58	73	6.3.17	
8185	A-13	89	300	0	10	60	30	0.3	4	36	6.3.17	A-13_D-02_250-500C_ 0.3Lmin_07032017
8185	D-02	90	500	0	10	60	30	0.3	59	40	7.3.17	
8185	D-02	91	400	0	10	60	30	0.3	30	11	7.3.17	
8185	C-13	92	250	0	10	60	30	0.3	0	0	8.3.17	
8185	C-13	93	300	0	10	60	30	0.3	2	9	8.3.17	
8185	C-13	94	350	0	10	60	30	0.3	7	6	8.3.17	C-13_C-02_250-500C_ 0.3Lmin_08032017
8185	C-13	95	400	0	10	60	30	0.3	40	60	8.3.17	
8185	C-13	96	450	0	10	60	30	0.3	60	72	8.3.17	
8185	C-13	97	500	0	10	60	30	0.3	74	89	8.3.17	
8185	C-02	98	250	0	10	60	30	0.3	2	21	14.3.17	
8185	C-02	99	300	0	10	60	30	0.3	12	27	14.3.17	
8185	C-02	100	350	0	10	60	30	0.3	95	100	14.3.17	C-13_C-02_250-500C_ 0.3Lmin_14032017
8185	C-02	101	400	0	10	60	30	0.3	95	100	14.3.17	
8185	C-02	102	450	0	10	60	30	0.3	87	98	14.3.17	
8185	C-02	103	500	0	10	60	30	0.3	77	92	14.3.17	
8185	C-02	104	250	0	10	60	30	0.3	2	39	15.3.17	
8185	C-02	105	300	0	10	60	30	0.3	13	36	15.3.17	
8185	C-02	106	350	0	10	60	30	0.3	44	71	15.3.17	C-13_C-02_250-500C_ 0.3Lmin_15032017
8185	C-02	107	400	0	10	60	30	0.3	63	91	15.3.17	
8185	C-02	108	450	0	10	60	30	0.3	74	94	15.3.17	
8185	C-02	109	500	0	10	60	30	0.3			15.3.17	

GHSV (h^{-1})	Name	# SP	Temp	P	CO2	H2	N2	F (L/min)	X_{CO2} %	S_{CH4} %	Date	Name of the file
8185	C-13	110	250	0	10	60	30	0.3	1	67	16.3.17	
8185	C-13	111	300	0	10	60	30	0.3	7	76	16.3.17	
8185	C-13	112	350	0	10	60	30	0.3	45	86	16.3.17	C-13_C-02_250-500C_ 0.3Lmin_16032017
8185	C-13	113	400	0	10	60	30	0.3	78	97	16.3.17	
8185	C-13	114	450	0	10	60	30	0.3	86	98	16.3.17	
8185	C-13	115	500	0	10	60	30	0.3	81	94	16.3.17	
8185	D-12	116	250	0	10	60	30	0.3	2	40	17.3.17	
8185	D-12	117	300	0	10	60	30	0.3	5	37	17.3.17	
8185	D-12	118	350	0	10	60	30	0.3	27	60	20.3.17	D-12_E-12_250-500C_ 0.3Lmin_17032017
8185	D-12	119	400	0	10	60	30	0.3	42	65	20.3.17	
8185	D-12	120	450	0	10	60	30	0.3	60	92	20.3.17	
8185	D-12	121	500	0	10	60	30	0.3	61	89	20.3.17	
8185	E-12	122	250	0	10	60	30	0.3	2	29	20.3.17	
8185	E-12	123	300	0	10	60	30	0.3	6	37	20.3.17	
8185	E-12	124	350	0	10	60	30	0.3	38	62	20.3.17	D-12_E-12_250-500C_ 0.3Lmin_20032017
8185	E-12	125	400	0	10	60	30	0.3	42	73	20.3.17	
8185	E-12	126	450	0	10	60	30	0.3	60	92	20.3.17	
8185	E-12	127	500	0	10	60	30	0.3	39	22	20.3.17	
8185	D-12	128	250	0	10	60	30	0.3	1	30	21.3.17	
8185	D-12	129	300	0	10	60	30	0.3	12	37	21.3.17	
8185	D-12	130	350	0	10	60	30	0.3	25	51	21.3.17	D-12_E-12_250-500C_ 0.3Lmin_21032017-2
8185	D-12	131	400	0	10	60	30	0.3	44	76	21.3.17	
8185	D-12	132	450	0	10	60	30	0.3	52	82	21.3.17	
8185	D-12	133	500	0	10	60	30	0.3	56	83	21.3.17	

GHSV (h^{-1})	Name	# SP	Temp	P	CO2	H2	N2	F (L/min)	X_{CO2} %	S_{CH4} %	Date	Name of the file
8185	E-12	134	250	0	10	60	30	0.3	0	0	23.3.17	
8185	E-12	135	300	0	10	60	30	0.3	2	56	23.3.17	
8185	E-12	136	350	0	10	60	30	0.3	8	53	23.3.17	A-01_E-12_250-500C_ 0.3Lmin_23032017
8185	E-12	137	400	0	10	60	30	0.3	25	56	23.3.17	
8185	E-12	138	450	0	10	60	30	0.3	47	62	23.3.17	
8185	E-12	139	500	0	10	60	30	0.3	62	75	23.3.17	
8185	A-01	140	250	0	10	60	30	0.3	4	95	22.3.17	
8185	A-01	141	300	0	10	60	30	0.3	15	95	22.3.17	
8185	A-01	142	350	0	10	60	30	0.3	47	95	22.3.17	A-01_E-12_250-500C_ 0.3Lmin_22032017
8185	A-01	143	400	0	10	60	30	0.3	78	98	22.3.17	
8185	A-01	144	450	0	10	60	30	0.3	87	99	22.3.17	
8185	A-01	145	500	0	10	60	30	0.3	79	97	22.3.17	
8185	D-11	146	250	0	10	60	30	0.3	2	40	24.3.17	
8185	D-11	147	300	0	10	60	30	0.3	5	52	24.3.17	
8185	D-11	148	350	0	10	60	30	0.3	8	64	24.3.17	A-01_D-11_250-500C_ 0.3Lmin_24032017
8185	D-11	149	400	0	10	60	30	0.3	47	76	24.3.17	
8185	D-11	150	450	0	10	60	30	0.3	52	83	24.3.17	
8185	D-11	151	500	0	10	60	30	0.3	61	89	24.3.17	
8185	D-11	152	250	0	10	60	30	0.3	2	39	27.3.17	
8185	D-11	153	300	0	10	60	30	0.3	6	36	27.3.17	
8185	D-11	154	350	0	10	60	30	0.3	22	52	27.3.17	D-11_250-500C_0.3Lmin_ 27032017
8185	D-11	155	400	0	10	60	30	0.3	-	-	27.3.17	
8185	D-11	156	450	0	10	60	30	0.3	51	84	27.3.17	
8185	D-11	157	500	0	10	60	30	0.3	-	-	27.3.17	

GHSV (h^{-1})	Name	# SP	Temp	P	CO2	H2	N2	F (L/min)	X_{CO2} %	S_{CH4} %	Date	Name of the file
8185	F-01	158	250	0	10	60	30	0.3	0	-	30.3.17	F-01-F-02_250-500C_0.3Lmin_30032017
8185	F-01	159	300	0	10	60	30	0.3	3	55	30.3.17	
8185	F-01	160	350	0	10	60	30	0.3	5	23	30.3.17	
8185	F-01	161	400	0	10	60	30	0.3	43	81	30.3.17	
8185	F-01	162	450	0	10	60	30	0.3	50	46	30.3.17	
8185	F-01	163	500	0	10	60	30	0.3	68	82	30.3.17	
8185	F-02	164	250	0	10	60	30	0.3	0	-	31.3.17	F-01-F-02_250-500C_0.3Lmin_31032017
8185	F-02	165	300	0	10	60	30	0.3	5	58	31.3.17	
8185	F-02	166	350	0	10	60	30	0.3	11	60	31.3.17	
8185	F-02	167	400	0	10	60	30	0.3	52	79	31.3.17	
8185	F-02	168	450	0	10	60	30	0.3	63	85	31.3.17	
8185	F-02	169	500	0	10	60	30	0.3	73	91	31.3.17	

APPENDIX 3. List of Reactor Tubes

Catalyst name	Definition	Slurry	Coated/Packed Reactor Tubes	Catalyst Amount (g)	Preparation method	Notes
LSC-20	17.75 w% Ni/Al2O3	SLURRY44	A-01	1.030	Incipient Wetness Impregnation	-
			A-02	1.410		-
			A-03	0.570		-
LSC-21	25 w% Ni/Al2O3	SLURRY46	A-11	0.333	Incipient Wetness Impregnation	-
			A-12	0.450		-
			A-13	0.568		-
LSC-23	0.5 Ni/Mg/Al HT	SLURRY47	B-01	0.368	Co-Precipitation	-
			B-02	0.330		-
			B-03	0.682		-
-	Ce-doped_HT	SLURRY49	C-01	-	Commertial	
			C-03	-		Unseccessful coating
LSC-25	2nd Batch 0.5 Ni/Mg/Al HT	SLURRY50	B-11	0.596	Co-Precipitation	
			B-12	0.654		With calcined catalyst
LSC-25	2nd Batch 0.5 Ni/Mg/Al HT	SLURRY52	B-13	0.825	Co-Precipitation	
			B-14 (E-03)	0.429		With dried catalyst
LSC-26	0.17 Ni/Mg/Al HT	SLURRY53	-	-	Co-Precipitation	
			E-01	-		Unseccessful coating
LSC-26	0.17 Ni/Mg/Al HT	SLURRY54	D-01	0.527	Co-Precipitation	With dried --> calcined catalyst
LSC-28	5 w% Ni/Mg/Al HT	-	C-11	0. 400	Sol-gel	Packed bed (not enough for coating)
LSC-29	Ni/Ce-doped_HT	SLURRY58	E-02	-	Wet Impregnation	Unseccessful coating
LSC-26	0.17 Ni/Mg/Al HT	-	D-02	0.363	Co-Precipitation	Packed
LSC-30	Ni/Zr-doped_HT	SLURRY55	E-12	0.499	Wet Impregnation	-
LSC-31	17.75 w% Ni/Ce-doped_HT	SLURRY56	E-11	-	Wet Impregnation	Unseccessful coating
LSC-32	17.75 w% Ni/Zr-doped_HT	SLURRY57	E-13	-	Wet Impregnation	Unsuccessful coating
LSC-28	5 w% Ni/Mg/Al HT	-	C-02	0.4	Sol-gel	Packed bed (not enough for coating)
LSC-31	17.75 w% Ni/Ce-doped_HT	-	C-13	0.4	Wet Impregnation	Packed bed
LSC-28	5 w% Ni/Mg/Al HT	SLURRY60	D-11	0.763	Sol-gel	-
LSC-34	15 w% Ni/Mg/Al HT	SLURRY59	D-12	0.676	Sol-gel	-
LSC-29	Ni/Ce-doped_HT	-	F-01	0.4	Wet Impregnation	Packed bed
LSC-32	17.75 w% Ni/Zr-doped_HT	-	F-02	0.415	Wet Impregnation	Packed bed